

AN INVESTIGATION OF BI-DIRECTIONAL
REFLECTANCE FROM RANDOMLY
ROUGH ENGINEERING
SURFACES

By

FRED EDWIN WALTER

"
Bachelor of Science
Montana State University
Bozeman, Montana
1958

Master of Science
University of Wyoming
Laramie, Wyoming
1963


Submitted to the faculty of the Graduate College
of the Oklahoma State University
in partial fulfillment of the requirements
for the Degree of
DOCTOR OF PHILOSOPHY
May, 1972

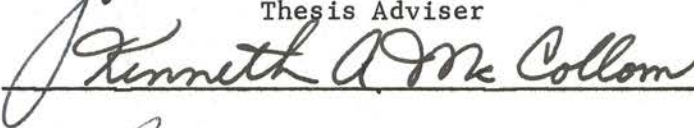
Thesis
19720.
W231i
wp2

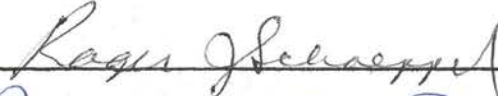
AUG 16 1973


AN INVESTIGATION OF BI-DIRECTIONAL
REFLECTANCE FROM RANDOMLY
ROUGH ENGINEERING
SURFACES


Thesis Approved:



Thesis Adviser








Dean of the Graduate College

ACKNOWLEDGMENTS

Many people offered assistance and encouragement to the author during this research effort. I wish to extend my sincere appreciation to these people and in particular to: Dr. J. A. Wiebelt, committee chairman and thesis adviser, for his guidance and especially his patience; Dr. C. E. Price, for his assistance in sample selection and photographic processing; Lt. Col. J. D. Pinson and Mr. Jim Roberson, of the United States Air Force, Wright-Patterson Air Force Base, for their facilities, equipment, and support in sample preparation and characterization; Dr. Richard Murray, Dr. Victor J. Anselmo, and Dr. John C. Thompson for their technical discussions and encouragement; Mr. Robert Thompson, Mr. John Levesque, and Capt. Harold Izzolino for their expert assistance in integrating digital computer subroutines; and most of all to my wife and family for their sacrifices and encouragement during the years of graduate study.

TABLE OF CONTENTS

Chapter	Page
I. INTRODUCTION	1
Background	1
Literature Survey	5
II. THEORETICAL ANALYSIS	13
III. EXPERIMENTAL DEVELOPMENT AND APPARATUS	19
Sample Selection and Preparation	19
Confirmation of Sample Surfaces	22
Optical Surface Characteristics	29
Surface Characteristics Apparatus	33
Bi-Directional Reflectances	35
IV. DATA REDUCTION	44
Bi-Directional Reflectance Data	48
Reflected Pattern	50
Calibration	52
Extrapolated Calibration Data	58
V. RESULTS AND CONCLUSIONS	61
Optical and Mechanical Surface Parameters	62
Theory Versus Data	64
1-D Data Versus Theory	65
2-D Data Versus Theory	67
Conclusions and Recommendations	68
SELECTED BIBLIOGRAPHY	71
APPENDIX A	74
APPENDIX B	95
APPENDIX C	107

LIST OF TABLES

Table	Page
I. Filter Calibration Data	39
II. Mechanical and Optical Surface Parameters	62

LIST OF FIGURES

Figure	Page
1. Angles of Incidence and Reflection	15
2. Sample Schematics	20
3. Photomicrographs of 1-D Samples	22
4. Photomicrograph of 2-D Sample	22
5. Proficorder Tracing	23
6. Schematic of Proficorder Tracing Digitizer	24
7. Normal Probability Graph - Sample 1	26
8. Normal Probability Graph - Sample 2	27
9. Normal Probability Graph - Sample 3	28
10. Schematic of Surface Characteristics Experiment	30
11. Wave Propagation	31
12. Schematic of Bi-Directional Reflectance Experiment	37
13. Densitometer Linearity Graph	42
14. Specular Reflectance Data - Sample 1	45
15. Specular Reflectance Data - Sample 2	46
16. Specular Reflectance Data - Sample 3	47
17. Specular Reflectance - Birkebak and Walter Data	49
18. Speckle Patterns	51
19. Typical Calibration Curve	53
20. Sample of Raw Data	54
21. Sample of Calibrated Data	55

Figure	Page
22. Sample of Curve-fit Data	57
23. Typical Characteristic Curve	60
24. Extrapolated Characteristic Curve	60
25. Raw Data - Sample 1 - $\psi = 0^\circ$	75
26. Raw Data - Sample 1 - $\psi = 10^\circ$	76
27. Raw Data - Sample 1 - $\psi = 15^\circ$	77
28. Raw Data - Sample 1 - $\psi = 30^\circ$	78
29. Raw Data - Sample 1 - $\psi = 45^\circ$	79
30. Raw Data - Sample 1 - $\psi = 60^\circ$	80
31. Raw Data - Sample 1 - $\psi = 75^\circ$	81
32. Raw Data - Sample 2 - $\psi = 0^\circ$	82
33. Raw Data - Sample 2 - $\psi = 10^\circ$	83
34. Raw Data - Sample 2 - $\psi = 15^\circ$	84
35. Raw Data - Sample 2 - $\psi = 30^\circ$	85
36. Raw Data - Sample 2 - $\psi = 45^\circ$	86
37. Raw Data - Sample 2 - $\psi = 60^\circ$	87
38. Raw Data - Sample 2 - $\psi = 75^\circ$	88
39. Raw Data - Sample 3 - $\psi = 5^\circ$	89
40. Raw Data - Sample 3 - $\psi = 15^\circ$	90
41. Raw Data - Sample 3 - $\psi = 30^\circ$	91
42. Raw Data - Sample 3 - $\psi = 45^\circ$	92
43. Raw Data - Sample 3 - $\psi = 60^\circ$	93
44. Raw Data - Sample 3 - $\psi = 75^\circ$	94
45. Theory Versus Data - Sample 1 - $\psi = 0^\circ$ and 10°	96
46. Theory Versus Data - Sample 1 - $\psi = 15^\circ$ and 30°	97

Figure	Page
47. Theory Versus Data - Sample 1 - $\psi = 45^\circ$ and 60°	98
48. Theory Versus Data - Sample 1 - $\psi = 75^\circ$	99
49. Theory Versus Data - Sample 2 - $\psi = 0^\circ$ and 10°	100
50. Theory Versus Data - Sample 2 - $\psi = 15^\circ$ and 30°	101
51. Theory Versus Data - Sample 2 - $\psi = 45^\circ$ and 60°	102
52. Theory Versus Data - Sample 2 - $\psi = 75^\circ$	103
53. Theory Versus Data - Sample 3 - $\psi = 5^\circ$ and 15°	104
54. Theory Versus Data - Sample 3 - $\psi = 30^\circ$ and 45°	105
55. Theory Versus Data - Sample 3 - $\psi = 60^\circ$ and 75°	106

NOMENCLATURE

A	area
$C(\tau)$	autocorrelation coefficient
E	electric field strength
E_2	scattered field
E_{20}	scattered field from smooth surface
k	propagation vector of electric field
L	half of the illuminated length of the surface
n	normal to the surface
p	fixed point in far-field space
\bar{P}	mean power reflection coefficient
P	modified mean power reflection coefficient
Q	mean scattered power
r	distance from the origin of the coordinate system to a point on the surface
\bar{R}	normalized reflectance
T	correlation distance
v	a vector equal to the incoming propagation vector minus the outgoing propagation vector
$v \cdot r$	scalar product
X	half the illuminated length in the x direction
Y	half the illuminated length in the y direction
∇	del-vector operator

Greek

θ	polar angle of reflection
λ	monochromatic wavelength of energy
μ	micron (micrometer)
ρ	bi-directional reflectance or scattering coefficient
$\rho\rho^*$	proportional to mean scattered power
σ	root-mean-square height of roughness elements
Φ	azimuth angle of reflectance
ψ	polar angle of incidence
$d\omega$	incoming solid angle

CHAPTER I

INTRODUCTION

The knowledge of how roughened surfaces reflect incident thermal energy (electromagnetic waves) is very important, especially for making heat balance calculations in space. The purpose of this dissertation was to investigate experimentally the applicability of using Beckmann's Bi-Directional Reflectance Model to predict reflectance from randomly rough surfaces with optical roughnesses less than one. In particular, two experiments were required, one to optically determine the surface parameters and one to obtain the bi-directional reflectances.

Thermal radiation (electromagnetic waves) is the only means of heat transfer in space, for in space there is no mass transfer between an object and its environment. This is unlike the earth's air environment where heat transfer is usually dominated by convection and conduction. Therefore, the space age has focused on the need for more knowledge in thermal radiation. A few of the many applications of thermal radiation in space are temperature control, generation of power from solar energy and heat rejection systems. The need for understanding all aspects and properties of radiant heat transfer will continue to grow as man advances in the utilization of space.

Background

Reflectance is a fundamental thermal radiation property. It is

often related to a specific material as a unique property of that material. However, reflectance is affected not only by the intrinsic properties of the material but also by the surface properties such as roughness, chemistry and physical state of the surface layer (1, 2). Only the effect of the roughness parameter is investigated in this research.

Surface damage and oxide films are two important surface parameters which substantially affect the inherent reflectance of a material and therefore, must be accounted for in any experimental technique employed in research. Both parameters are wavelength dependent (1, 2). Working a material results in lattice distortions that can extend to depths greater than the optical penetration depth. The result of the surface strain is a decrease in the inherent reflectance. Therefore, tabular values of reflectance are only approximate for materials that have been worked. Oxide films can also substantially reduce reflectance in the ultraviolet and visible wavelength ranges (2). The thickness of the oxide film significantly affects the amount that the reflectance is reduced and which wavelengths will experience lower reflectance. Thus in determining the overall reflectance of a material, not only the intrinsic properties and the surface roughness must be considered but the other surface properties as well.

The range of surface roughness is very significant as it affects the reflectance in different ways. A smooth surface reflects an incident wave specularly. That is, a specular reflection (coherent) has equal angles of incidence and reflectance, and the incident solid angle equals the reflected solid angle like light reflected from a mirror. A rough surface scatters or reflects the incident energy

nonspecularly in various directions though certain directions may receive more energy than others. The nonspecularly reflected energy (incoherent) from a slightly roughened surface is concentrated within a cone which may be centered on the specular direction. The rougher diffuse surface reflects all incident radiation nonspecularly into all directions in space with an energy distribution described by Lambert's cosine law (3). The incident electromagnetic energy is generally assumed to be reflected either specularly or diffusely. Each is a limiting case and the energy distribution from real surfaces is considered intermediate to these extremes.

The roughness range investigated is limited to an optical roughness less than unity. The optical roughness is defined as the ratio of the root-mean-square (rms) roughness of the surface divided by the wavelength (λ) of the incident energy. This range of roughness is of particular significance in space because a major portion of the sun's energy is emitted at wavelengths that are less than the surface roughnesses encountered in the normal milling, machining and finishing of spacecraft materials. These types of surfaces will be referred to as engineering surfaces and in space are often found on metallic materials.

Directional reflectance is not appreciably affected by the surface roughness when the optical roughness is small, although the spatial distribution is strongly influenced (4). In this range diffraction is the predominant effect of the surface roughness. Therefore, a bi-directional reflectance model is required to predict the energy scatter from the reflecting surface.

Many bi-directional reflectance models have been developed and researched, but to date there is no proven model which can quantitatively

predict the energy scatter. The interaction of the electromagnetic waves with a material boundary is very complicated in the reflection process and requires a solution of a system of partial differential equations with the associated boundary conditions. The laws for reflectance from plane surfaces are well established and exact solutions can be obtained. The reflectance distribution is predictable for surfaces with certain specified regular geometric forms; however, for irregular or random surfaces a priori predictions are unknown and solutions are approximate.

Most of the models assume a perfectly conducting material and require a physical description of the surface topography. This usually requires a characteristic dimension of the height of the irregularities (surface roughness) and often a characteristic dimension of the peak-to-peak distance (peak density). The surface roughness is usually defined as the arithmetic average or, most often, the root-mean-square (rms) roughness. Two terms often used to indicate peak density are the rms slope of the roughness elements and the autocorrelation distance (5).

The normal technique used to determine the surface parameters is to take a sample of the material to be investigated and trace its surface profile with a profilometer. This is a laboratory technique and often is destructive (scratches) to the surface. Statistical surface roughnesses and peak density terms can be analytically determined from the profile tracings. Optical techniques have also been used to determine the surface parameters but are usually compared to the parameters determined using the profilometer tracings to substantiate the optical measurements. These techniques are non-destructive

and research data indicates that they may be more accurate in the roughness range investigated.

This brief background indicates the relative importance of reflectance and how it is normally handled. A closer look at individual efforts to investigate the phenomena of reflectance is appropriate.

Literature Survey

Beckmann and Spizzichino's text (5) contains a survey and analytical review of some of the models used to predict scattering of electromagnetic waves from rough surfaces. In this text, Beckmann also develops his bi-directional reflectance model, the model used in this research.

In 1964, prior to Beckmann's text, H. Davies published the development of his model for bi-directional reflectance (6). The Davies model is widely used and is quite similar to Beckmann's but has some significant differences. Both Davies and Beckmann consider a perfectly conducting material with a random roughness distributed according to the Gaussian distribution with standard deviation and the correlation distance T . Physically, T represents the rms slope of the surface profile. Interreflection and shadowing effects are neglected, and the analysis is limited to ratios of correlation distance to incident wavelength which are much greater than unity (5). The two models are derived from different forms of the Helmholtz integral and differ in that Davies treats only the limiting optical roughness cases of $\sigma/\lambda \ll 1$ and $\sigma/\lambda \gg 1$. The result is that the terms for the coherent portions of the reflected radiation are identical but the terms for the incoherent portions are different.

In 1961, H.E. Bennett and J.O. Porteus (7) used Davies' model to study the relationship between surface roughness and specular reflectance at near normal incidence. The wavelength of the incident energy was shortened until the optical roughness increased to the extent that most of the energy was scattered outside the specular region. Thus as σ/λ increased, the relative reflectance decreased from unity to smaller and smaller values.

They found that by using the coherent portion of Davies' model to predict the reflectance, the data was well fitted until a relative reflectance of 0.9 was reached. However, beyond a relative reflectance of 0.75 even the inclusion of the incoherent term did not make the predictions fit the data. Their conclusion was that the requirement that $\sigma/\lambda \ll 1$ was violated. They suggested that this optical technique could be used to accurately determine the surface roughness if radiation of sufficiently long wavelengths was used. Analysis and data were presented to substantiate this suggestion.

R. C. Birkebak (8), and R. C. Birkebak in conjunction with E. R. G. Eckert (9) also investigated the effects of roughness of metal surfaces on angular distribution of monochromatic reflected radiation and used Davies' model to analyze the data. Two groups of samples were studied; aluminum-coated ground glass and ground nickel. The optically measured roughnesses were larger by factors of 1.76 to 2.86 than the mechanically measured (profilometer) roughnesses. In both sample groups, the specular reflectance increased with increasing wavelengths of the incident radiation. Normalized reflectances showed decreasing reflectance with increasing roughness. This was to be expected; however, the relative reflectance ratios for

nickel surfaces were considerably smaller than for the aluminum-coated glass and this was unexplained. They postulated that the ground glass had a much higher peak density (scattering) term and that this may account for the difference (4). Limited correlation between Davies' model and the data was obtained.

K. F. Torrance and F. M. Sparrow (10, 11) not only researched bi-angular reflectance from randomly rough metals but also investigated nonmetals. They observed that reflectance from a roughened non-conductor followed the same trends as that from a conductor even though a difference in the reflection characteristics of conductors and non-conductors would be expected. That is, the reflection process for a metal (conductor) is essentially a surface phenomenon, while that for a nonmetal (non-conductor) involves both surface and internal reflections. About 90 per cent of the incident radiation in metals is reflected and that portion which is transmitted is quickly absorbed by the metal. In contrast, about 10 per cent of the incident radiation in nonmetals is reflected. That which is transmitted is internally scattered and ultimately a significant portion reflected back through the surface. Magnitudes of reflectance for the two types of material are not comparable. A polished non-conductor may have a specular reflectance of about 0.25, whereas the specular reflectance for a conductor may be near unity. This phenomenon is wavelength dependent and true only at the shorter wavelengths. In fact, at longer wavelengths the ratio of the specular reflectances becomes inverted.

Torrance and Sparrow (10) showed that for a non-conductor:

1. A given surface approaches a diffuse distribution at short wavelengths and a specular distribution at long wavelengths.

2. An increased surface roughness favors the more rapid approach toward diffuse characteristics at short wavelengths and conversely decreased surface roughness favors the more rapid approach toward specular conditions at long wavelengths.
3. The large off-specular reflectance is accented at short wavelengths and at a given wavelength the position of the off-specular peak moves to larger polar angles with increasing surface roughness.

These trends are the same as those for metallic surfaces. Points (1) and (2) are identical to those found by Birkebak (8) for metals. Thus, the qualitative effect of roughness on the bi-angular reflectance distributions is the same for electric conductors as for electric non-conductors (10). This tends to substantiate the effects of surface roughness on reflectance and gives confidence that other surface phenomena are not the controlling factors in this roughness range.

Torrance and Sparrow also found that the specular reflectance was not the limiting case. Their data demonstrated that off-specular peaks, three or four times as large as the specular peak, would occur in certain ranges of optical roughness for some angles of incidence. Some general trends they found for the off-specular peaks are:

1. For a given σ/λ the angular position of the off-specular peak moves to larger polar angles with increasing incident angle.
2. The magnitude of the reflectance at the off-specular peak relative to that in the specular direction increases with increasing angle of incidence. (This was true for angles $> 30^\circ$.)

3. The off-specular peak is accentuated at large values of σ/λ and generally decreases with decreasing σ/λ until at $\sigma/\lambda < 0.6$ it no longer appears.

Torrance and Sparrow concluded that at near normal incidence (angles less than 10°), the specular and diffuse reflections may be properly regarded as limiting cases for the angular distribution for the reflected radiation. For intermediate and large angles of incidence the limiting extreme of specular reflection is true, but the diffuse model of reflection does not represent a valid limiting case. They also believe that the shadowing effect due to the angle of incidence must be included in any theory on the cause of the off-specular peaks. The off-specular peak roughness range is not included in this investigation.

Comparative studies on Davies' Bi-Directional Reflectance Model and Beckmann's Bi-Directional Reflectance Model were made by R. G. Hering, A. F. Houchens and T. Smith (4). Radiant energy conservation was used to compare their ranges of applicability. That is, for a perfectly conducting material, all the incident energy must be reflected. The Davies and the Beckmann equations were numerically integrated over hemispherical space to obtain the directional reflectance. Davies' model was only valid for $\sigma/\lambda < 0.04$, which is almost optically smooth. Beckmann's model was still satisfying the energy conservation requirement at $\sigma/\lambda = 0.5$ where Hering terminated his calculations.

Hering found limited data to compare with Beckmann's model and emphasized that more measurements were necessary. He did perform further analysis for validity by comparing it to the data collected by Birkebak (8). The coherent component, which is the same in the

Beckmann and the Davies' model, has been adequately verified by many other investigators and was not re-addressed. In trying to verify the incoherent portion of Beckmann's model, Hering found that the surfaces did not have unique values for the correlation distance T . It was necessary to reduce the values of T for a given sample to make the computed values fit the distributions for larger values of σ/λ .

Comparisons of Birkebak's data from the aluminum samples versus the nickel samples showed that for nearly identical optical roughnesses the reflectance distributions were quite different. Therefore, the optical roughness by itself was not sufficient to characterize the spatial distribution of reflected energy and the significance of the peak density term (incoherent portion) was verified. A review of Torrance and Sparrow's data (10) indicates support of this conclusion.

Subsequently, T. F. Smith and R. G. Hering (12) made some specular bi-directional reflectance measurements for rough metallic samples with optical roughness values less than one. Their facility utilized a globar light source, coaxial rotary tables for angular positions, and a monochrometer for selecting the wavelength and collecting the energy. An optical technique was used to measure the surface parameters. The data (specular reflectance only) was then compared to Beckmann's model. They got correlation with test data to $\sigma/\lambda = 0.05$, by using the optical roughness portion of the model only. When the rms peak density term was added, correlation was obtained to $\sigma/\lambda = 0.2$. The theoretical analysis showed that for $\sigma/\lambda = 0.1$, the contribution of scattered energy to the specular reflectance was small but it increased rapidly until for $\sigma/\lambda = 0.2$ the scattered energy was nearly the sole contributor. Comparisons of the data with the predictions of

the model demonstrated that the model exhibited trends and characteristics similar to the measurements.

Dupree Maples (13) used Beckmann's model for a periodically roughened surface to investigate experimentally the electromagnetic scattering from a saw tooth surface profile. A profilometer was used to measure the roughness and the geometry of the surface profile was used to calculate the correlation distance. A photographic technique was used to record the scattered energy. It should be noted that energy was reflected from periodical surfaces in lobes versus a concentration around the specular direction for reflectances from a randomly rough surface. Maples concluded that the model predicted the approximate location of the reflected energy but that it did not predict the magnitude of the reflected energy.

J. E. Lochrlin, E. R. F. Winter and R. Vishanta (14) presented a photographic technique for measuring the angular distribution of energy reflected from surfaces. The technique utilized a sphere lined with film versus a cylinder used by D. Maples and J. A. Wiebelt (15). Measurements using this technique were made but the samples investigated were in the optical roughness range $\sigma/\lambda > 1.0$. Some of their data supported the occurrence of off-specular peaks as had been found by Torrance and Sparrow (11).

D. C. Look, Jr. and T. J. Love (15) suggested that a third in-surface parameter was necessary for an accurate description of the total reflected distribution. Not only must the roughness and the peak density be measured but a dimension in the plane of the surface that represents the portion of the surface that contributes to the regularly reflected (coherent) component. That is, a peak roundness

parameter or that part of the surface which is essentially flat. Their approach used a Monte Carlo technique in a digital computer program to investigate the action of energy bundles in the plane of incidence. Their model closely fitted the data of Birkebak (9), and Torrance and Sparrow (10). It did not fit the data of Herold and Edwards (17) and Francis (18) quite as well.

In summary, the literature surveyed showed the importance of the effect of surface roughness on reflectance. The theoretical solutions predicting reflectance were based on simplifying assumptions, and verification through experimentation had not been complete. Indications were that Beckmann's model for bi-directional reflectance might be applicable over a wider range of roughnesses than other models. Therefore, Beckmann's Bi-Directional Reflectance Model was selected to be examined experimentally to see if it would predict the scatter from randomly rough surfaces.

CHAPTER II

THEORETICAL ANALYSIS

Reflectance of electromagnetic waves from a smooth plane surface is very well understood. The laws have been well established and if the wavelength, angle of incidence and electrical properties of the material are known, the energy reflected can be quantitatively predicted. This is not true for irregular or roughened surfaces. Because the interaction of electromagnetic wave radiation with a rough surface is very complicated, mathematical solutions are usually not practical or feasible. Therefore exact solutions are not known and simplifying assumptions have to be made to get approximate solutions. A comprehensive review of many of the mathematical models used to describe reflectance from rough surfaces is given by P. Beckmann and A. Spizzichino (5). The various simplifying assumptions and the specific surfaces addressed are explained. Beckmann also presents a complete development of his Bi-Directional Reflectance model for randomly rough surfaces with optical roughnesses less than one. This model was used in the research for this dissertation.

In the general development of his model, Beckmann uses Kirchoff's approximation of the boundary conditions to evaluate the Helmholtz integral. The Helmholtz integral is developed by applying the Divergence Theorem to a bounded volume, substituting continuous scalar functions which satisfy the wave equation $\nabla^2 E + k^2 E = 0$, and thus

through manipulation obtaining Green's First Theorem, Green's Second Theorem and finally the Helmholtz integral for the field at a point.

$$E(P) = \frac{1}{4\pi} \iint_S \left(E \frac{\partial}{\partial n} \frac{e^{ikr}}{r} - \frac{e^{ikr}}{r} \frac{\partial E}{\partial n} \right) \partial S \quad (1)$$

The simplifying assumptions used by Beckmann to obtain numerically calculable solutions are:

1. The radius of curvature of the scattering elements is taken to be much greater than the wavelength of the incident radiation.
2. Shadowing effects are neglected.
3. Only the far field is calculated.
4. Multiple scattering is neglected.

The general solutions obtained for a scattering coefficient from one-dimensional (1-D) and two-dimensional (2-D) rough surfaces are shown below. The angles of incidence and reflection are shown in Figure 1.

$$\text{1-D} \quad \rho = \pm \sec \psi \frac{1 + \cos(\psi + \theta)}{\cos \psi + \cos \theta} \frac{1}{2L} \int_{-L}^L e^{iv \cdot r} dx + \frac{e^{\pm(L)}}{2L} \quad (2)$$

$$\text{where } e^{\pm(L)} = \frac{i \sec \psi \sin \psi}{k (\cos \psi + \cos \theta)} e^{iv \cdot r(x)} \Big|_{-L}^L$$

$$k = \frac{2\pi}{\lambda} \quad v \cdot r = \frac{2\pi}{\lambda} [(\sin \psi - \sin \theta)x - (\cos \psi + \cos \theta)\zeta(x)]$$

$$\begin{aligned} \text{2-D} \quad \rho &= \frac{1 + \cos \psi \cos \theta - \sin \psi \sin \theta \cos \Phi}{\cos \psi (\cos \psi + \cos \theta)} \frac{1}{A} \int_{-X}^X \int_{-L}^L e^{iv \cdot r} dx dy \\ &+ \frac{e(x,y)}{A} \end{aligned} \quad (3)$$

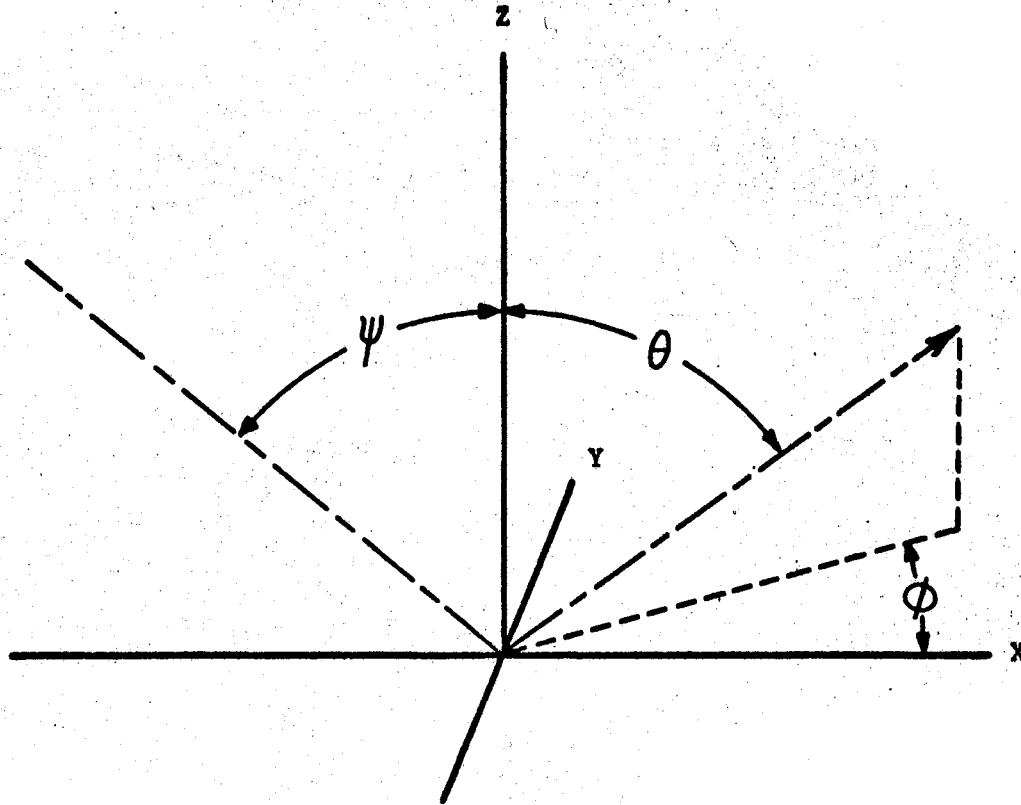


Figure 1. Angle of Incidence and Reflection

The scattering coefficient is defined as $\rho = E_2/E_{20}$, where E_{20} is the field reflected in the direction of specular reflection ($\psi = \theta$) by a smooth, perfectly conducting plane of the same dimensions under the same angle of incidence, and E_2 is the field reflected from the rough surface to the point of observation.

Beckmann develops the general solution to apply to periodic and randomly rough surfaces, where a randomly rough surface is defined as one that would be generated by a continuous stationary random process and thus a normally distributed surface. Two statistical functions are

used to describe the surface, the rms roughness (σ) and the correlation distance (T). The correlation distance is defined as the distance in which the autocorrelation coefficient $C(\tau)$ drops to the value e^{-1} . τ is the separation parameter ($\tau = x_1 - x_2$). Beckmann shows that it is sufficient to define this autocorrelation coefficient as:

$$C(\tau) = e^{-\frac{\tau^2}{T^2}}$$

Beckmann observes that ρ is a complex quantity and its mean value is of little use except as a stepping stone to determine the mean value of the complex conjugate quantity:

$$\langle \rho \rho^* \rangle = \left\langle \left| \frac{E_a}{E_{a0}} \right|^2 \right\rangle.$$

The asterisk, $*$, denotes the complex conjugate, $\langle \rangle$ means mean value, and $| \ |$ means absolute value. $\langle \rho \rho^* \rangle$ is proportional to the mean scattered power and is represented by:

$$\begin{aligned} \text{1-D } \langle \rho \rho^* \rangle &= \exp \left[-\frac{4\pi^2 \sigma^2}{\lambda^2} (\cos \psi + \cos \theta)^2 \right] \rho_0^2 & (4) \\ &+ \exp \left[-\frac{4\pi^2 \sigma^2}{\lambda^2} (\cos \psi + \cos \theta)^2 \right] \times \\ &\left[\frac{\sqrt{\pi} T}{2 L} \left(\sec \psi \frac{1 + \cos(\psi + \theta)}{\cos \psi + \cos \theta} \right)^2 \right] \\ &\sum_{m=1}^{\infty} \frac{\left[\frac{4\pi^2 \sigma^2}{\lambda^2} (\cos \psi + \cos \theta)^2 \right]^m}{m! m} \times \\ &\exp \left[-\frac{T^2}{4m} \left(\frac{2\pi}{\lambda} \right)^2 \left(\sin^2 \psi + 2 \sin \psi \sin \theta + \sin^2 \theta \right) \right] \end{aligned}$$

$$\begin{aligned}
2-D \quad \langle \rho \rho^* \rangle &= \exp \left[-\frac{4\pi^2 \sigma^2}{\lambda^2} (\cos \psi + \cos \theta)^2 \right] \rho_0^2 \quad (5) \\
&+ \exp \left[-\frac{4\pi^2 \sigma^2}{\lambda^2} (\cos \psi + \cos \theta)^2 \right] \times \\
&\left[\frac{\pi \Gamma^2}{A} \left(\frac{1 + \cos \psi \cos \theta - \sin \psi \sin \theta \cos \Phi}{\cos \psi [\cos \psi + \cos \theta]} \right)^2 \right] \\
&\cdot \sum_{m=1}^{\infty} \frac{\left[\frac{4\pi^2 \sigma^2}{\lambda^2} (\cos \psi + \cos \theta)^2 \right]^m}{m! m} \times \\
&\exp \left[-\frac{\Gamma^2 \pi^2}{m \lambda^2} (\sin^2 \psi - 2 \sin \psi \sin \theta \cos \Phi + \sin^2 \theta) \right]
\end{aligned}$$

The 2-D equation was used in the scatter experiment.

It should be noted that the solutions consist of two terms:

$$\rho = \text{coherent term} + \text{incoherent term.}$$

The coherent term is for that portion of the reflected energy which has not been scattered but reflected as if from an optically smooth surface. The incoherent term is for that portion of the energy which has been scattered.

The mean power reflection coefficient of a surface of illuminated area A was found to be:

$$\bar{P} = \frac{\text{Power Out}}{\text{Power In}} = \langle \rho \rho^* \rangle |E_{20}|^2 \quad (6)$$

$$\text{where } |E_{20}|^2 = \frac{A^2 \cos^2 \theta}{\lambda^2 \rho^2}$$

This equation was used in optically determining the surface parameters.

The simplifying assumption that the material is a perfect conductor must be accounted for in any experimental set-up, as real materials have finite conductivity. Bennett and Porteus (7) and Beckmann (5) suggest that the scatter coefficient for finite conductivity can be represented by multiplying the scatter coefficient for

infinite conductivity by the bi-directional reflectance of the actual material with an optically smooth surface. This in effect normalizes the rough sample reading by the specular reading from a smooth sample. This will not rigorously account for the finite conductivity but should generally account for its effect and also tend to minimize any other surface parameters that are characteristic to the sample material. Normalizing approaches were used in setting up the experiments.

CHAPTER III

EXPERIMENTAL DEVELOPMENT AND APPARATUS

An essential preliminary part of the experimental development was to determine the type of surfaces to be investigated, to determine how to manufacture the samples, and to ascertain that the finished samples did indeed have the desired surface characteristics.

It was decided that the surface roughness parameters required in Beckmann's model should be measured optically and that the equations used to obtain these characteristics from the experimental data should be Beckmann's equations. Optical parameters should be more accurate and when determined by using Beckmann's equations should be more compatible to and make Beckmann's Bi-Directional Reflectance Model more accurate. This should give the best opportunity to evaluate the applicability of using Beckmann's model to predict the scatter pattern. Therefore, experimental development evolved into three areas: (1) selection, preparation and conformation of samples, (2) an optical experiment to determine surface characteristics, and (3) a bi-directional reflectance experiment to determine the scatter patterns.

Sample Selection and Preparation

The types of engineering surfaces one would encounter in space applications are generally metallic materials whose rms roughnesses range from 0.25 to 1.0 micron for normal machining, grinding, and

polishing techniques (4). Many machined surfaces have preferential directions where all the ridges and valleys run parallel to each other, such as the ridges on the surface of a board after it has been planed. Therefore, samples were made which have a variable random roughness in the X direction only (1-D). Not all finishing or manufacturing techniques leave preferential directions or paths in the surface, but the roughness is random in whatever direction it is measured. This is considered a limiting case for engineering type surfaces and therefore, a sample was made with variable roughness in the X and Y directions (2-D). A randomly rough surface was assumed to be an isotropic Gaussian surface. Schematics of the samples are shown in Figure 2.

SAMPLE SCHEMATICS

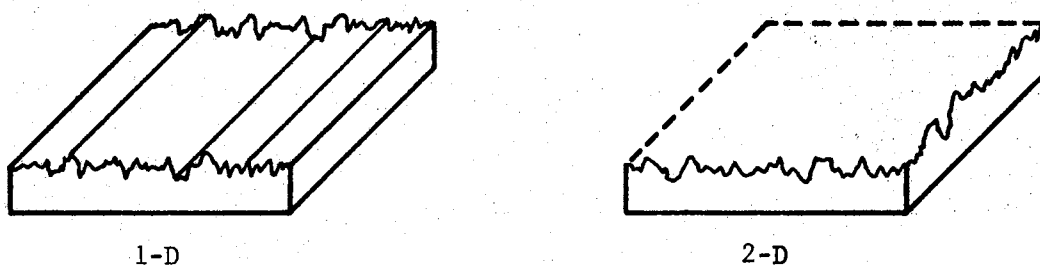


Figure 2. Sample Schematics

Selection of the metal to be used required consideration of electrical properties of the material and the susceptibility of the

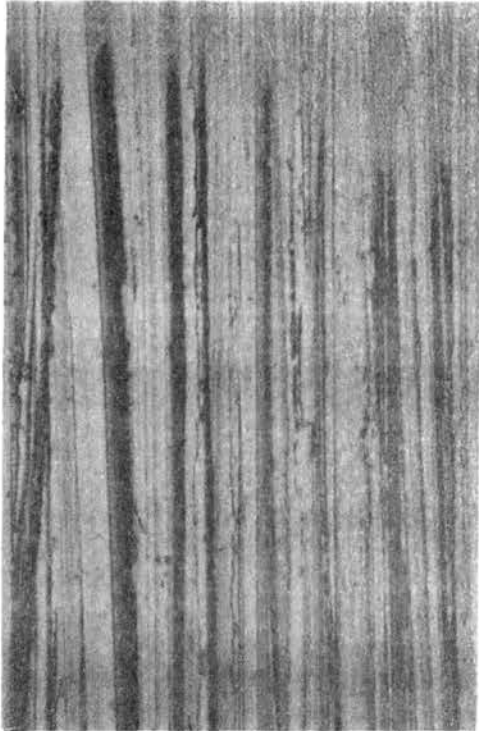
material to surface damage and contamination; though, as previously stated, these effects can be minimized by normalizing the reflectances. It is still desirable that these effects be further minimized as much as possible by having the intrinsic properties match those of the theory as closely as possible.

A 99.999% pure nickel was selected as the metal for the test samples because it was a good conductor and not susceptible to contamination by oxidation. An additional benefit from using nickel was that others have done bi-directional reflectance research on roughened nickel samples and thus, this research would provide comparable sets of data and enlarge the technical base.

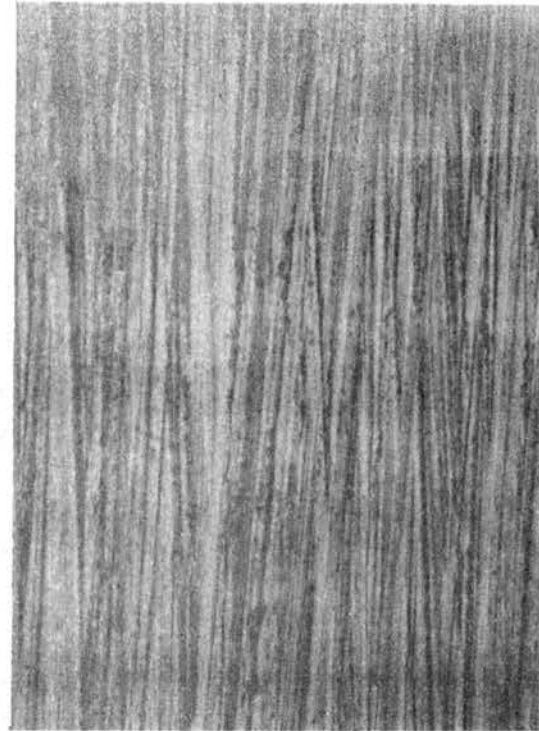
Several techniques were investigated to see what methods could be used to manufacture 1-D and 2-D randomly rough surfaces. Etching, sandblasting and electron bombardment were seriously considered. These methods could not produce 1-D samples and appeared to give a more uniformly rough rather than a randomly rough 2-D surface. Quantitative tests were run on the manufacturing techniques used.

The nickel samples of 3/4" diameter by 1/4" thick were mounted in 1 $\frac{1}{4}$ " diameter phenolic blocks. They were polished by standard polishing techniques and then roughened. The 1-D samples were carefully drawn in one direction across emery paper. Sample 1 used a 240 grit emery paper whose grit was approximately 0.5 micron diameter. Sample 2 used a 400 grit emery paper whose grit was approximately 0.375 micron diameter. Photomicrographs of Samples 1 and 2 with 500x magnification are shown in Figure 3.

The 2-D sample was placed in a 12-inch diameter SYNTRON vibramet for 60 minutes with a water and 320 carbonite grit solution. A 320



Sample 1



Sample 2

Figure 3. Photomicrographs of 1-D Samples



Sample 3

Figure 4. Photomicrograph of 2-D Sample

grit is approximately 0.44 micron diameter. Preliminary test runs of 15, 30, 60, and 120 minutes were made using the 320 grit, and the 60 minute run was found to give the best surface. A photomicrograph of Sample 3 with 500x magnification is shown in Figure 4.

Confirmation of Sample Surfaces

The surface characteristics of the samples were examined to confirm that the samples were truly 1-D and 2-D randomly rough surfaces and would also subsequently be used to provide a comparison to the optically measured surface parameters. This examination was based on surface profile traces made at Wright-Patterson Air Force Base on a Bendix Micrometrical Proficorder using a stylus of 0.0005 inch diameter. A tracing is not expected to give an exact copy of the surface because the finite size of the stylus prohibits it from following the contour to the bottoms of all the valleys. Figure 5 is a typical section of the traces obtained.

PROFICORDER TRACING

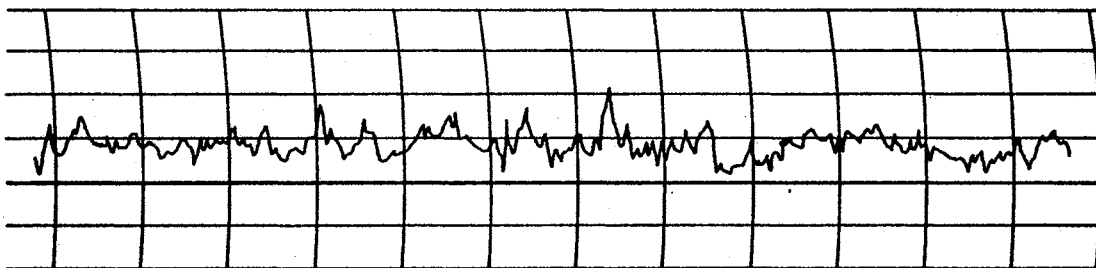


Figure 5. Proficorder Tracing

The tracings were digitized to provide statistical data for analysis to determine the degree of confidence that the surfaces were truly randomly rough. The tracings are sampled at equal intervals. This sampling distance (Δx) had to be sufficiently small so that the location of each peak and valley would be recorded as this data contains 90% of the statistical information. Thus a minimum criterion was established that Δx not exceed the half cycle of the highest frequency contained in the tracings. A $\Delta x = 0.1$ inch was selected. A schematic of the digitizer apparatus is shown in Figure 6.

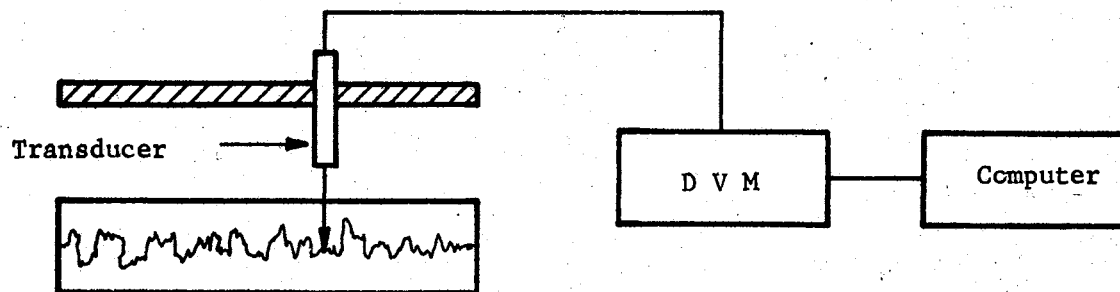


Figure 6. Schematic of Proficorder Tracing Digitizer

A linear transducer was mounted on a geared screw. The stylus of the transducer was moved on the tracing and the transducer output was recorded through a digital voltmeter which was interfaced to a paper tape punch. This output was correlated to the height scale on the tracing. The transducer output was checked and found linear over the range of displacements needed to cover the tracing. Several sets of

data were rerun to determine reproducibility of the transducer readings. It was found that the readings varied only 2.3 per cent about the mean value for the point, indicating a maximum deviation of less than 5 per cent.

The geared screw gave positive control of the Δx needed to give an equal interval sample of the surface. The transducer was advanced in only one direction to keep any play in the gear train from affecting the Δx . Samples of 500 points were obtained and three separate samples were taken from each tracing. Taking separate sections from each sample gave an estimate of the uniformity of the roughness over the entire surface of the sample. The rms roughnesses over the three areas did not vary more than 5 per cent.

Chi-Square distributions were calculated from this data and it was found that within a 95 per cent confidence factor the samples came from a random surface. This is shown more graphically when the cumulative percentages are plotted at the corresponding class boundaries on arithmetic probability graph paper, Figures 7, 8, and 9. The units on the abscissa are arbitrary and used only to establish class boundaries. They are related to the voltage output of the transducer. The probability scale was so designed that any cumulative normal distribution would graph as a straight line.

This digitized data was also used to calculate correlation distances. A Control Data Corporation autocorrelation coefficient subroutine was modified to give the correlation distance. The subroutine was designed to calculate the autocorrelation coefficient for a sequence of time-dependent observations that oscillate or fluctuate about a constant mean. Distance on the tracings is equivalent

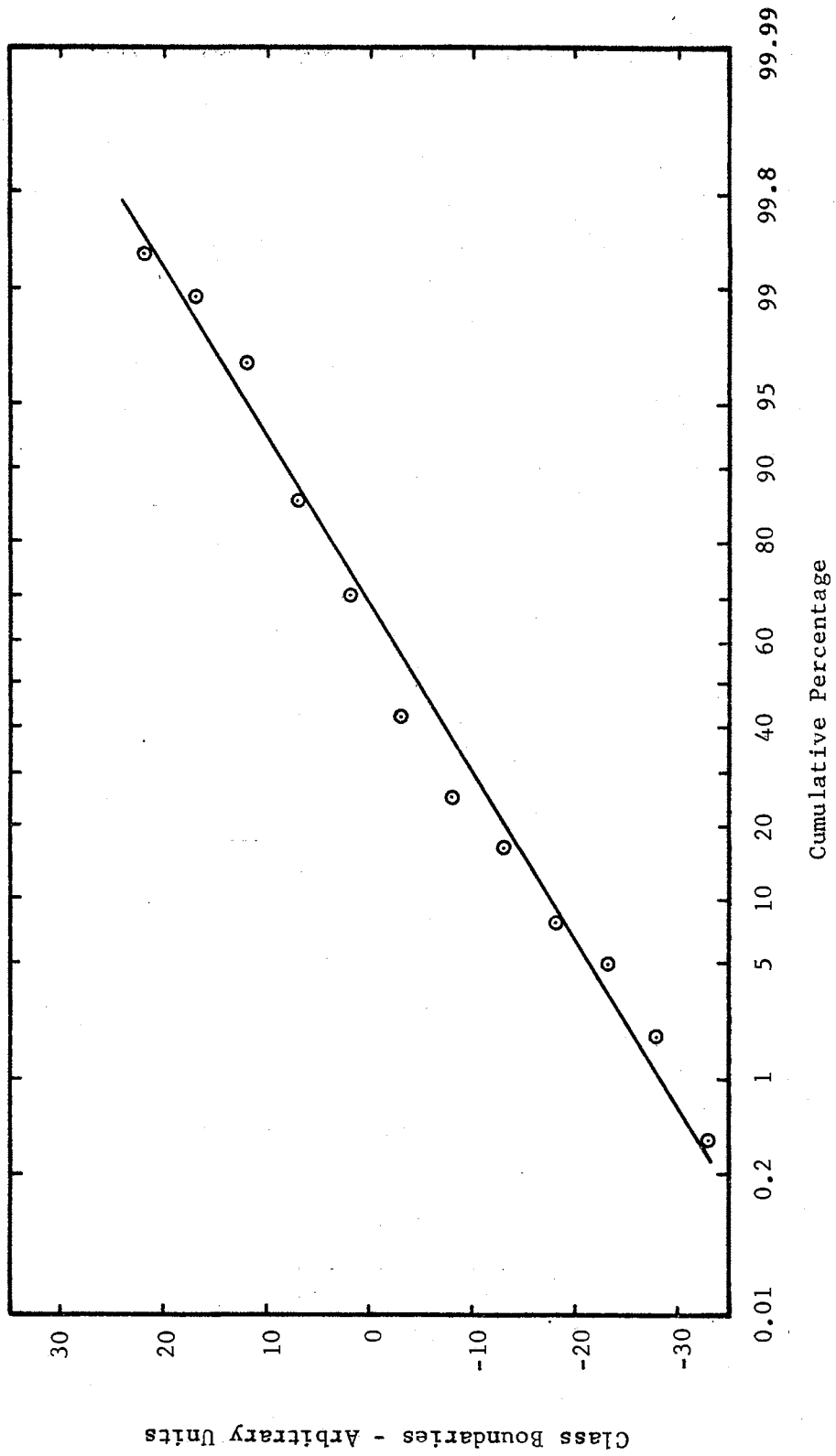


Figure 7. Normal Probability Graph Sample 1

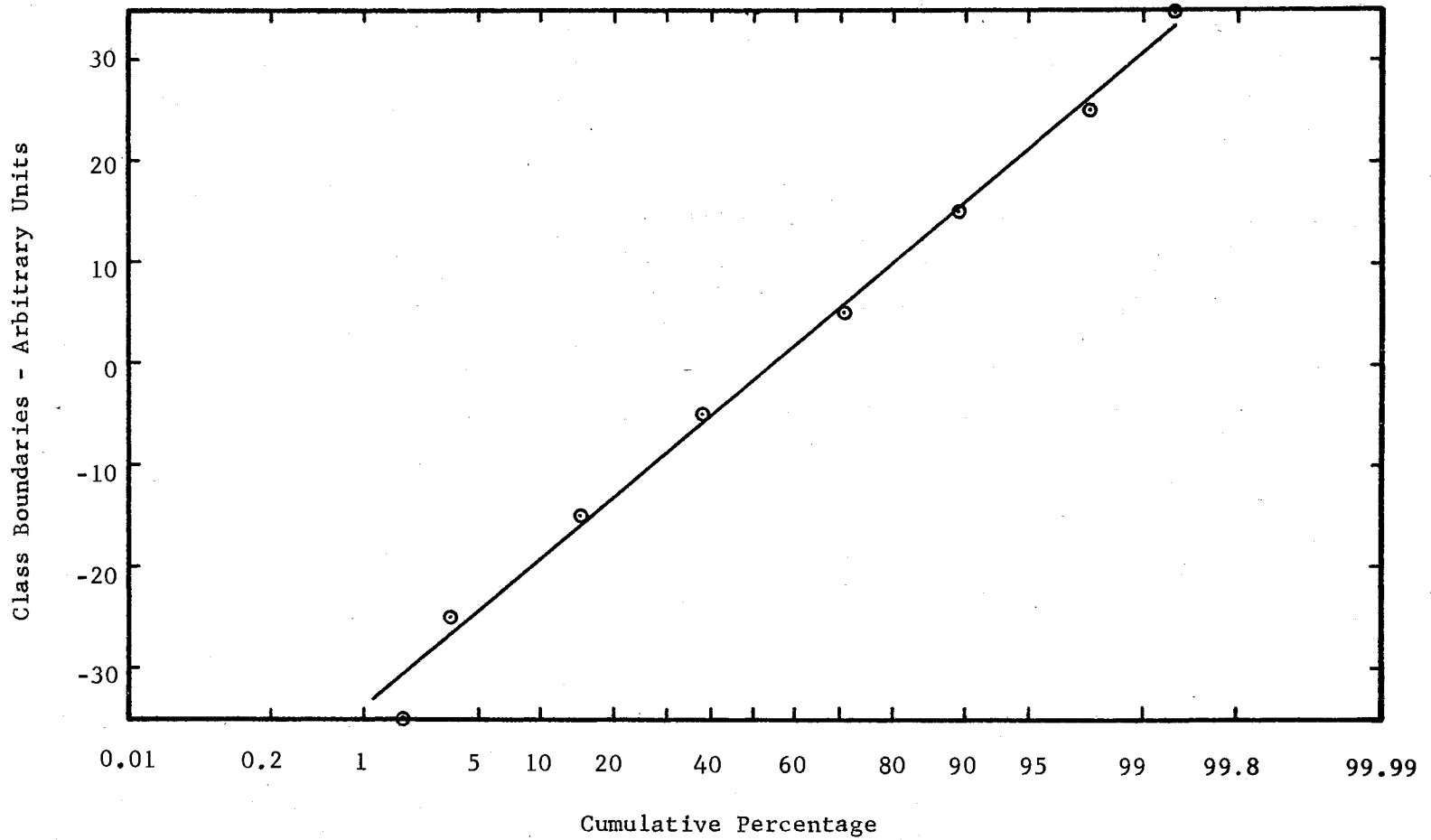


Figure 8. Normal Probability Graph Sample 2

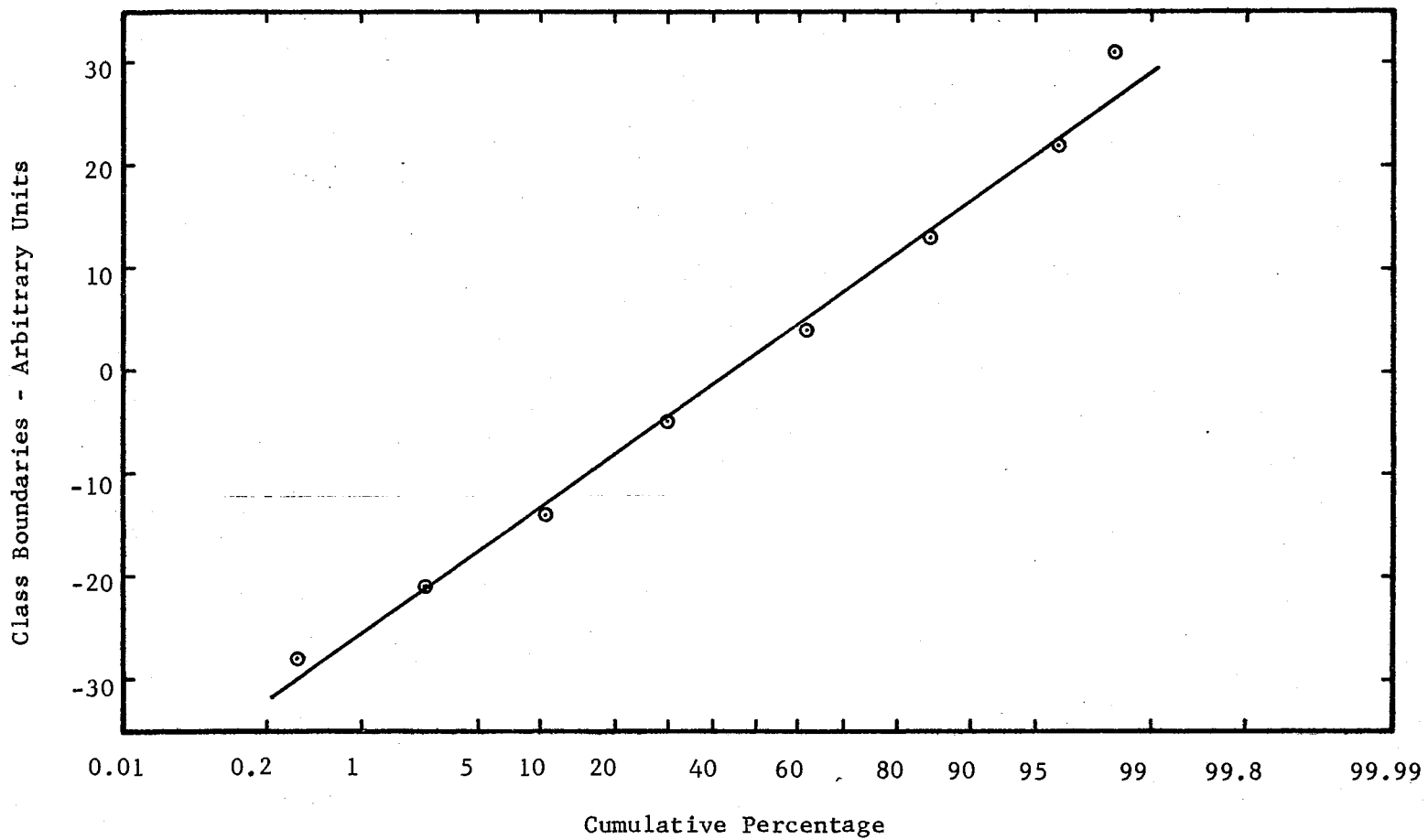


Figure 9. Normal Probability Graph Sample 3

to a time function in the subroutine. The subroutine required equally-spaced time points (distance points) which, as previously described, were used. These correlation distances are presented in Table II, Chapter V.

It can be concluded from the above data that these selected samples have the desired surface characteristics and are 1-D and 2-D randomly rough surfaces. Therefore, experiments using these samples can be designed with confidence that any anomalies in the data will not be the effects of anomalies in the surfaces.

Optical Surface Characteristics

The experimental set-up used to optically determine the surface parameters of rms roughness and correlation distance is illustrated in Figure 10. The solid line represents the ray path through the apparatus. The broken line indicates this is no longer a ray path but the flow line for obtaining the data. As indicated by the ray line, only specular reflectance data was required and these measurements were taken at various wavelengths from first a smooth sample and then a rough sample. All other variables were held constant.

This set-up provided extremely fine resolution of the energy reflected into the specular direction because the thermocouple detector is only 0.2×2 millimeters. Thus the solid angle contained between the surface of the sample and the reflector can be neglected and the energy can be considered to be recorded at a point. This fine resolution feature is very important for the optical roughness ranges investigated where much of the energy is specularly reflected. This resolution was verified in that slight misalignment of the thermocouple

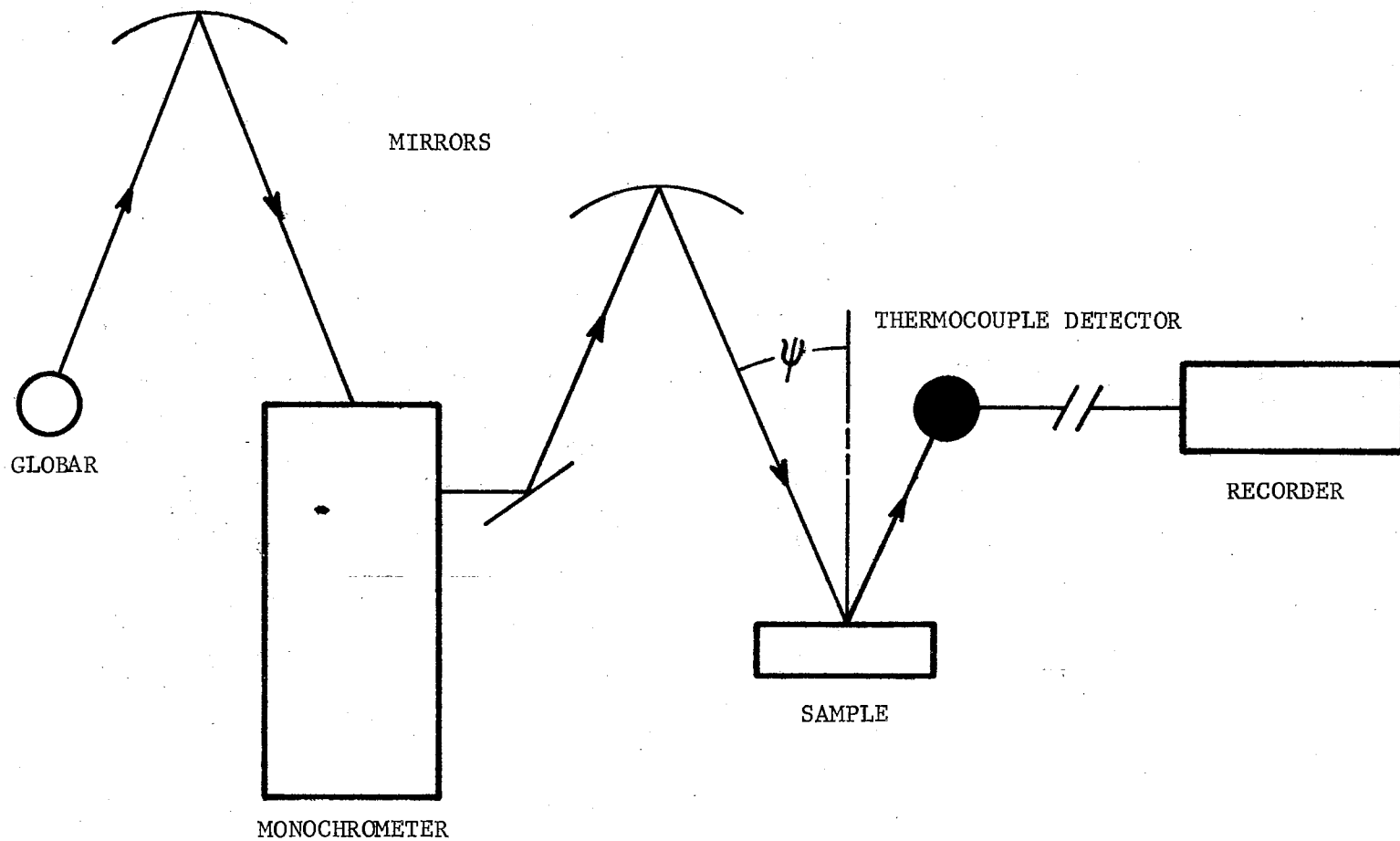


Figure 10. Schematic of Surface Characteristics Experiment

would greatly affect its output. To insure proper alignment the system was optically aligned using a laser beam.

Beckmann's mean power reflection coefficient, "Power Out" versus "Power In", Equation 6, Chapter II, was modified to model this experimental set-up. Modification was required to account for use of a spherical wave instead of the theoretical plane wave. The spherical wave propagation in the experiment is illustrated in Figure 11.

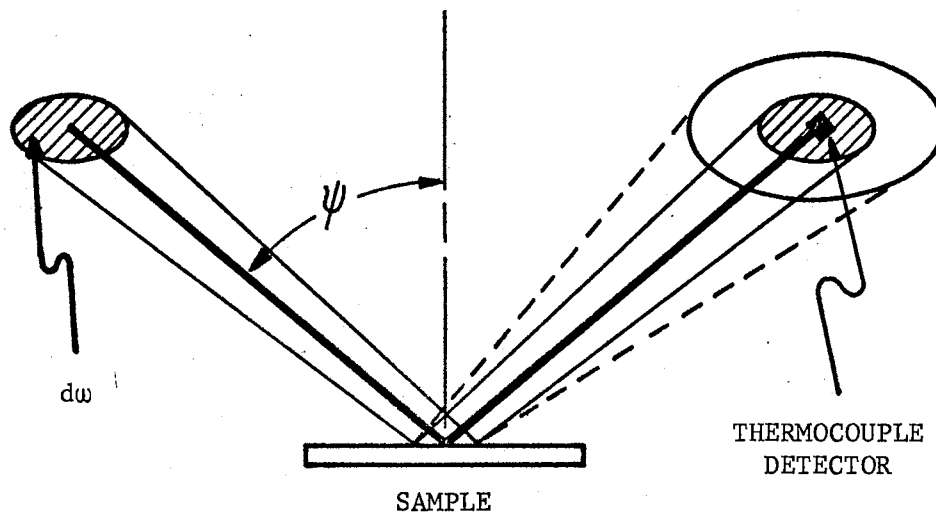


Figure 11. Wave Propagation

When the specular reflectance from the smooth sample (S_1) was taken, the thermocouple detector was recording the thin pencil of rays contained in the detector's surface area as illustrated by the solid ray line in Figure 11. This in effect was a measurement of the incoming intensity because this signal was not affected by the size of

the illuminated area of the incident energy being spherical waves instead of plane waves. The finite conductivity factor of the nickel (C) did affect this signal. The signal S_1 can be considered the "Power In" term and can be represented by:

$$S_1 = CI \quad I = \text{Incoming intensity} \quad (7)$$

When the specular reflectance from the rough sample (S_2) was taken, the thermocouple was recording the "Power Out". If the incident energy were a plane wave, Beckmann's scattered power equation would be:

$$Q = CI \langle \rho \rho^* \rangle |E_{20}|^2 \quad (8)$$

and would apply directly to S_2 . However, the sample was illuminated with a spherical wave and the "Power Out" had to be modified to account for this. A modification for the spherical waves effect on the incoherent portion of the energy can be represented by $\cos \psi d\omega$, where $d\omega$ is the incoming solid angle (3). Thus the signal from the rough sample is represented by:

$$S_2 = CI \cos \psi d\omega \langle \rho \rho^* \rangle |E_{20}|^2 \quad (9)$$

Thus the mean power reflection coefficient for this experimental set-up is:

$$\begin{aligned} P &= \frac{\text{Power Out}}{\text{Power In}} = \frac{S_2}{S_1} = \frac{CI \cos \psi d\omega \langle \rho \rho^* \rangle |E_{20}|^2}{CI} \\ &= \cos \psi d\omega \langle \rho \rho^* \rangle |E_{20}|^2 \end{aligned} \quad (10)$$

It should be noted that the modifiers to $\langle \rho \rho^* \rangle$ affect only the incoherent portion of the reflected energy. Thus P can be shown as:

$$P = \text{coherent} + \text{incoherent} (\cos \psi d\omega) (|E_{20}|^2) \quad (11)$$

At the longer wavelengths, where P almost equals one, only the coherent term is contained in P. The coherent term is a function of the rms roughness only. Using the method suggested by H. E. Bennett

and J. O. Porteus (7) the rms roughness was determined by plotting the specular reflectance ratios for the longer wavelengths on semilog paper. The resultant slope is directly proportional to the rms roughness squared (σ^2). The equation plotted is:

$$\ln P = \sigma^2 [4\pi^2 (\cos \psi + \cos \theta)^2] \left[\frac{1}{\lambda^2} \right] \quad (12)$$

At the shorter wavelengths coherent and incoherent light contributes to the specular reflectance from the rough samples and both surface parameters are coupled in P. However, since σ has already been determined it is substituted into P, Equation 10, and T is calculated.

One other factor must be considered which modifies the $\langle \rho\rho^* \rangle$ equations used in the 1-D experiments. That is, Beckmann's one dimensional general solution is for an illuminated infinite strip, whereas in the experiments only a finite area is illuminated. The basic Helmholtz Integral and Maxwell boundary conditions apply to both the one and two-dimensional theoretical developments. Only the limits of integration were affected by using a finite area instead of an infinite strip. Therefore it was assumed that the two-dimensional model of $\langle \rho\rho^* \rangle$ developed for a finite illuminated area might apply to the one-dimensional experiments where only a finite area could be illuminated. Therefore, the 2-D model was used in all the analysis of the 1-D data.

Surface Characteristics Apparatus

Light Source, Mirrors and Apertures

A global light source was used. It was masked until its focused image was fully contained on the reflecting sample. Two unmasked

spherical mirrors were used with the incoming solid angle to the sample limited to 0.0795 steradian by an aperture. The sample's illuminated area was 0.0995 inch wide and 0.439 inch long or an area of 27.3×10^8 square microns.

Monochromator

A Perkin-Elmer Model 99 double pass monochromator with a sodium chloride (NaCl) prism was used to select the monochromatic wavelength of light desired for each set of readings. The theoretical relationship between the number of turns on the monochromator dial for the wavelength of the (NaCl) prism was plotted on a wavelength calibration graph and used to correlate the dial reading to the output wavelength. It should be noted that the complete globar image was focused to just fill the monochromator entrance slit.

Sample Holder

The sample holder was designed and fabricated at Oklahoma State University. It was firmly bolted to the optics table and each sample securely held in place by an internal steel spring. The plane of the surface of the sample was controlled by three screws equilaterally located on the back of the sample receptacle. Once the sample holder was oriented, the smooth and rough samples could be repeatedly interchanged without disturbing the optical alignment.

No provision was built into the sample holder to orient the grooves at a particular angle. Since the energy was collected at the specular reflectance point, rotation of the sample should not affect this reading. Such an experiment was run and this was found to be the case.

Thermocouple

A Perkin-Elmer thermocouple for the model 99 monochromator was used to record the energy reflected in the specular direction. It had a cesium-bromide (CsBr) window and a target area of 0.2×2 millimeters. An experiment was run to see if there was interreflection within the thermocouple that would affect the output and thus the effective target area. Interreflections did not affect the output. Optical alignment of the thermocouple was critical and required careful manipulation. The thermocouple was aligned by monitoring the output of the thermocouple on the recording device. When the maximum output was obtained, the thermocouple was on the specular angle and was firmly secured.

Recorder

The Perkin-Elmer monochromator recorder was used. Calibration and background noise checks were made. The chopped incoming signal gave a steady output which was recorded manually. Consistency of the input signal was continually checked. First the smooth sample reading for a given wavelength of light was taken. The rough sample was then inserted and its reading was recorded. Prior to selecting the next wavelength of light, the smooth sample was reinserted and the recorded signal compared to the first reading. These readings did not vary more than 2 per cent.

Bi-Directional Reflectances

A photographic technique was chosen to record the scattered energy because it established an instantaneous permanent record and it was easy

to obtain a maximum number of data points from the film. Other techniques required large numbers of readings and thus much equipment manipulation over an extended period of time. In such an apparatus only a very limited number of data points could be obtained from the infinite number available in the spread of the energy.

Schematics of the photoreflectometer system used is shown in Figure 12. The upper schematic is a side view which shows the ray path of the laser beam through the different pieces of apparatus. The lower schematic, a top view, illustrates how the laser beam is scattered onto the film-lined cylinder by the roughened sample. The break in the solid line from the camera indicates a change from the ray path to a flow line representing the sequence of equipment needed to extract the data from the film for use on a computer.

The cylindrical camera gave an undistorted record in the plane of incidence. For the 1-D samples all the energy was contained in the plane of incidence; for the 2-D sample the information contained in the plane of incidence was considered indicative of the bi-directional reflectance. The microdensitometer system recorded the average energy deposited on small incremental areas of the film along the spread of the energy in the plane of incidence. The energy recorded in the specular direction was used to normalize the other readings and, as previously mentioned, accounted for the finite conductivity of the samples.

The use of the digital computer was required because of the quantities of the bi-directional reflectance data and the large number of theoretical calculations. Therefore a digital voltmeter (DVM) coupled to a paper tape punch was used to digitize the microdensitometer signal.

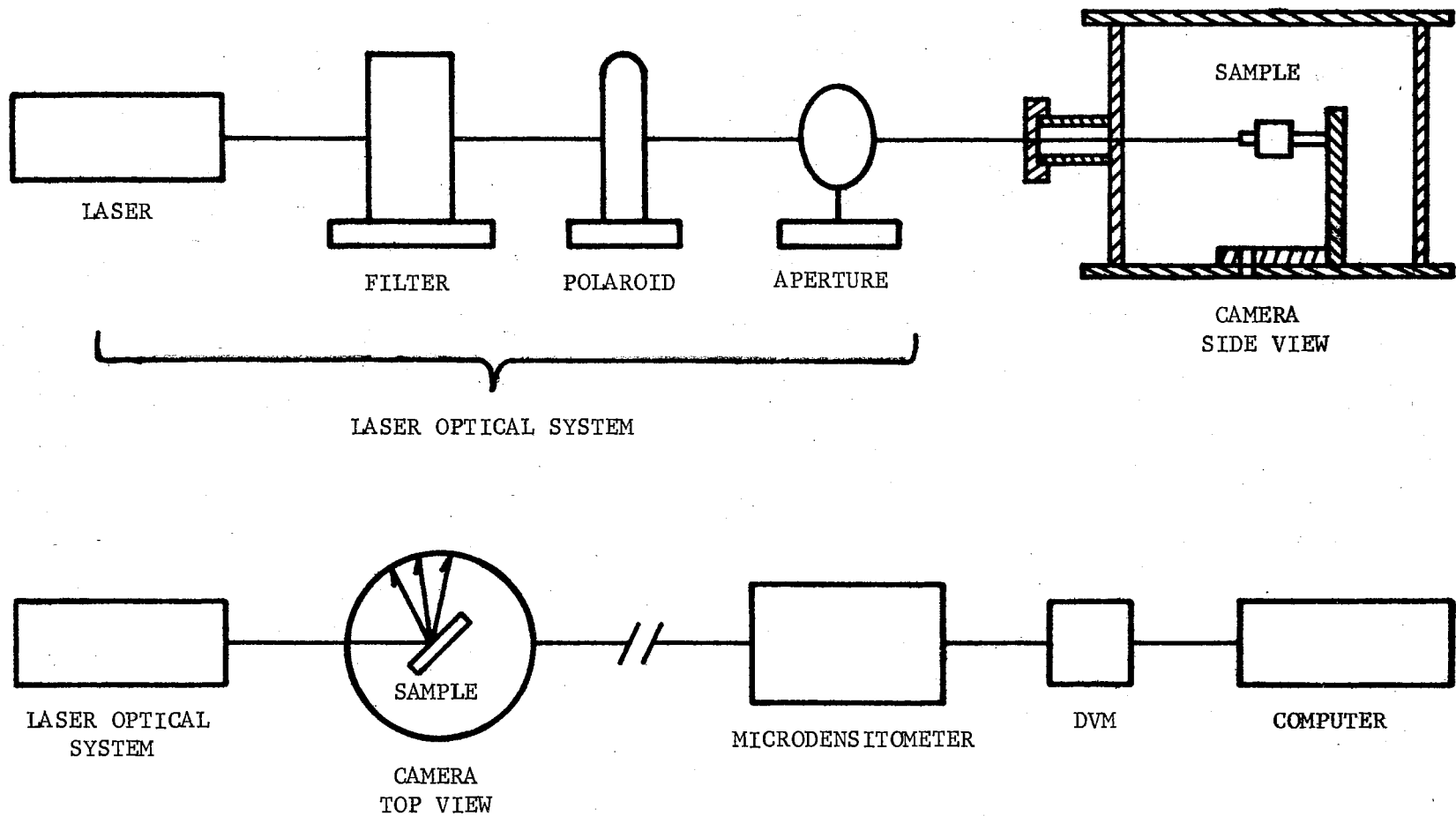


Figure 12. Schematics of Bi-Directional Reflectance Experiment

The experimental set-up was modeled by using Beckmann's scattering coefficient equation, Equation 5, Chapter II. Experimental and theoretical results were compared by use of a Fortran IV digital computer program.

Since the laser beam was essentially a plane wave, no modifiers for spherical waves were needed in this case. Additionally the terms needed to change the electric field equations to power equations canceled each other because a normalized reflectance (\bar{R}) was used. Thus Beckmann's scattering coefficient equation is all that was required and the resultant normalized reflectance was:

$$\bar{R} = \frac{\text{Signal Off-Specular}}{\text{Signal Specular}} = \frac{\langle \rho\rho^* \rangle \text{ Off-Specular}}{\langle \rho\rho^* \rangle \text{ Specular}} \quad (13)$$

Bi-Directional Reflectance Apparatus

Laser

A model 130B Spectra-Physics helium-neon gas laser was used to provide the monochromatic, plane polarized light source. The laser was operated at 0.6328 micron wavelength. The output of the laser increased for approximately 20 minutes after start-up and then stabilized. Therefore a warm-up time of 30 minutes was allowed. Amplitude stability, peak to peak, then varied less than 3 per cent over a five minute interval.

Filters

A Jarrell-Ash Co. (JACO) seven-step filter was used to calibrate each film strip. The transmissibility of the filter was determined in the laboratory using the laser light source. The laser beam was

focused so that it was completely contained within each step of the filter. The energy transmitted was recorded by the thermocouple. This data is presented in Table I.

TABLE I
FILTER CALIBRATION DATA

Step No.	Transmitted Light
1	1.000
2	0.646
3	0.421
4	0.272
5	0.185
6	0.129
7	0.094

It was found that the filter distorted the shape of the laser beam. This did not affect the calibration of the film but this could have affected the scatter pattern. Therefore after the calibration of each film strip, the filter was removed from the system before the sample was irradiated.

Polaroids

Two polaroid discs were used to control the amount of energy input to the camera. The amount of energy needed to expose the film for the scatter patterns was much larger than that required to calibrate the film because a much larger area needed to be exposed. The angle of incidence also affected the energy requirement. The larger the angle, the less the scatter and therefore the less area exposed and the less energy required. Experiments were run to obtain the multiple settings necessary to properly expose and calibrate the different strips of the film.

Aperture

An aperture was used to eliminate secondary reflections from the polaroids and the filter. It was adjusted to just pass, untouched, the complete laser beam and was located in front of the shutter.

Camera

The camera consisted of a shutter and an 8-inch diameter cylinder lined with film. It should be noted that the sample was mounted internal to and on the center line of the camera. The shutter speed was set at 1/200 second. The film was held firmly in place against the sides of the cylinder by a steel spring. A separate strip of film was required for each angle of incidence for each sample. Each strip of film was exposed eight separate times to obtain the seven calibration points and the scatter pattern. The camera was opened and the film repositioned for each exposure. Therefore, the experiments were run under

total darkness. Because of the multiple exposures, experiments were run to see if there was any interreflections. No interreflections were detected for the power settings used.

Film Processing

The exposed Kodak Tri-X Pan Sheet Film (ESTAR Thick Base) was immediately processed upon its removal from the camera. The film was continuously agitated for 3 minutes in a tray filled with Kodak DK-50 developer at 75°F, rinsed for 15 seconds in Kodak Indicator Stop Bath, fixed for 5 minutes in Kodak Rapid Fixer, and then washed for 30 minutes in running water at 75°F.

Sample Holder

The sample holder allowed six-degree-of-freedom control over positioning of the sample. The sample was placed in the holder and its surface aligned with the centerline of the cylinder. The laser beam was directed through the shutter onto the sample. The sample was adjusted until the beam was reflected back upon itself. This positioned the surface of the sample perpendicular to the incident beam. A graduated strip, inscribed with the angles, was centered at the shutter opening and extended along the cylinder wall. The sample holder was rotated about the centerline until the ray of light was focused on the desired specular angle. The sample holder was then secured, dark room conditions obtained, and the camera loaded with film. The angles were incrementally set at 0, 10, 15, 30, 45, 60, 75° for the 1-D samples, and 5, 15, 30, 45, 60, and 75° for the 2-D sample.

Microdensitometer

A Jarrell-Ash Model JA200, direct-reading microdensitometer was used to measure the energy deposited on the film. The slit opening of the densitometer was set at 0.5 millimeter height and 50 microns width. Linearity of the densitometer was checked using polaroids. The cosine of the cross angle of the polaroids squared gave the per cent of the signal which would pass through the polaroids. This comparison was made and the results shown in Figure 13.

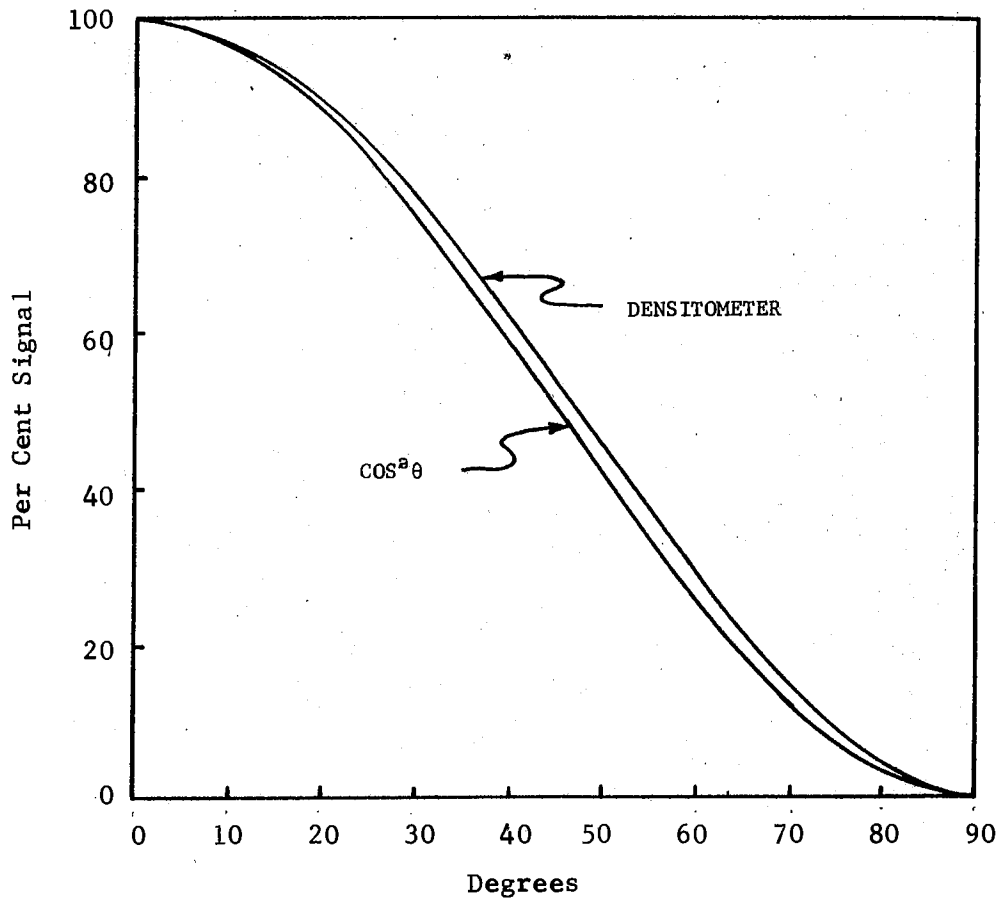


Figure 13. Densitometer Linearity Graph

The drive mechanism of the densitometer was connected to a constant speed, 5 RPM, AC motor. The exposed film was then moved across the photocell field and the photocell output was recorded by a digital voltmeter. The response time of the densitometer was checked to see if the traverse speed would affect the output. Readings using the 5 RPM motor compared within 5 per cent to those obtained using a 1 RPM motor. This deviation alternated plus and minus and confirmed that the photocell output was not affected by the traverse speed used.

Digital Voltmeter

The digital voltmeter was interfaced with a paper tape punch. The DVM recording cycle averaged the output signal from the microdensitometer photocell for 1 second, skipped 0.118 second of photocell output to initiate the paper punch and then recycled. The background signal with the DVM short-circuited was 0.0005 volt; therefore, the last digit was not used. It should be noted that the paper tape was in turn converted to cards for use on the CDC 6600 computer.

Computer

A Control Data Corporation 6600 Scope 3.2 Version 52 computer and a CALCOMP 160 Plotter was used to process and graph the data.

CHAPTER IV

DATA REDUCTION

The specular reflectance data collected in the surface parameters experiment are shown in Figures 14, 15, and 16. The energy which is reflected coherently is superimposed on the graph as a dashed line. The dashed line is based on the theoretical predictions and indicates the relative amounts of coherent versus incoherent energy contained in the specular reflection. As previously stated in Chapter III, these relative amounts of energy are important in selecting data used in calculating a parameter.

The rms roughness was calculated using the long wavelength data where little or no energy is reflected incoherently. The data was substituted into equation 10, Chapter III and the results plotted on semi-log paper. The four longest wavelength data points plotted as a straight line. The slope of the line continually changed when the shorter wavelength data points were plotted. Thus only the four longer wavelength data points had insignificant amounts of incoherent energy in the specular reflectance and could be used to calculate the rms roughness. The results of the calculations are presented in Table II, Chapter V.

The correlation distances were calculated using the shortest wavelength data point and also presented in Table II, Chapter V. Since the correlation distance is only a function of the scattered

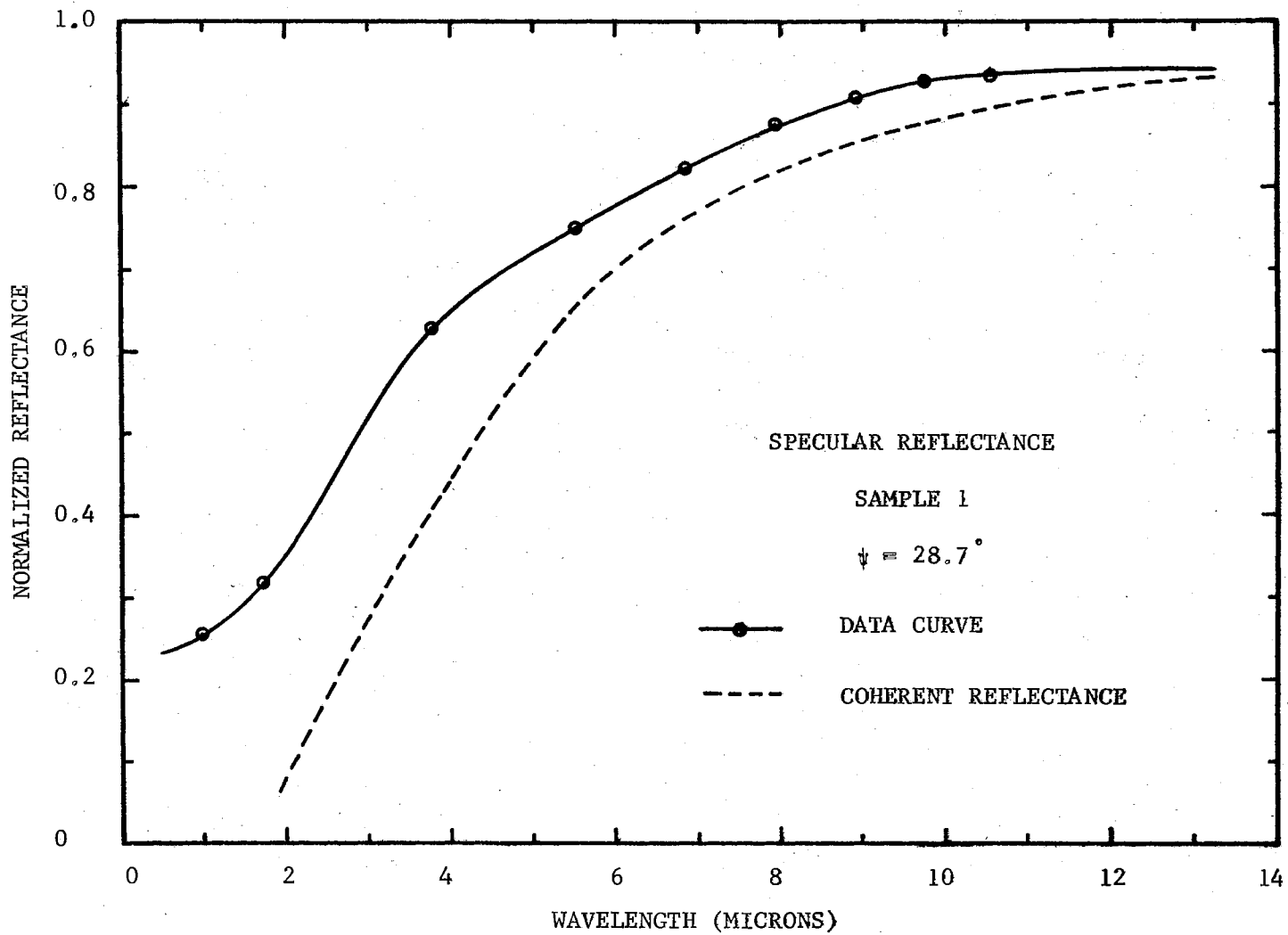


Figure 14. Specular Reflectance Data - Sample 1

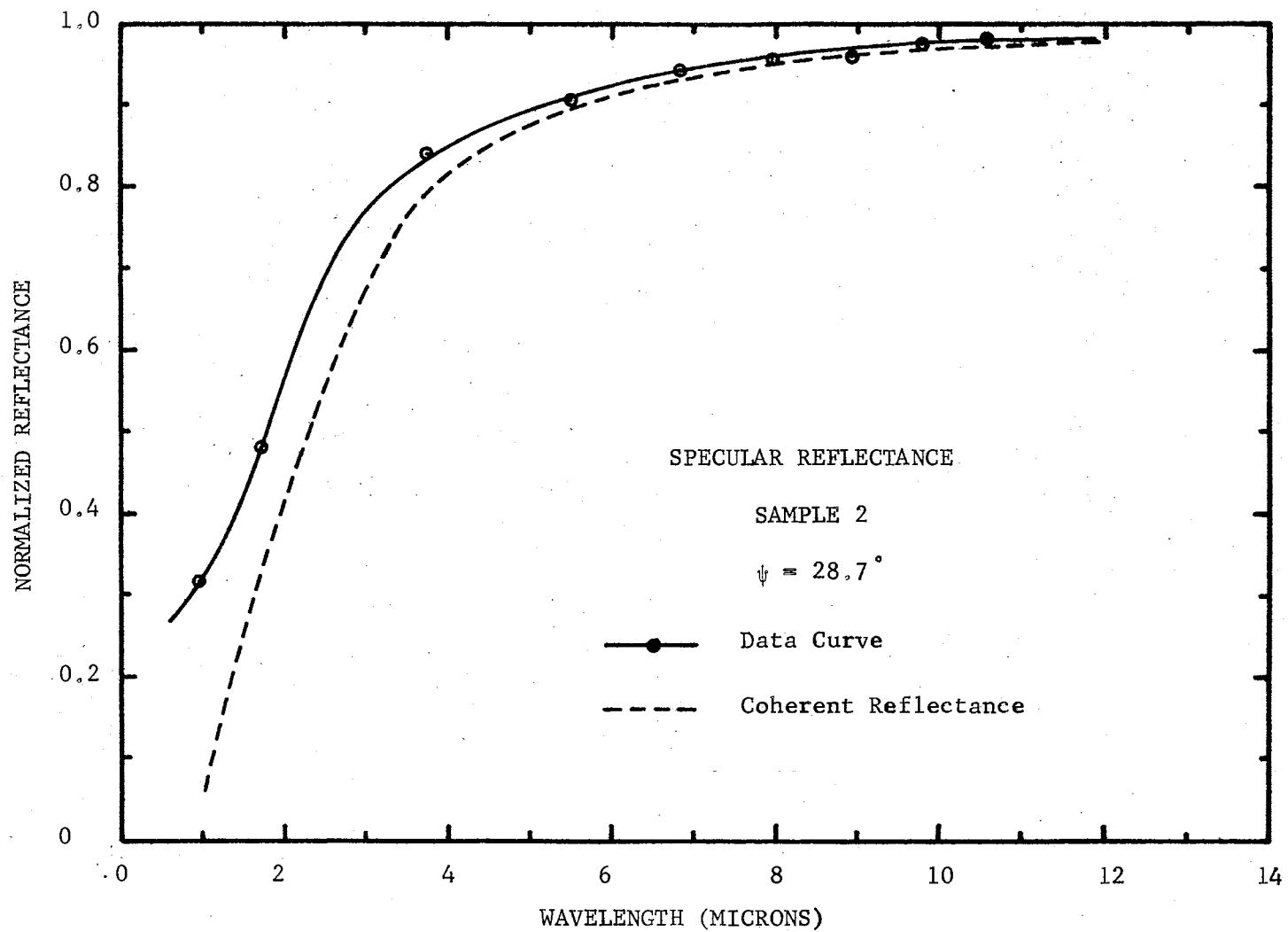


Figure 15. Specular Reflectance Data - Sample 2

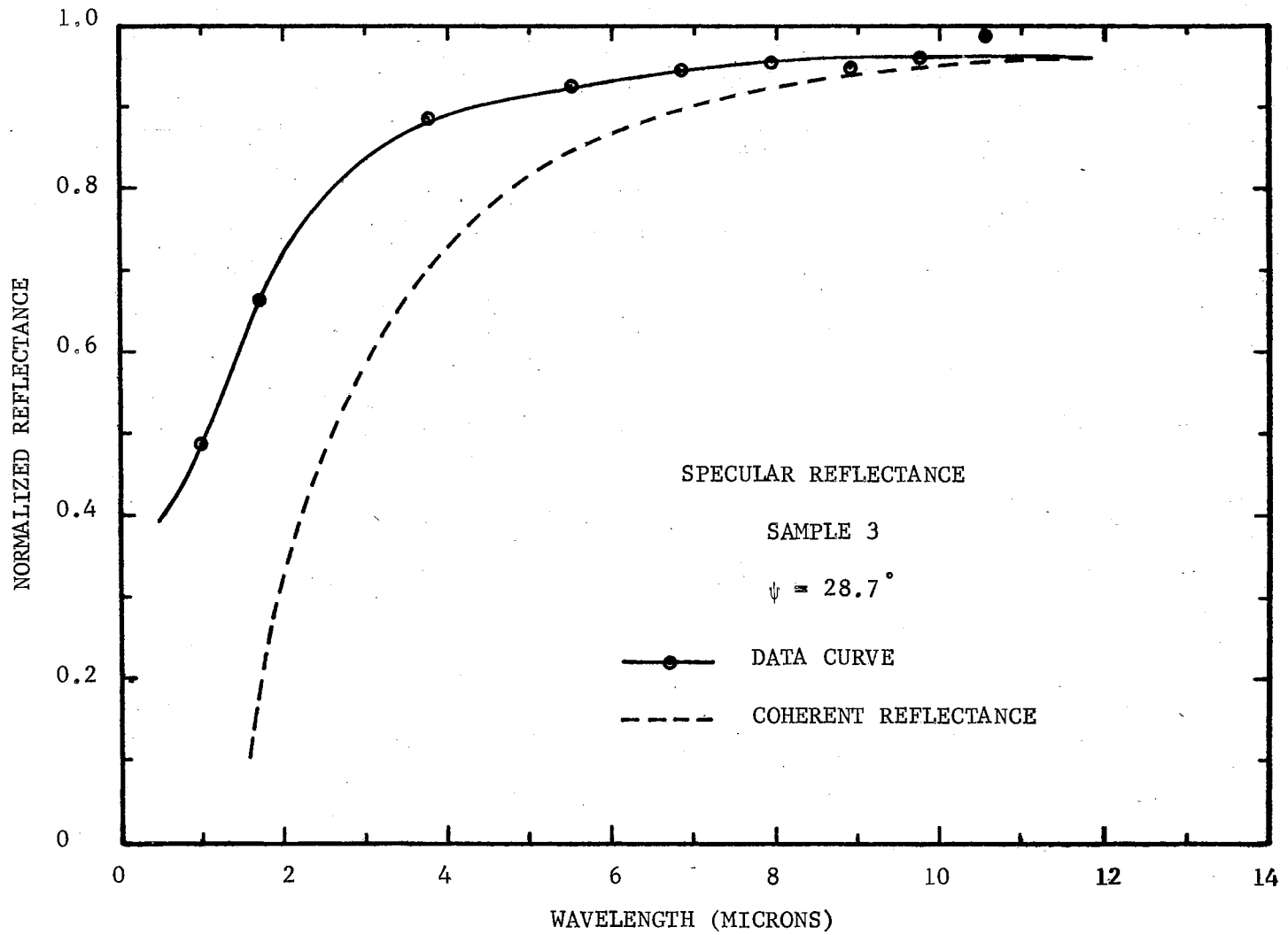


Figure 16. Specular Reflectance Data - Sample 3

energy, it was desirable that the data used to determine this parameter consist primarily of incoherent energy. At the short wavelength the specular reflectance was almost entirely composed of incoherent energy. In fact, the theory predicts that at the short wavelengths less than 10 per cent of the energy received at the thermocouple detector had been reflected coherently. Only one data point was required for this calculation; therefore, the shortest wavelength data point in each set was used.

It is significant to note that the specular reflectance data is similar to that collected by H. E. Birkebak (8). Birkebak's research was done on samples which had higher optical roughnesses and his specular reflectance data was collected at an angle of incidence of 10° versus this angle of incidence of 28.7° . Therefore a direct comparison cannot be made. However, Figure 17 is a comparison of the data from the two samples most nearly alike, Birkebak's smoothest sample versus the roughest used in this work, Sample 1. It is evident that the characteristics of the curves are the same. The curves would be even closer if the angle of incidence were the same, as changing the angle from 28.7° to 10° would lower the curve.

Bi-Directional Reflectance Data

Two effects necessitated special handling of the photographic data. A speckle pattern was recorded on the film versus the expected continuously exposed area, and a few data points were outside of the range of the calibration curves.

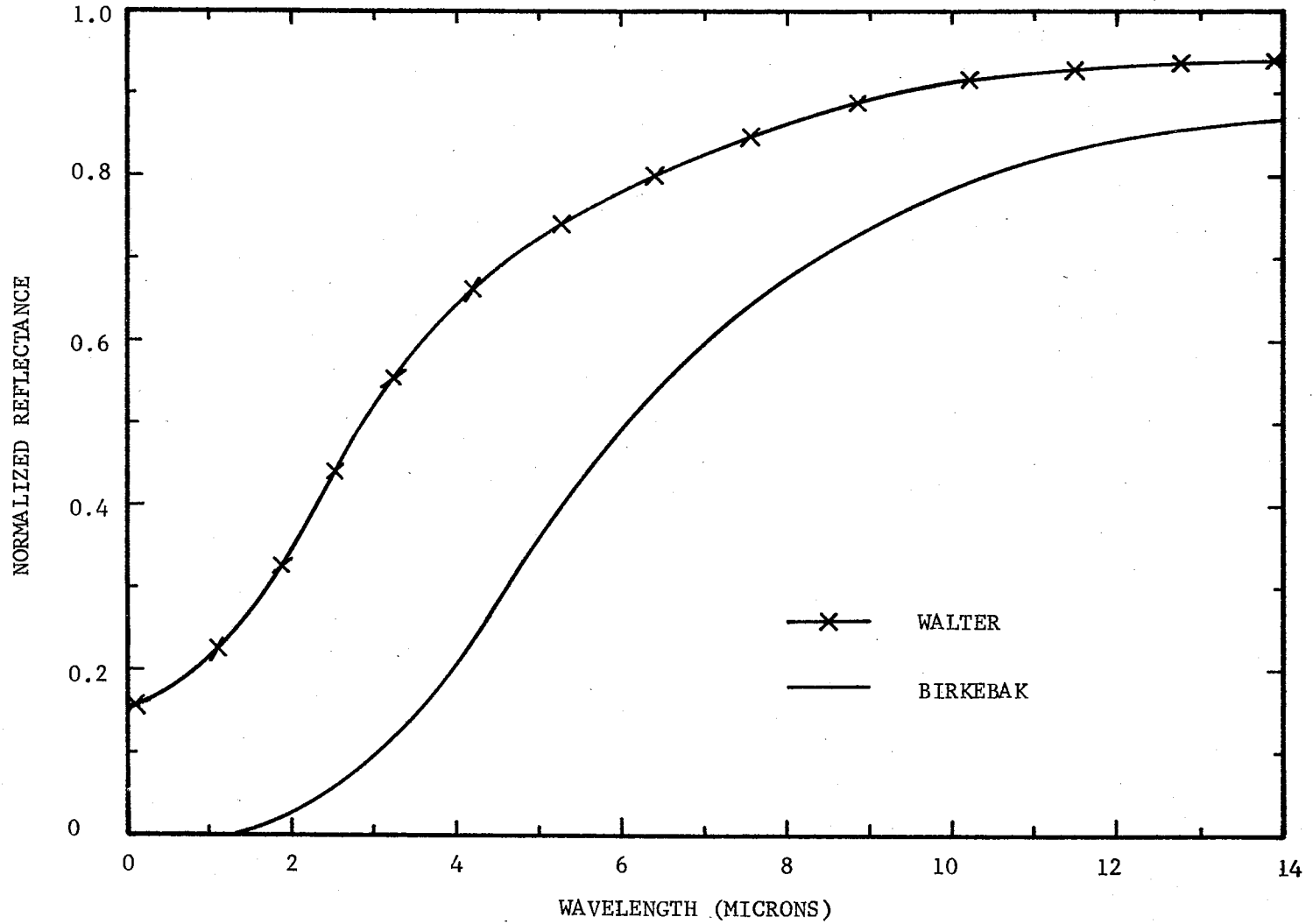


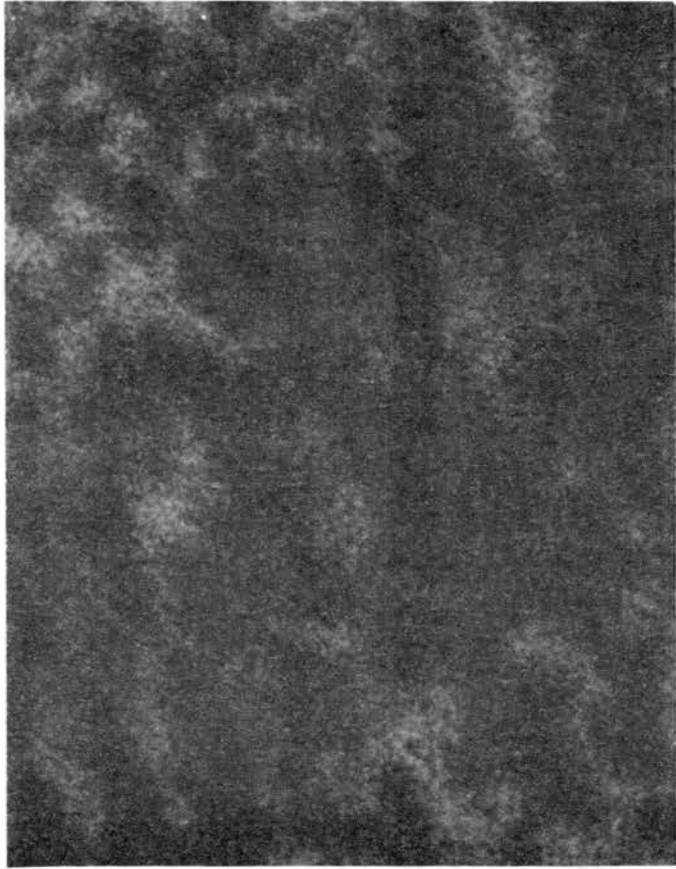
Figure 17. Specular Reflectance - Birkebak and Walter Data

Reflected Pattern

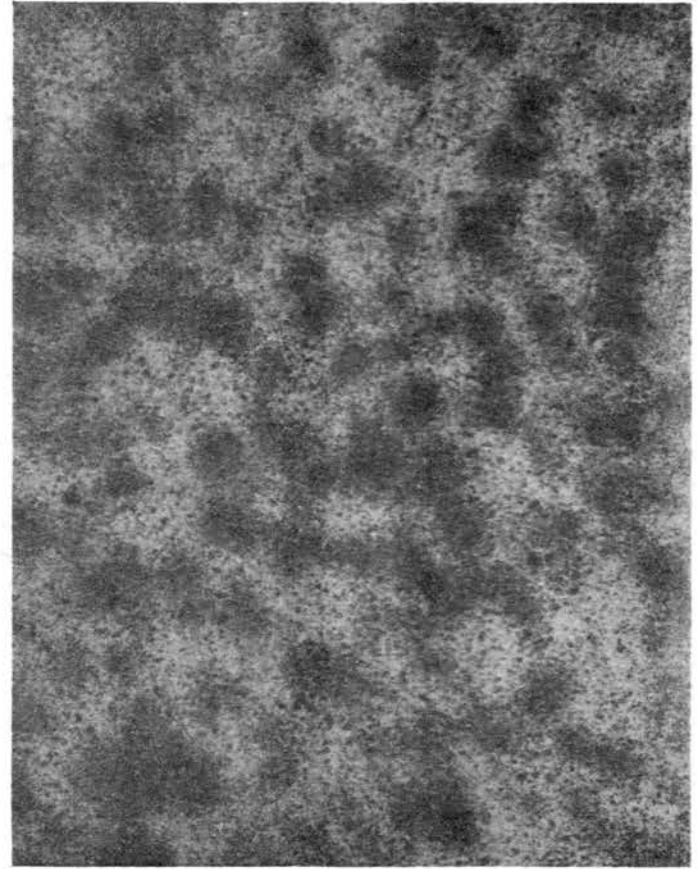
The scatter pattern recorded on the film was indeed a speckle pattern as is shown in Figure 18. Instead of a continuously exposed field, the field was a collection of dots. It was expected that the scattered energy would have exposed the whole area covered by the speckle pattern with the majority of the energy deposited in the specular direction and exponentially decreasing in intensity to the edge of the scatter pattern. The dots became less densely packed and each dot contained less energy as one moved away from the specular direction and thus the speckle pattern did give a diminishing intensity about the specular direction.

The speckle pattern was an interference pattern caused by using a laser light source. It was not a function of the granularity of the film as the exposed dots were much larger than the grain size of the film. Two comprehensive discussions of speckle patterns are given by L. I. Goldfisher (19) and G. Stavis (20). The reradiating surface can be considered filled with elemental emitters having random phase, amplitude and position. The diffraction pattern generated by these random emitters results in the speckle pattern.

Because this was an interference pattern, the film was recording the constructive interference and was not exposed by the destructive interference. Therefore it was assumed that if the energy deposited over a finite area of the film, having both exposed and unexposed areas, were averaged, the constructive interference energy and the destructive interference energy would average out. Thus, the speckle



Specular



Off-Specular

Figure 18. Speckle Patterns

pattern necessitated an averaging technique to estimate the reflected energy distribution.

The effective area of film which was averaged by the microphotometer and DVM was 0.5 millimeter high by 0.0928 millimeter wide. This resulted in 0.0652 degree between data points. Averaging over this small area for a data point still gave substantial variation in the reading from one data point to another. Further averaging was obtained by curve-fitting the data.

Calibration

The microdensitometer transmissibility data which is raw data, must be converted to energy to compare to the theoretical predictions. The calibration points obtained by using the JACO seven-step filter give the basis to convert the transmissibility readings to energy. Each step in the filter reduces the energy input a fixed amount as is given in Table I, Chapter III. Each calibration point is read individually on the microdensitometer for each strip of film. This data was input to a computer subroutine which calculated spline curve fits (21, 22) to the calibration data, Figure 19. Each data point can now be substituted into the graph to get its relative energy. By using the computer, the raw data, Figure 20, was input to the spline equations and calibrated and plotted as shown in Figure 21.

The calibrated data appears inverted compared to the raw data. This is because the raw data measured transmissibility of the film. The more energy deposited on the film the greater the exposure and the less transmissibility. Thus when the transmissibility readings are converted to energy deposited, the curves become inverted.

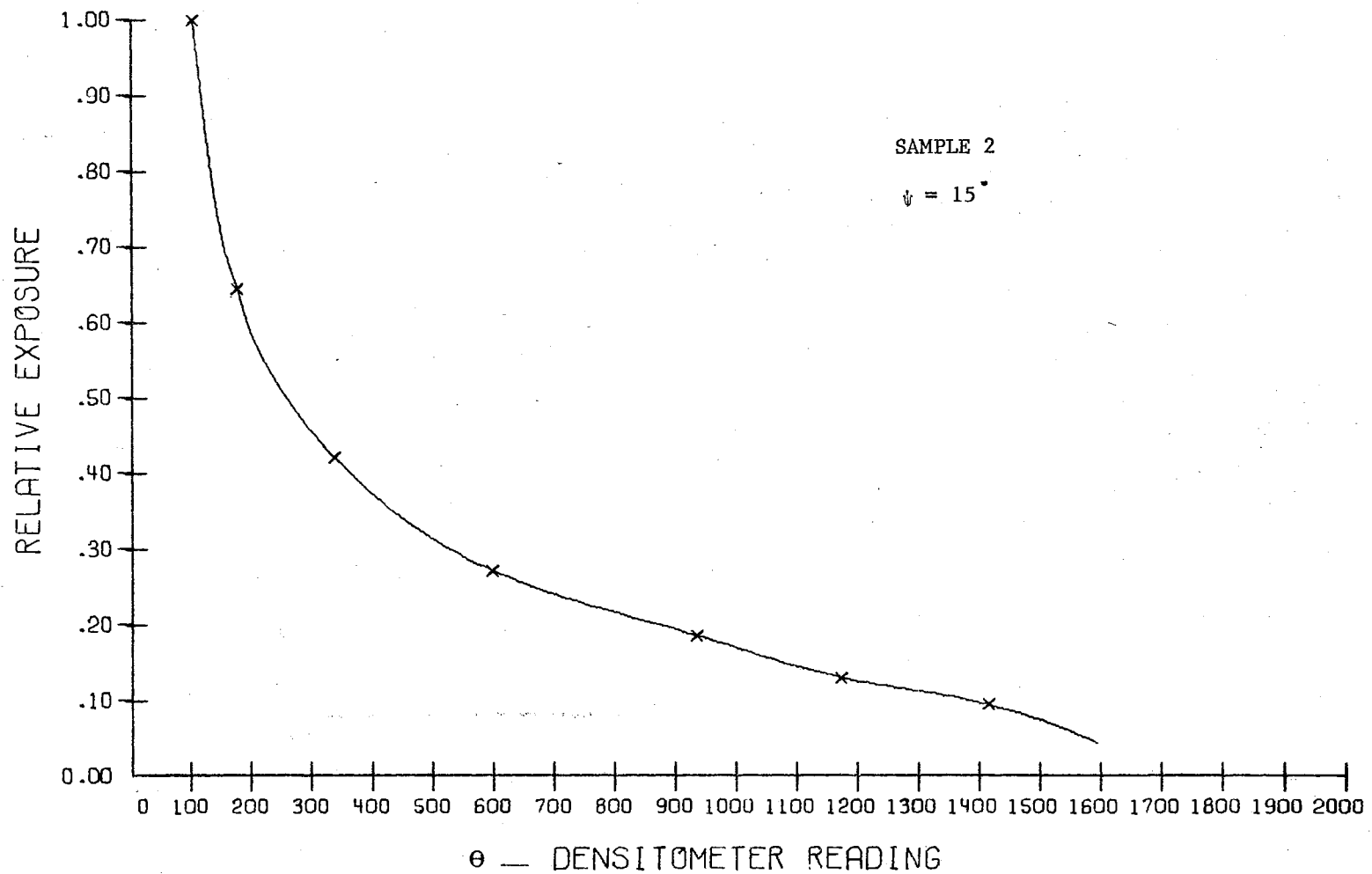


Figure 19. Typical Calibration Curve

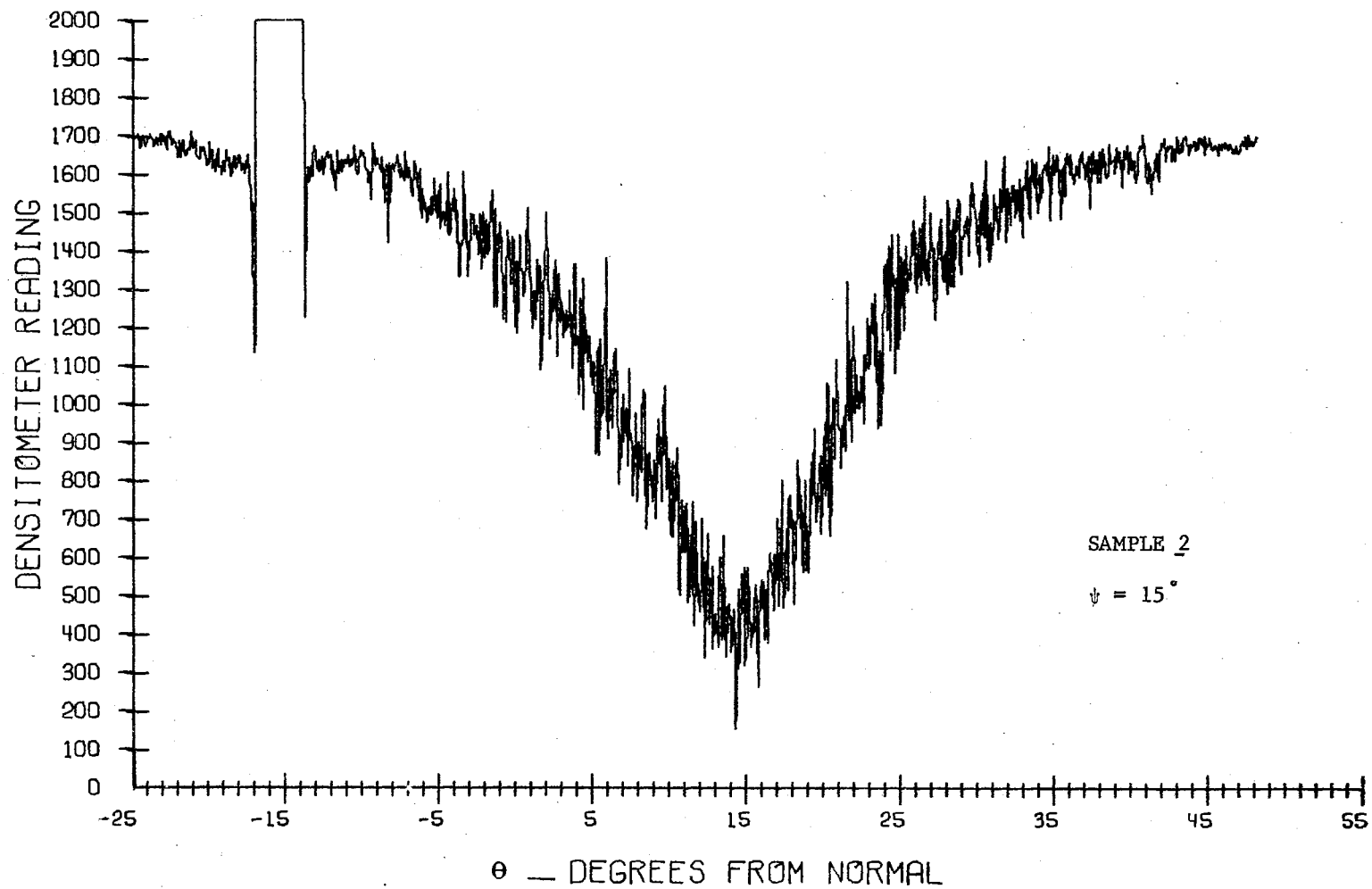


Figure 20. Sample of Raw Data

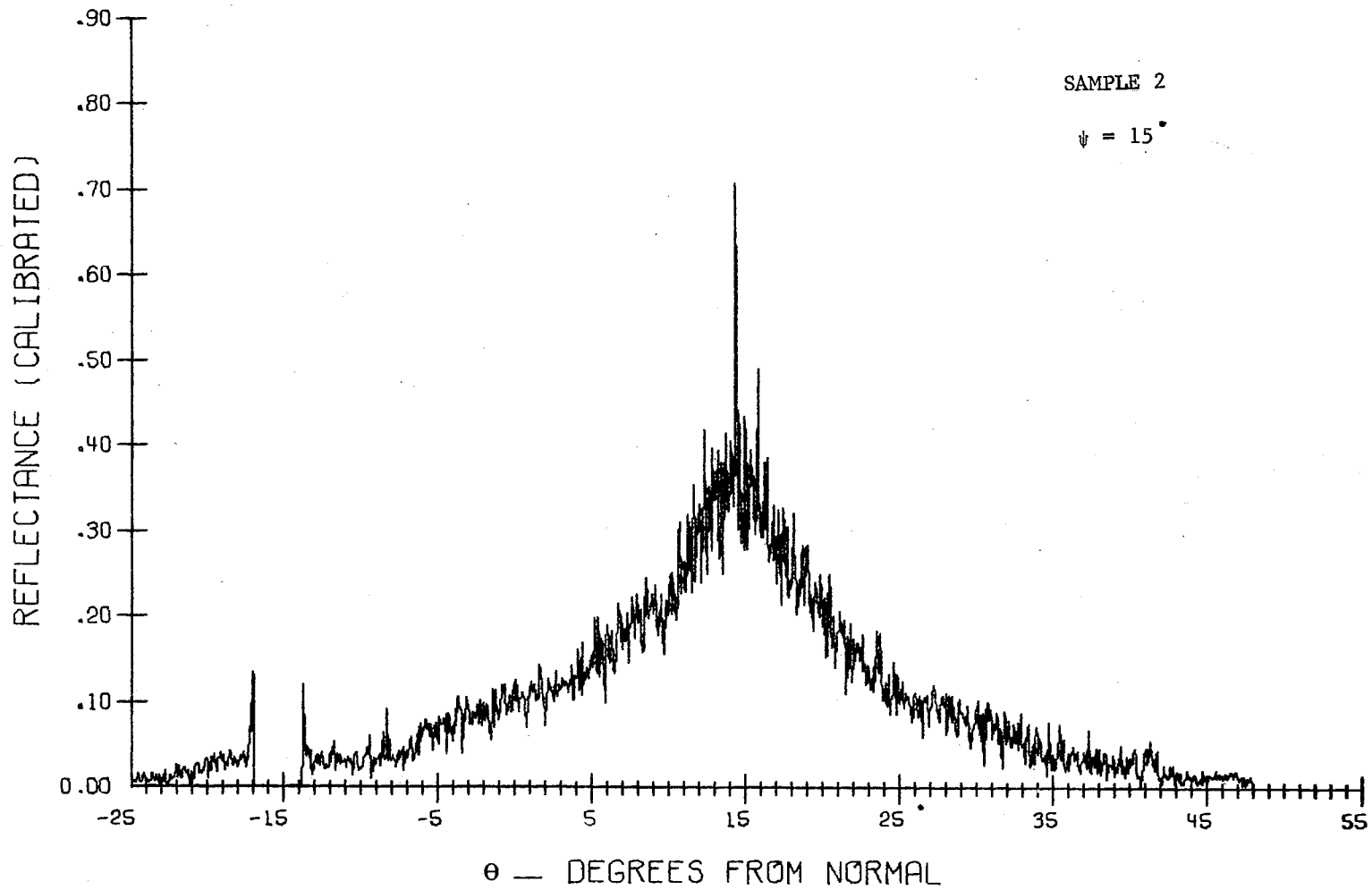


Figure 21. Sample of Calibrated Data

The data of Figure 21 must be curve-fit, normalized, and superimposed onto the theoretical predictions. Many computer curve-fit routines were tried but none performed satisfactorily. The high order, high frequency curve-fits could fit the peaks of the specular reflectance, but had oscillations in the lower level scatter data. Weighting function routines did not bring the curve-fits up to the specular reflectance peaks, particularly on the data from Sample 3. Therefore, curve-fits by hand, using the human eye and a french curve, gave the best results.

The specular reflectance value, which is the highest point in the curve-fit and also the value which will be used to normalize the data, had to be determined more accurately. This value was established by averaging a selected number of points about the specular direction. It was necessary to use averaged data due to the large variation of magnitude for adjacent points. Studies of expanded plots of the data were made. From these, a center grouping of data points appeared to give a bounded specular region and were therefore averaged. The data on either side of this region decreased rapidly and thus provided the basis for this decision. In the case of Sample 3, as few as four data points were averaged and in Sample 1, as many as 12 data points.

An additional check was made to verify this sample size for the normalizing value. The computer was given the sample size and incrementally searched either side of specular direction and compared the specular sample average to adjacent averages. The specular direction averages gave the highest values. The width of the area on the film covered by these sample sizes was less than the laser beam diameter.

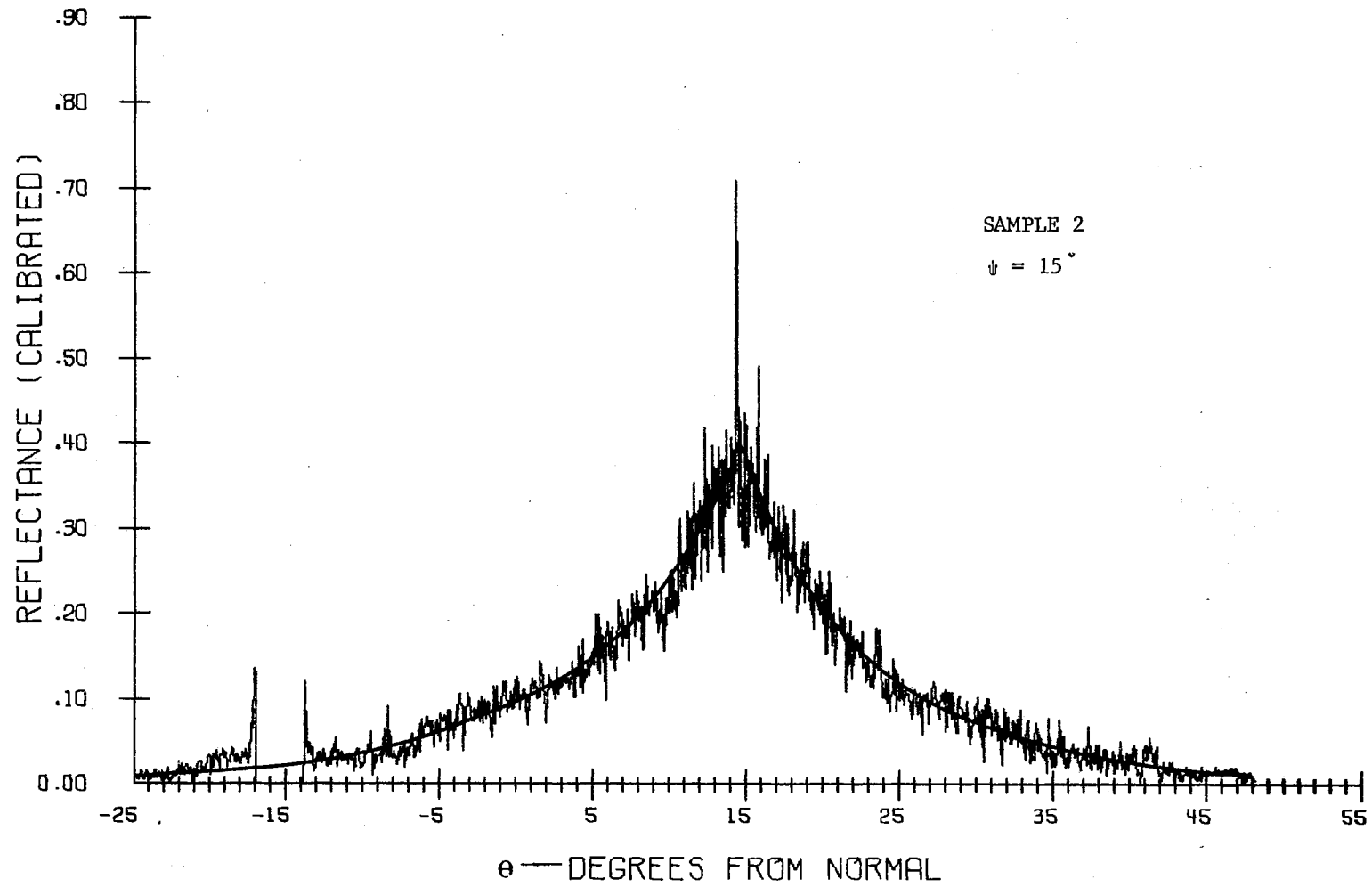


Figure 22. Sample of Curve-fit Data

A curve-fit was superimposed on the data as shown in Figure 22. These curve-fits were digitized using a Data Instruments, TELEREDEX, Model 29E-17, and input to the computer to be plotted versus the theoretical predictions.

Extrapolated Calibration Data

The initial photographic trial experiments were used to establish polaroid settings for all of the subsequent tests. The polaroids were used to control the energy so that the film would not be over or underexposed and to range the calibration data to cover the exposures. The initial trials underdetermined the energy that would be specularly reflected at the large angles of incidence, particularly from Sample 3. Therefore, some specular data points, in all cases less than 3 per cent of any one data set, were overexposed and thus were beyond the range of the calibration curves.

Sensitivity of the film had to be determined to establish criteria upon which to extrapolate the calibration curves. A complete discussion of film sensitivity is contained in reference (23). One feature of sensitivity, the characteristic curve, needs to be discussed here because it was used to extrapolate the calibration curve.

The characteristic curve is a plot of the transmission of the film versus the exposure, Figure 23. The significant features are the toe, which is the transmission of the base material (fog level); the straight line, where the transmission decreases linearly with increasing exposure; and the shoulder, the region of overexposure where the gradient of the curve decreases with increased exposure and eventually becomes horizontal.

A set of calibration points was taken in the over-exposed region on one film strip to provide upperbound information. It was not anticipated that this data be used, but it provided the base line upon which the calibration curves were extrapolated. This over-exposed data was used to define the shoulder for the characteristic curve. The transmissibility of the most over-exposed data point was studied relative to the over-exposed calibration data and from this comparison the flat portion of the shoulder of the characteristic curve was set. The toe and straight line portions were accurately established by the calibration data from that particular film strip. A representative type curve was used to connect the straight line segment to the flat shoulder segment. The extrapolated characteristic curve for Sample 3, $\psi = 15^\circ$, is given in Figure 24.

These extrapolated characteristic curves were used to calibrate the overexposed data. This data could then be handled in the normal fashion. It should be re-emphasized that only a few film strips had overexposed data points and at most only 3 per cent of the points were overexposed.

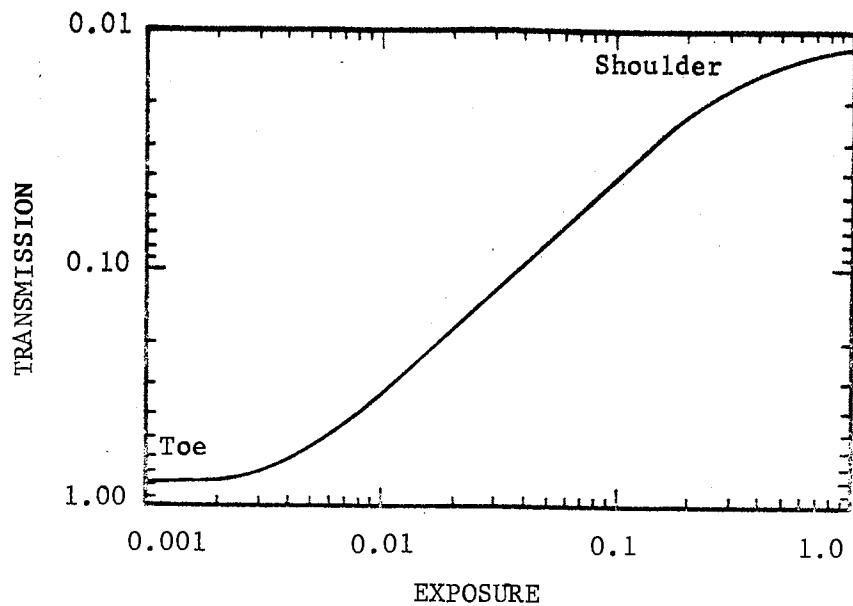


Figure 23. Typical Characteristic Curve

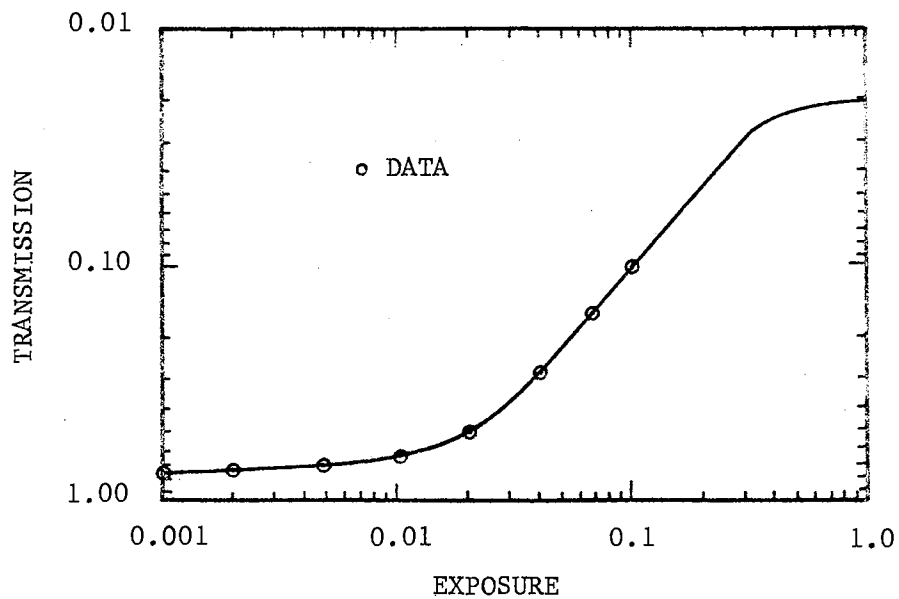


Figure 24. Extrapolated Characteristic Curve

CHAPTER V

RESULTS AND CONCLUSIONS

The purpose of this dissertation, as previously stated, was to investigate experimentally the applicability of using Beckmann's Bi-Directional Reflectance Model to predict reflectance from randomly rough surfaces with optical roughnesses less than one.

Two types of randomly rough surfaces were investigated, the 1-D rough surface and the 2-D rough surface whereas past research has been limited to the 2-D case. This investigation extended research to 1-D rough surfaces as well as adding information about reflectance from 2-D rough surfaces.

This investigation successfully employed an optical technique to measure surface parameters, and a photographic technique to record the reflected energy scatter pattern from the randomly rough nickel surfaces. The optically determined surface parameters are compared to mechanically determined surface parameters in Table II and significant disparities are discussed. The comparisons of the predicted scatter patterns to the actual scatter patterns indicated that Beckmann's Bi-Directional Reflectance Model may be used as a tool to approximate energy scatter from 2-D engineering type surfaces, but not from 1-D surfaces. The more pertinent aspects of the theoretical predictions versus the data will be discussed.

Optical and Mechanical Surface Parameters

The optically determined surface parameters are compared to the mechanically determined parameters in Table II. Correlation between the parameters obtained from these two techniques should not necessarily be expected. There are inherent errors in the mechanical technique, and optical techniques have not been completely proven and accepted.

TABLE II
MECHANICAL AND OPTICAL SURFACE PARAMETERS

Sample	rms Roughness		Correlation Distance	
	Optical	Mechanical	Optical	Mechanical
1. (1-D)	0.322	0.201	21.6	744
2. (1-D)	0.162	0.097	11.9	487
3. (2-D)	0.202	0.047	18.1	776

The surface roughnesses correlated best, however, the optical roughness was larger than the mechanical roughness. This would be expected because the finite diameter of the stylus tip prohibited it from following the surface contour to the bottoms of the valleys. Thus this difference in the mechanical and optical values would increase as the roughness decreased, as illustrated in the data in Table II. Other investigators (7, 12) have also found that for the rms roughnesses, optical techniques gave larger values than mechanical techniques. Therefore, it appears that for engineering type surfaces

the optical techniques determined the surface roughnesses better than mechanical techniques.

The optically determined and mechanically determined correlation distances did not compare. The optical correlation distances were much smaller than the unrealistically large mechanical correlation distances. The values differed by more than an order of magnitude. This wide divergence can not be explained. The optical correlation distances were realistic.

Initial parameter studies on the 1-D data indicated that correlation distances between 22 and 3 would be practical and give reasonable predictions. These values were obtained independently of the surface parameters experiment. The scatter data was used and the computer routine for the theoretical predictions was modified to allow the correlation distance T to vary until the predictions intersected the scatter data; at least at one point other than the normalized specular direction. Though unique values of T were not found, the above range of T values was established. The fact that the optical correlation distances obtained in the surface parameters experiment were similar to the values needed to fit the data from the scatter experiment gives added credence to the optical technique.

The fact that the mechanical correlation distances are unrealistically large can be ascertained by comparing the mechanical correlation distance to the surface rms roughness height. This large correlation distance indicates that the sample contours would have very wide valleys and very rounded peaks. This was not the case as illustrated in Figure 6, Chapter III. If the mechanical correlation distances were valid, given the height of the first point in Figure 6, one would be able to

reasonably predict the height of the last point in Figure 6. It is obvious from the tracing of the surface profile and the random roughness calculations that such a surface continuity does not exist. Also, when these mechanical values are substituted into the theory, the theory predicts no incoherent component of reflectance. Therefore, the surface would have to be essentially optically smooth to have such correlation distances. The tracings and the scatter data prove this is not the case. Postulated causes of the differences are: The stylus' finite radius producing inherent errors, the profilometer and strip chart recorder having mechanical operations errors, or the techniques used in data sampling affecting the results.

Because of the inherent errors in obtaining a mechanical rms roughness and the unrealistically large mechanically determined correlation distances, it is concluded that in the roughness range of $\sigma/\lambda < 0.3$ an optical technique will give a better determination of the surface parameters than a mechanical technique.

Theory Versus Data

The second phase of the investigation was to use the optically determined surface parameters in Beckmann's theoretical model and see if it would predict the scatter patterns obtained from the experiments. Again, the theory was applied to two surfaces of interest, the 1-D surfaces which are considered representative of a large class of engineering type surfaces and 2-D surfaces which are obtained from some manufacturing techniques and considered one limit of engineering type surfaces.

All the data collected from both the 1-D and 2-D samples are consistent with and confirm previously established reflectance trends:

1. Each sample becomes increasingly specular as the wave lengths increase.
2. A rough surface reflects more specularly as the angle of incidence increases.

Theory also predicts that the energy would be scattered in one lobe about the specular direction for both the 1-D and 2-D surfaces, and the experimental data does indeed show that randomly rough surfaces do scatter the energy in one lobe about the specular direction. Comparison of the theoretical predictions to the data reveals that the spread of the lobe is approximately predicted for the 2-D sample but that the spread of the lobe is greater than predicted for the 1-D samples. However, the trend of the lobe size for the 1-D samples is consistent with the roughness parameters of the surface in that the energy was scattered over a larger area for the rougher sample.

Comparisons of the predicted energy distributions to the recorded scatter pattern, Appendix A, showed very good correlation between theory and data for the 2-D sample and relatively poor correlation for the 1-D samples. Therefore the result of applying the theory to the 1-D case was not successful but the application to the 2-D case showed close correlation. Closer inspection and separate analysis of the two areas is appropriate.

1-D Data Versus Theory

The major disagreement between the theory and 1-D data is that the theory predicts that the energy would be scattered over a much smaller

area than that which was actually exposed on the film. This divergence is illustrated in all the 1-D figures.

The difference in the spread is substantial for both Sample 1 and Sample 2. The smoother Sample 2 shows the widest disagreement. Figure 46a shows a theoretical spread of 12° (theta) about the specular direction versus a spread of 68° for the data. The data spread of the energy remains approximately the same until the angle of incidence (ψ) becomes larger than 45° . The spread then becomes smaller and smaller as ψ increases. However, for $\psi > 45^\circ$ the theory shows no scatter for the roughness parameters of Sample 2 but the data shows substantial scatter. Similar trends are shown in the Sample 1 data, except because of the larger roughnesses the theoretical reflectance does not become specular until $\psi = 75^\circ$.

It appears that the 1-D model closely predicts the energy scatter at large angles. However, trend 2, page 64, must be considered. The reason it appears to more closely predict the scatter is that practically all of the reflected energy is reflected specularly. The theory is predicting a single narrow lobe of energy and the data still shows scattered energy even though it is of low magnitude. This is best illustrated in Figures 48b and 49.

Some differences in the magnitudes of relative reflectances for a given theta might be expected due to the averaging techniques used to interpret the energy deposited on the film. However, the spread of the energy about the specular direction should be the same if the theory is predicting the scatter pattern.

It is of interest to note in Figures 48b and 49 that the back scatter ($\theta < \psi$) is higher than the forward scatter ($\theta > \psi$). The

off-specular peaks observed by Torrance and Sparrow (11) would indicate that the forward scatter should be the larger as the large off-specular peaks occurred at angles greater than the specular. However, their optical roughnesses were larger than those investigated here so no direct comparisons can be made but the difference in trend is interesting.

Because the 2-D theory correlates well with the experimental data one might expect the 1-D theory to correlate better. Since it does not, it would appear that the version of Beckmann's Bi-Directional Reflectance model used in the 1-D data analysis may be wrong. In Chapter III it was assumed that the 2-D model could be applied to the 1-D samples because the 1-D illuminated area was a finite area and not the infinite strip of the 1-D theory.

It should be noted that if the optically determined correlation distances were smaller, the spread of the energy would increase and more nearly match the data. The same is true of an increased rms roughness. The changes required to make the theory fit the data are greater than can be accounted for by experimental error but not so large that additional investigation in applying Beckmann's model to 1-D surfaces is warranted.

2-D Data Versus Theory

The correlation of the 2-D data and the 2-D theory is quite good as illustrated in Figures 54 through 56. In Figures 54a and 54b the spread of the energy is almost the same. The magnitudes of the normalized reflectances do differ and the theory predicts that more energy is scattered in the non-specular directions. Figure 55 illustrates that as the angle of incidence increases more energy is specularly

reflected. Though closer, the theoretical values are still higher than the data, and the theoretical spread is somewhat larger than the data spread. When the angle of incidence is increased to 45° , Figure 55b, the spread is equal and the theoretical values are now slightly less than the data. Thus for the 2-D case the theoretical predictions have bounded the data. In Figures 55b and 56 the theory predicts essentially a specular reflectance and the data has only low-level scatter near the specular direction.

In analyzing this low-level scatter two basic assumptions in the theoretical development should be considered. These assumptions are no inter-reflections and no shadowing effects. At large angles of incidence both effects are probably present and would show up as an additional scatter component in the photographic data. Therefore, at the large angles it is probable that the theory may not be applied directly to predict the scatter. That is, beyond a given angle of incidence and peak density, shadowing and interreflections will affect the scatter pattern and modify or limit the range of applicability of the model.

In summary, the 2-D data shows that the energy scatter from the 2-D sample is approximately predicted by the model. The spread of the energy is very close for angles of incidence of 45° and less. The theoretical magnitudes of the reflectances are higher for angles less than 45° and lower for angles greater than 45° . Thus the data is bounded by theoretical predictions.

Conclusions and Recommendations

Beckmann's Bi-Directional Reflectance model, using the optically determined surface parameters, predicts an energy scatter pattern that

correlates well with the experimental data from the 2-D sample. This indicates that Beckmann's model may be applicable as a prediction tool for reflectance from metallic surfaces, however, further substantiation is required.

The fact that the surface parameters used in the model were obtained optically and thus non-destructively can be very significant. It suggests the possibility that a simple apparatus could be constructed to optically measure the surface parameters of a material anywhere in the field, without item damage, and with relative ease. Present techniques require laboratory analysis of representative samples of the surface. With such an apparatus field parameters can be obtained directly from the space vehicle and substituted into Beckmann's model for accurate reflectance predictions. This would greatly simplify present procedures and increase accuracy and thus be a very viable tool to assist in heat transfer calculations for space.

Because of the relative success of this investigation it is recommended that additional research be done to more completely determine the degree of applicability of Beckmann's Bi-Directional Reflectance model to predict thermal energy scatter from rough surfaces. In particular, it is recommended that the following areas be investigated:

1. Establishment of confidence limits and ranges of validity for Beckmann's 2-D Bi-Directional Reflectance Model.
2. Determination of the feasibility of applying a modified Beckmann's 1-D model to roughened surfaces.
3. Evaluation of the effect of roughness on reflectance from non-conductors.

4. Firm establishment of the validity of using an optical versus mechanical technique to determine surface characteristics.
5. Design of an optical surface characteristics measuring device.

SELECTED BIBLIOGRAPHY

1. Rolling, R. E., A. I. Funai, and J. R. Grammer. "Investigation of Effect of Surface Condition on the Radiant Properties of Metals." A. F. Materials Laboratory, RTD, AFSC, WPAFB, Ohio, Technical Report, AFML-TR-64-363, 1964.
2. Bennett, H.E. "Influence of Surface Roughness, Surface Damage, and Oxide Films on Emittance." NASA SP-55, 1965, pp. 145-152.
3. Wiebelt, J. A. Engineering Radiation Heat Transfer. Holt, Rhinehart, and Winston, 1966.
4. Hering, R. G., A. F. Houchens, T. Smith. "Theoretical Study of Radiant Heat Exchange for Non-Gray Non-Diffuse Surfaces In a Space Environment." NASA-CR-76764, CFSTI, 1966.
5. Beckmann, Peter, and Andre Spizzichino. The Scattering of Electromagnetic Waves from Rough Surfaces. Pergamon Press Limited - Distributed MacMillan Co., Oxford, England.
6. Davies, H. "The Reflection of Electromagnetic Waves From a Rough Surface." Proc. I.E.E., Pt. III, Vol. 101, 1954, pp. 209-214.
7. Bennett, H. E., and J. D. Porteus. "Relation Between Surface Roughness and Specular Reflectance at Normal Incidence." Journal of Optical Society of America, Vol. 51, No. 2, Feb. 1961, pp. 123-129.
8. Birkebak, R. C. "Monochromatic Directional Distribution of Reflected Thermal Radiation From Roughened Surfaces." Ph.D. Dissertation, University of Minnesota, 1962.
9. Birkebak, R. C., and E. R. Eckert. "Effects of Roughness of Metal Surfaces on Angular Distribution of Monochromatic Reflected Radiation." Journal of Heat Transfer, Vol. 87, No. 1, 1965, pp. 85-94.
10. Torrance, K. E., and E. M. Sparrow. "Biangular Reflectance of an Electric Non-Conductor as a Function of Wavelengths and Surface Roughness." ASME Paper No. 64-WA/HT-6, 1964.
11. Torrance, K. E., and E. M. Sparrow. "Off Specular Peaks in the Directional Distribution of Reflected Thermal Radiation." Journal of Heat Transfer, Vol. 88, No. 2, 1966, pp. 223-230.

12. Smith, T. F., and R. G. Hering. "Comparison of Bi-Directional Reflectance Measurements and Model for Rough Metallic Surfaces." Dept. of Mechanical and Industrial Engineering, University of Illinois, Urbana, Illinois, 1970.
13. Maples, Dupree. "Experimental and Theoretical Investigations of Electromagnetic Scattering From a Known, Rough Surface." Ph.D. Dissertation, Oklahoma State University, 1967.
14. Loehrlin, J. E., E. R. F. Womter, and R. Viskantor. "Measurement of Bi-Directional Reflectance Using a Photographic Technique." AIAA Paper No. 70-859, June, 1970.
15. Maples, D., and J. A. Wiebelt. "Experimental and Theoretical Investigation of Electro-Magnetic Scattering from a Known Rough Surface." AIAA Paper No. 68-29, 1968.
16. Look, D. C., Jr., and T. J. Love. "Investigation of the Effects of Surface Roughness Upon Reflectance." AIAA Paper No. 70-820, June, 1970.
17. Herold, L. M., and D. K. Edwards. "Bi-Directional Reflectance Characteristics of Rough Sintered-Metal." 3rd Aerospace Science Meeting (AIAA), 24-26, January, 1966.
18. Francis, R. E. "The Experimental Determination of Reflectance Function for Type 302 Stainless Steel." Master's Thesis, Aerospace and Mechanical Engineering Department, University of Oklahoma, Norman, Oklahoma, 1967.
19. Goldfisher, L. I. "Autocorrelation Function and Power Spectral Density of Laser-Produced Speckle Patterns." Journal of the Optical Society of America, Vol. 55, No. 3, March 1965, pp. 247-253.
20. Stavis, G. "A Laser Velocimeter." General Precision Inc., TNB, Vol. 8, No. 4, Pleasantville, New York, 1965.
21. Walsh, J. L., J. H. Ahlberg, E. N. Nilson. "Best Approximation Properties of the Spline Fit." Journal of Mathematics and Mechanics, Vol. 11, 1962, 225-234.
22. Schoenberg, I. J. "Spline Interpolation and Best Quadrature Formulae." American Mathematical Society Bulletin, Vol. 70, 1964, pp. 143-148.
23. Eastman Kodak Company. Kodak Plates and Films for Science and Industry, Kodak Publication No. P-9, Rochester, New York, 1963.
24. Stevison, Donald F. "Effect of Surface Roughness on the Reflectance of Refractory Metals." A.F. Materials Lab, RTD, AFSC, WPAFB, Ohio, Technical Report, AFML-TR-66-232, 1966.

25. Birkebak, R. L., E. M. Sparrow, E. R. G. Eckert, and J. W. Ramsey. "Effect of Surface Roughness on the Total Hemispherical and Specular Reflectance of Metallic Surfaces." Journal of Heat Transfer, Vol. 86, 1964, pp. 193-199.
26. Scott, O. T. "A Method of Signal Recovery From High Random Noise." Mechanical Engineering 510 Report, Oklahoma State University, 1967.
27. Richmond, J. C., D. P. Dewitt, and W. D. Hayes, Jr. "Procedures for Precise Determination of Thermal Radiation Properties," A. F. Materials Laboratory, RTD, AFSC, WPAFB, Ohio, Technical Report, ML-TDR-64-257, January 1965.
28. Dunn, S. T., J. C. Richmond, and J. F. Parmer. "Survey of Infrared Measurement Techniques and Computational Methods in Radiant Heat Transfer." AIAA Paper No. 65-657, September 1965.
29. Houchens, A. F., and R. G. Hering. "Bi-Directional Reflectance of Rough Metal Surfaces." AIAA Paper 67-319, 1967.
30. Hildebrand, F. B. Advanced Calculus for Applications, Prentice-Hall, 1962.
31. Miller, I., and J. E. Freund. Probability and Statistics for Engineers. Prentice-Hall, 1965.
32. Alder, H. L., and E. B. Boessler. Introduction to Probability and Statistics. W. H. Freeman, 1964.
33. Kruse, P. W., L. D. McGlauchlin, and R. E. McQuistan. Elements of Infrared Technology, John Wiley and Sons, 1963.

APPENDIX A
EXPERIMENTAL BI-DIRECTIONAL
REFLECTANCE DATA

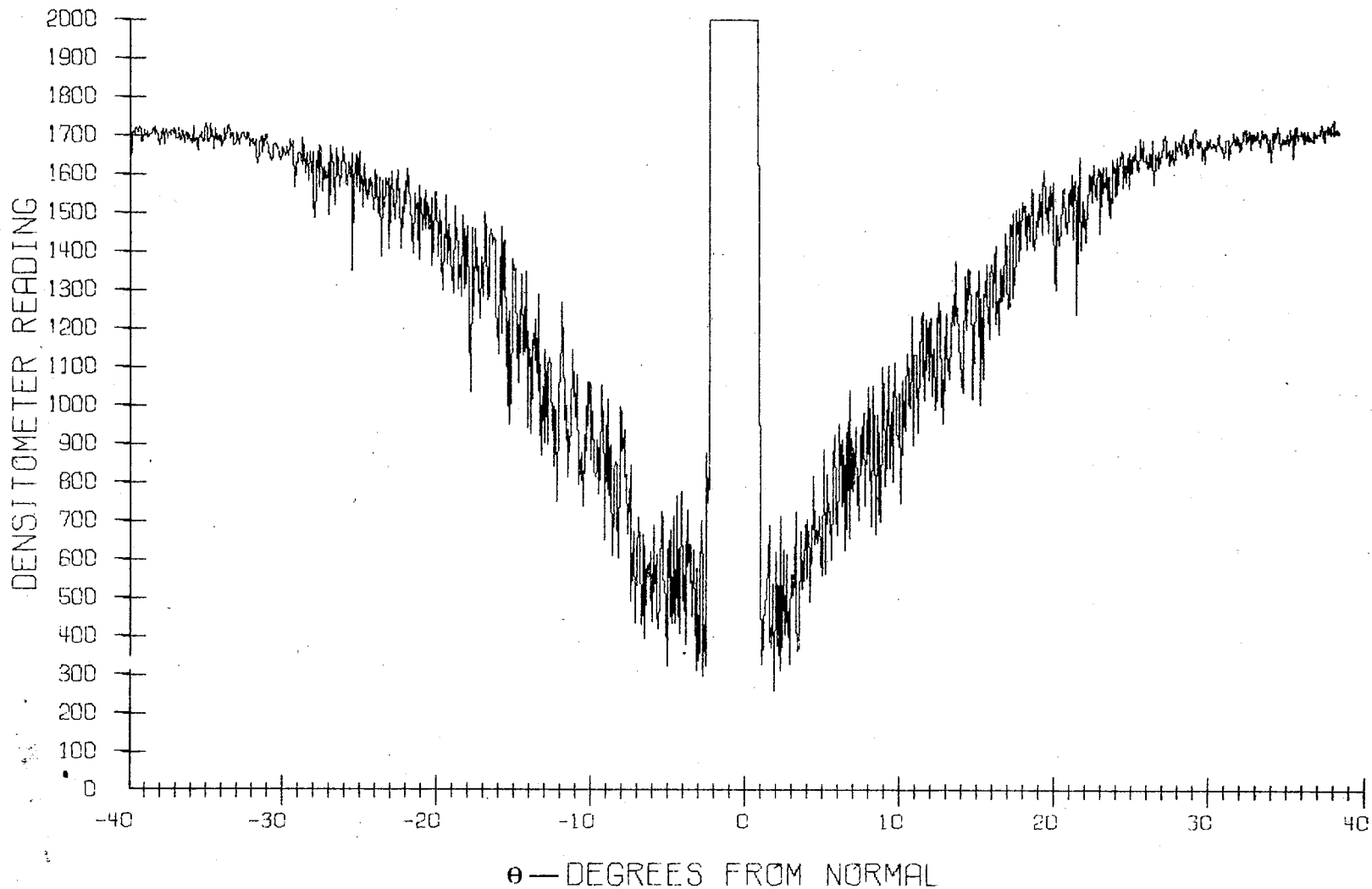


Figure 25. Raw Data—Sample 1— $\psi = 0^\circ$

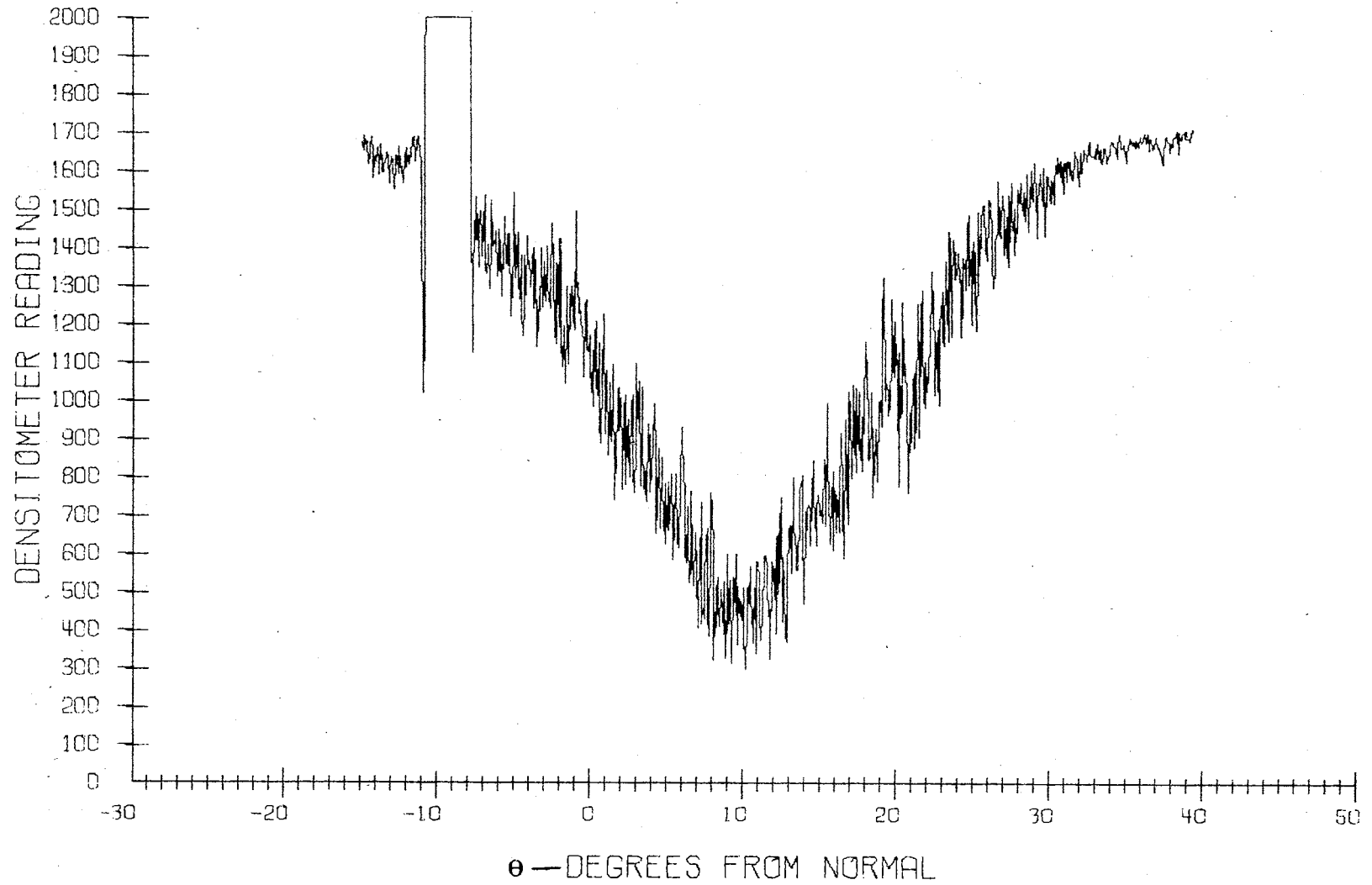


Figure 26. Raw Data—Sample 1— $\psi = 10^\circ$

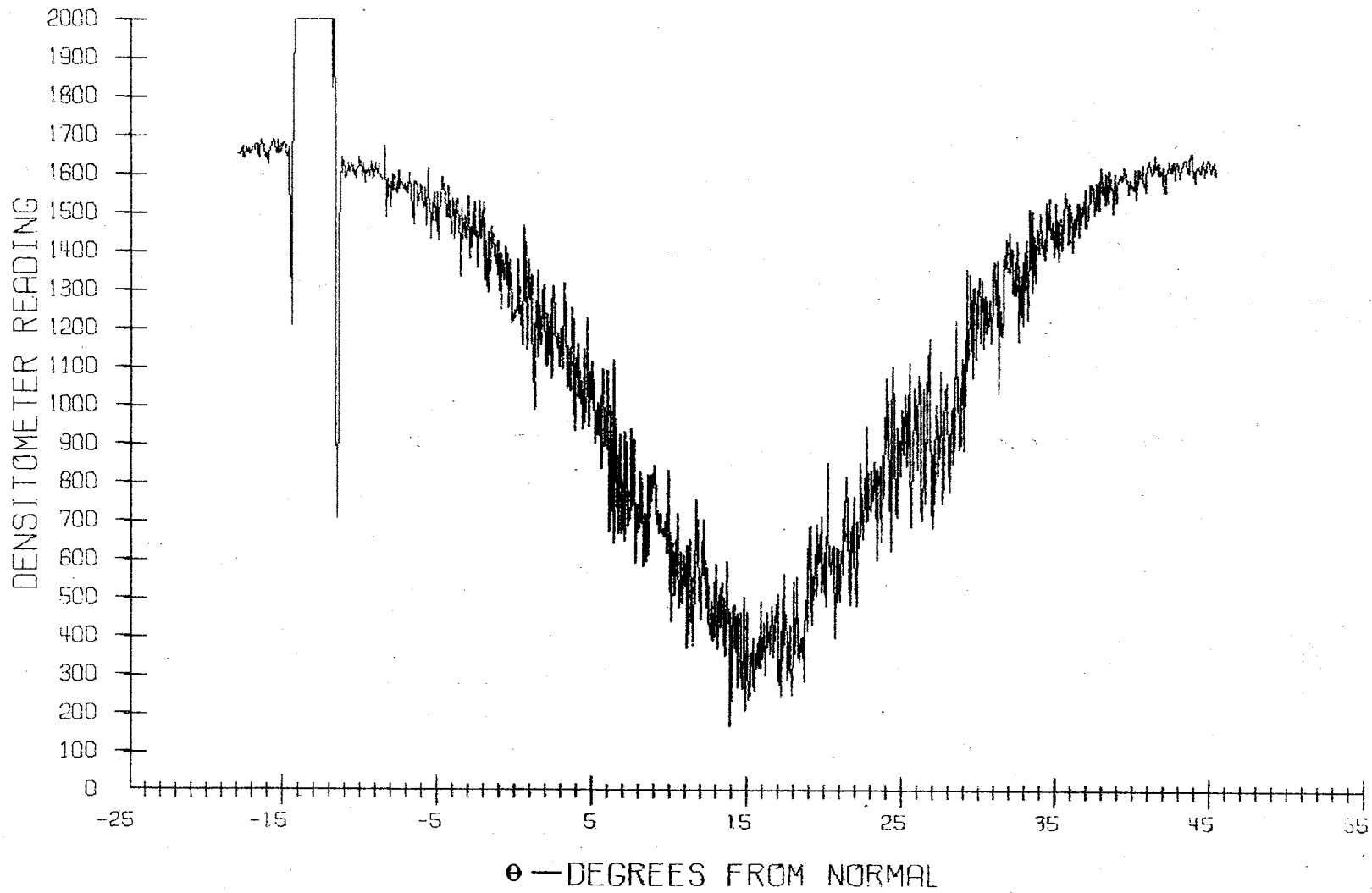


Figure 27. Raw Data—Sample 1— $\psi = 15^\circ$

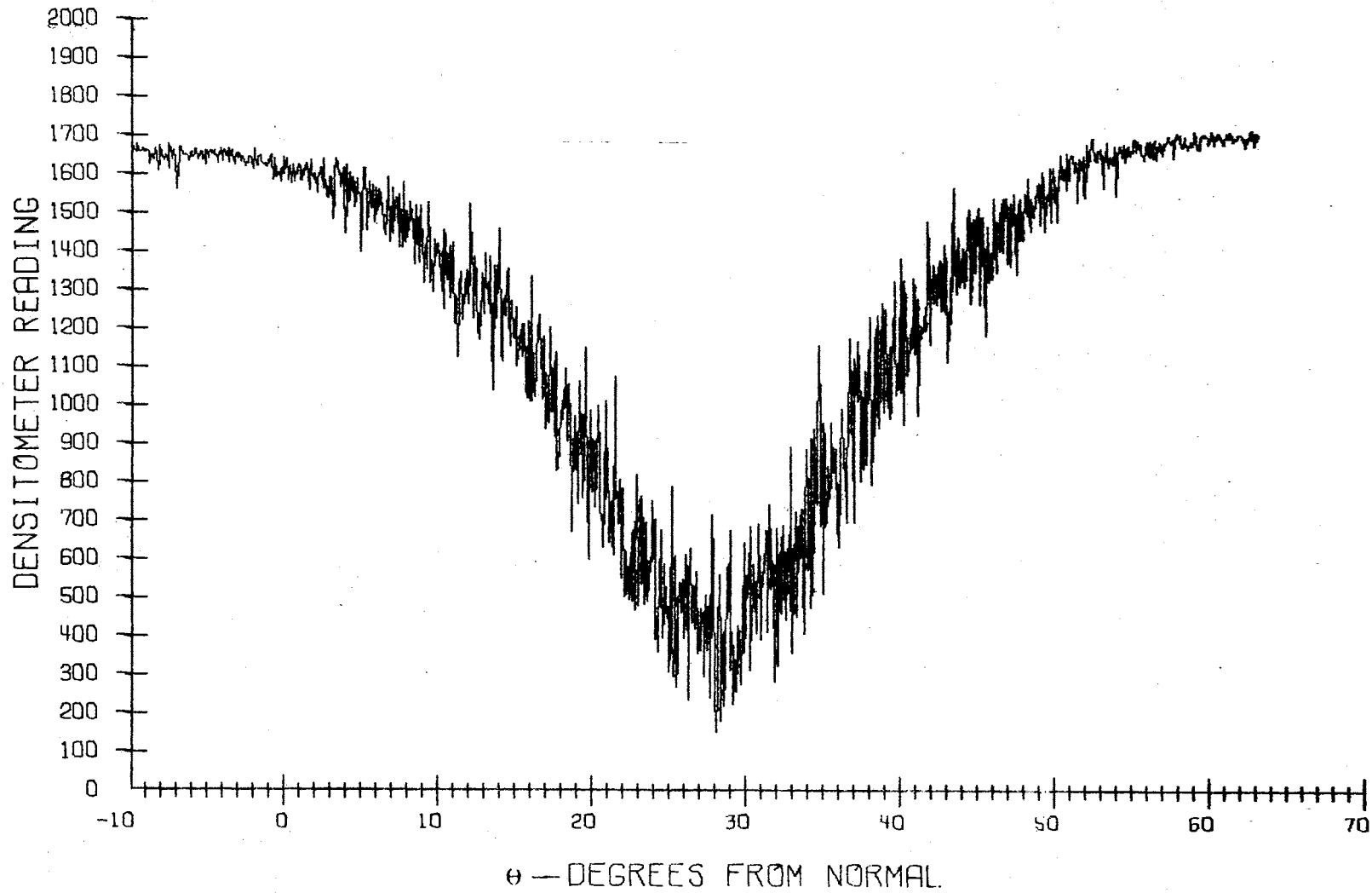


Figure 28. Raw Data - Sample 1 - $\psi = 30^\circ$

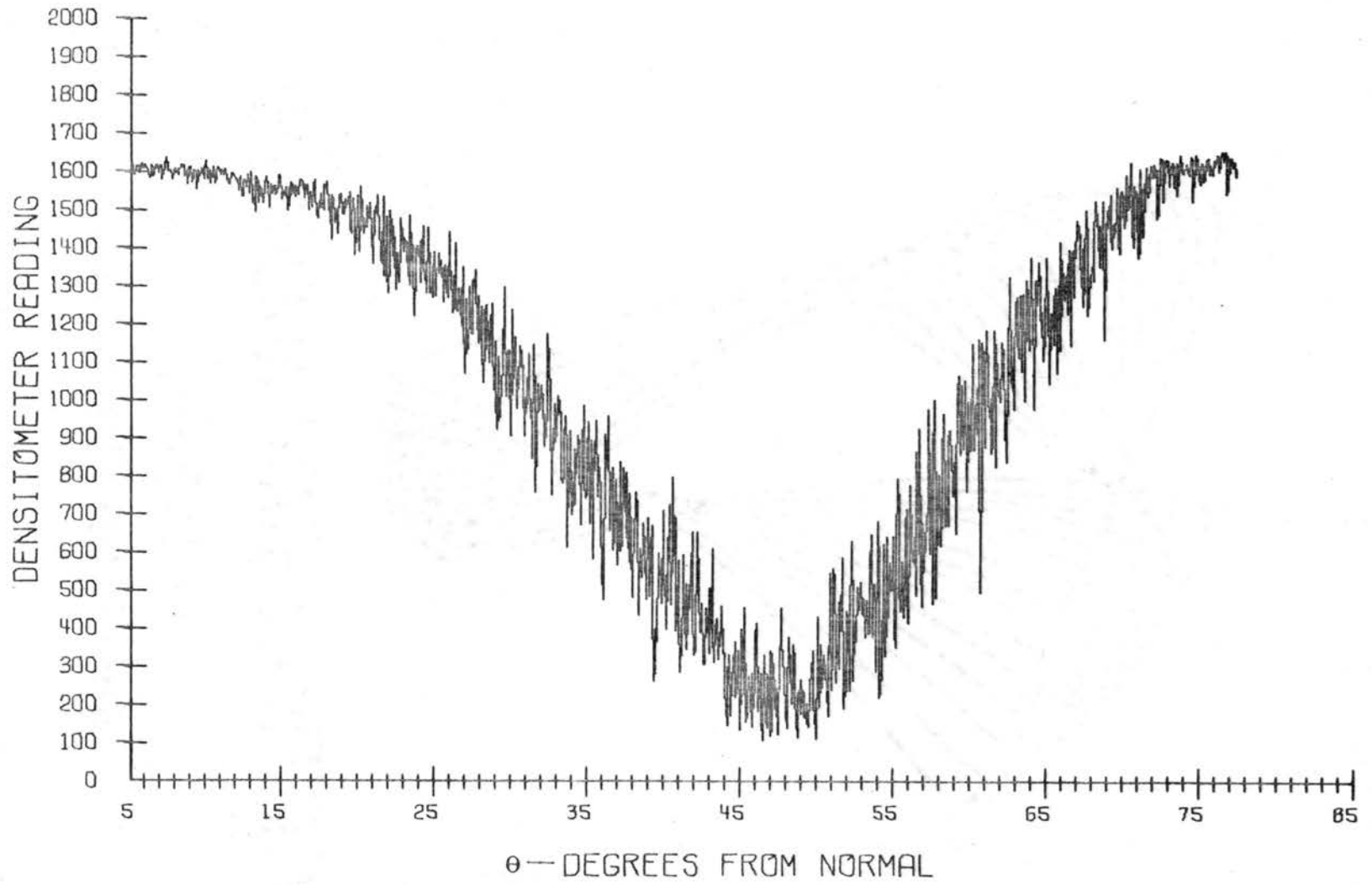


Figure 29. Raw Data - Sample - $\psi = 45^\circ$

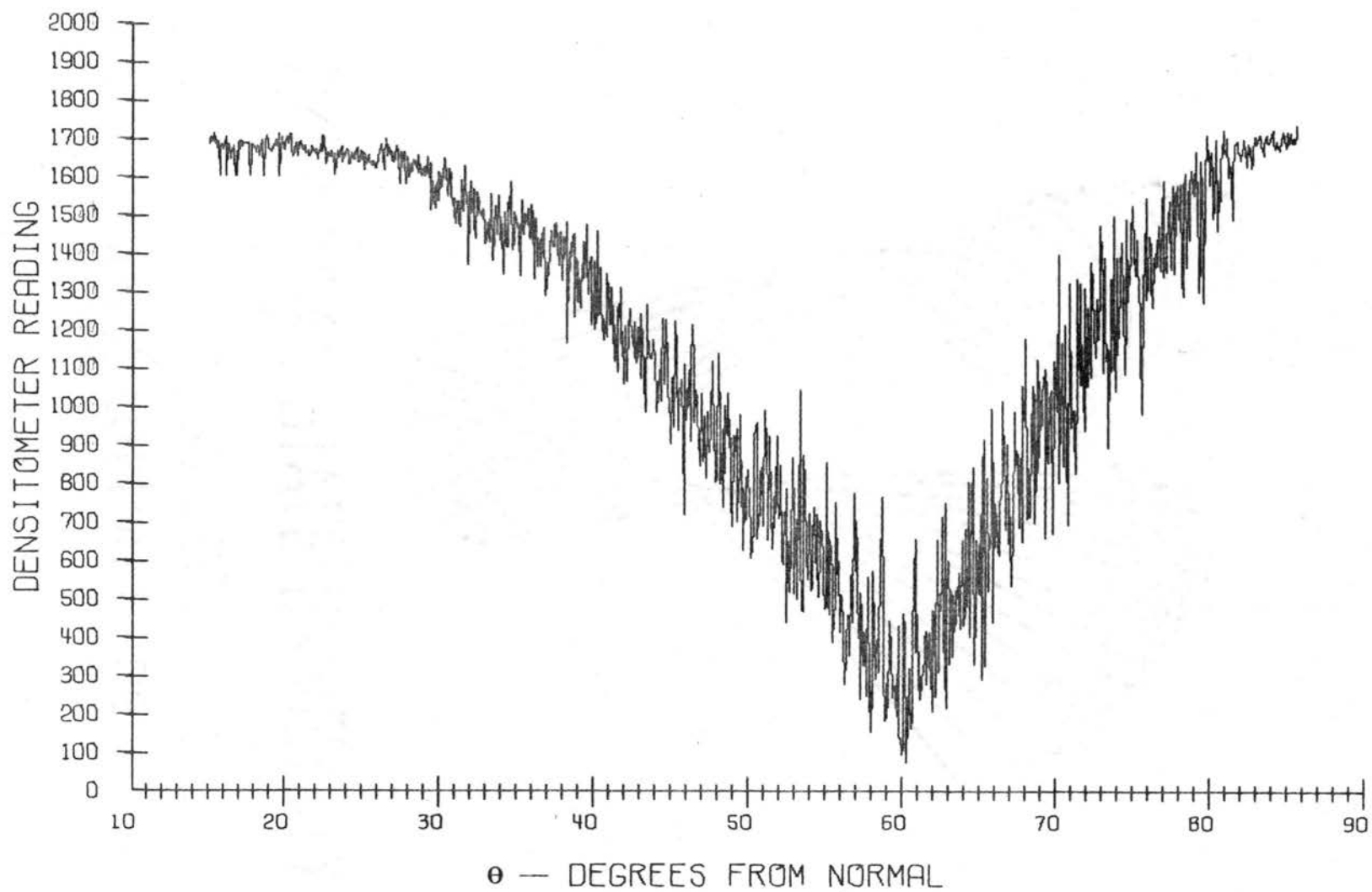


Figure 30. Raw Data - Sample 1 - $\psi = 60^\circ$

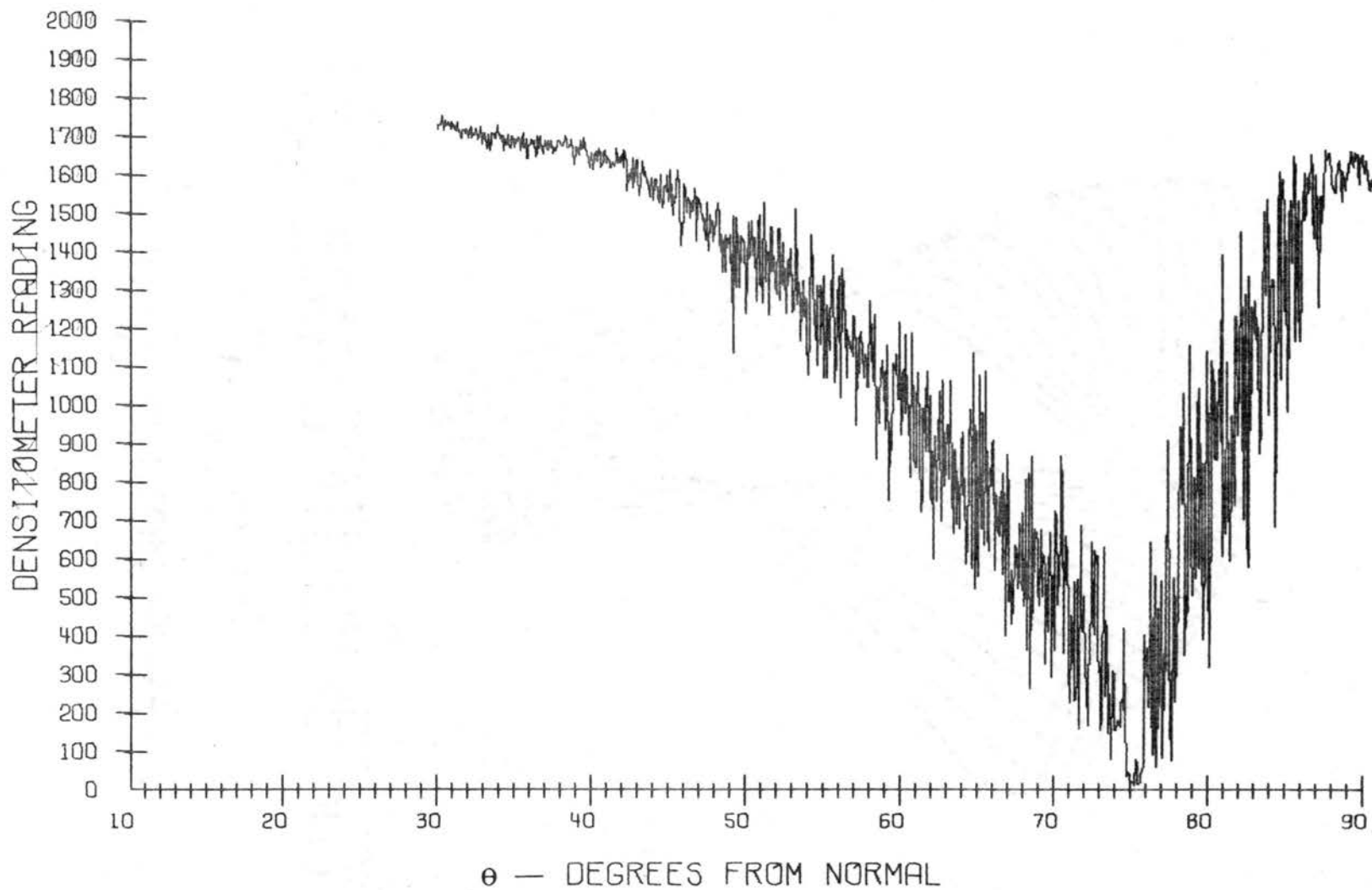


Figure 31. Raw Data - Sample 1 - $\psi = 75^\circ$

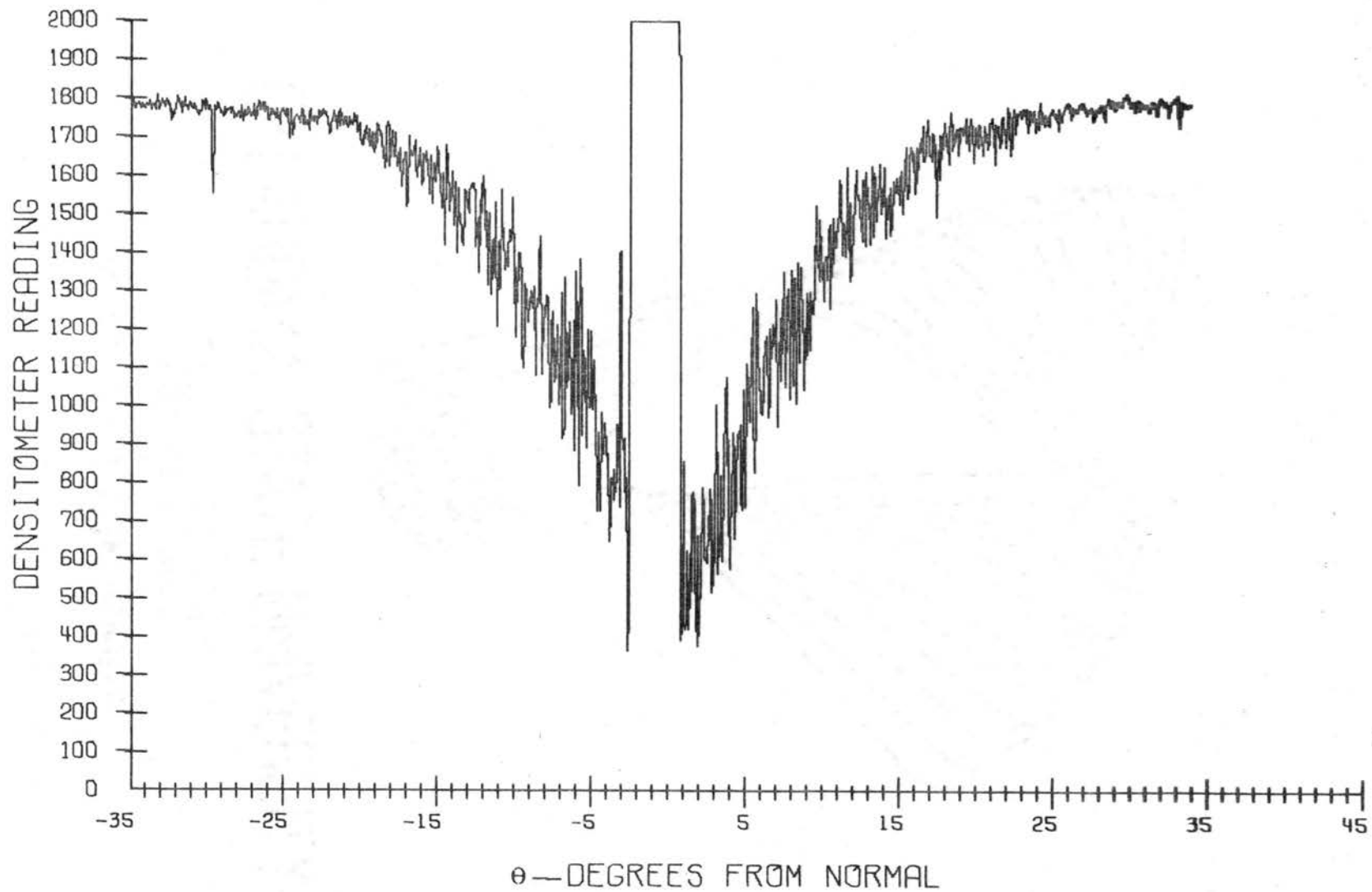


Figure 32. Raw Data—Sample 2— $\psi = 0^\circ$

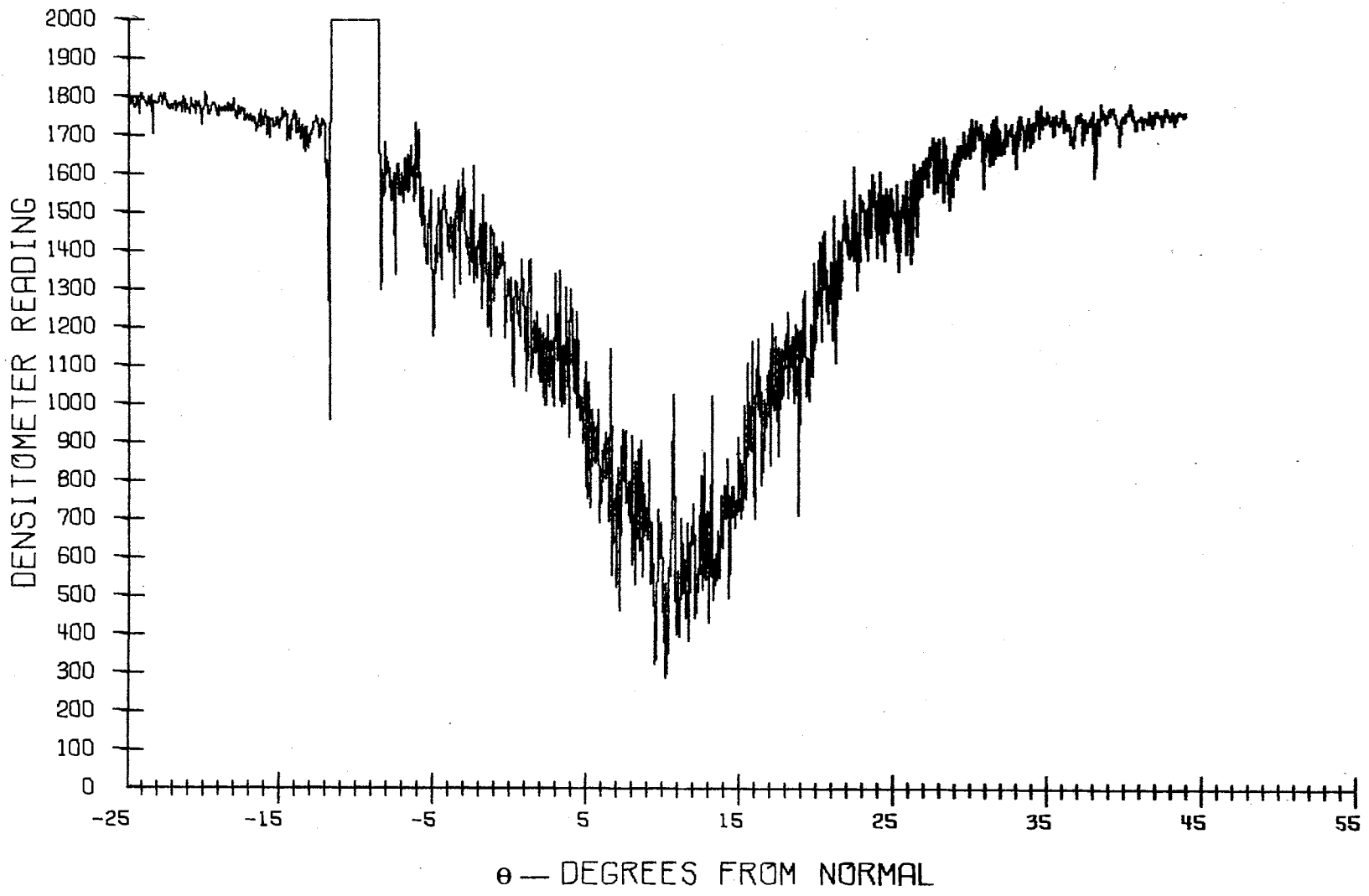


Figure 33. Raw Data—Sample 2— $\psi = 10^\circ$

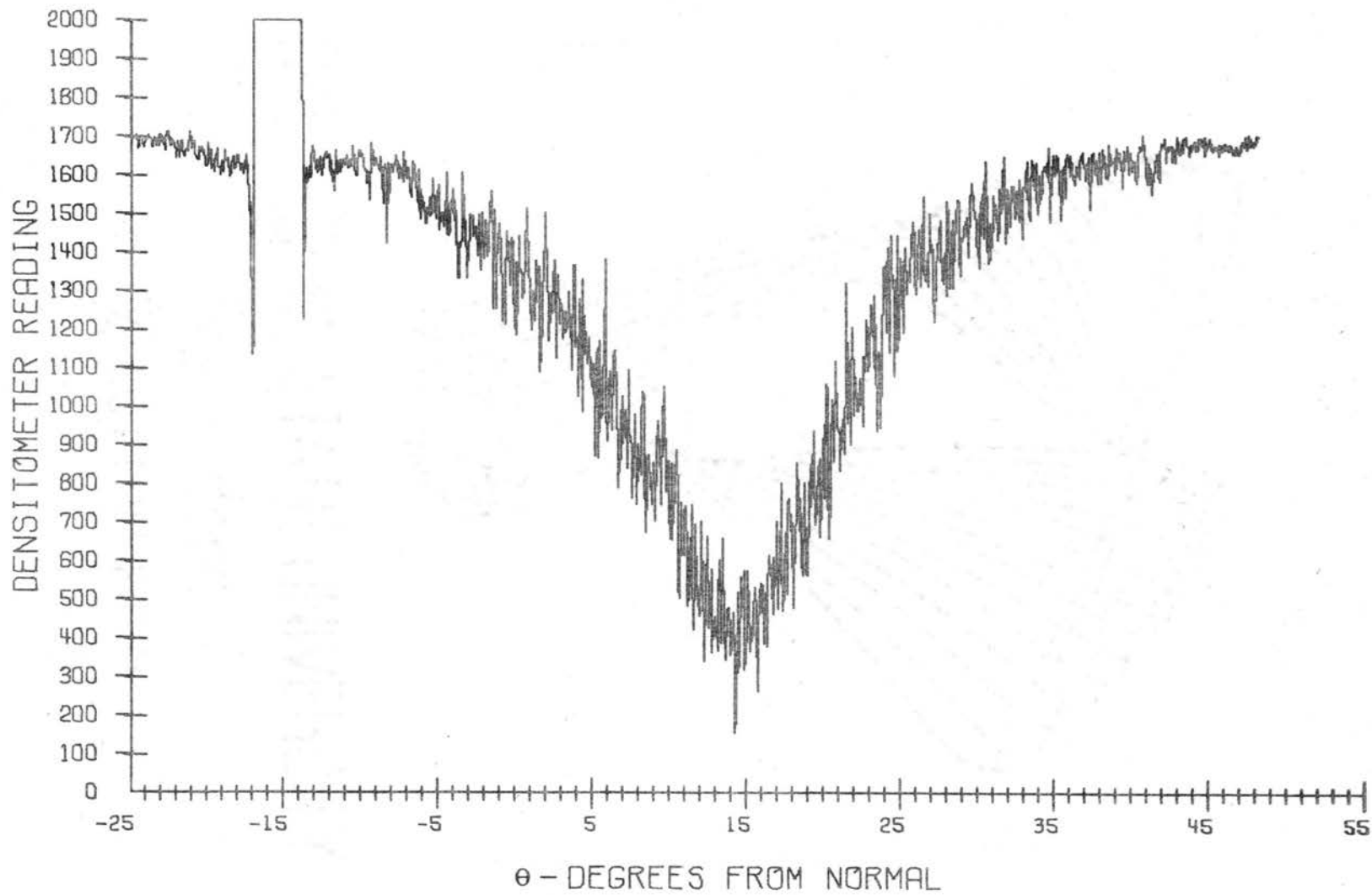


Figure 34. Raw Data—Sample 2— $\psi = 15^\circ$

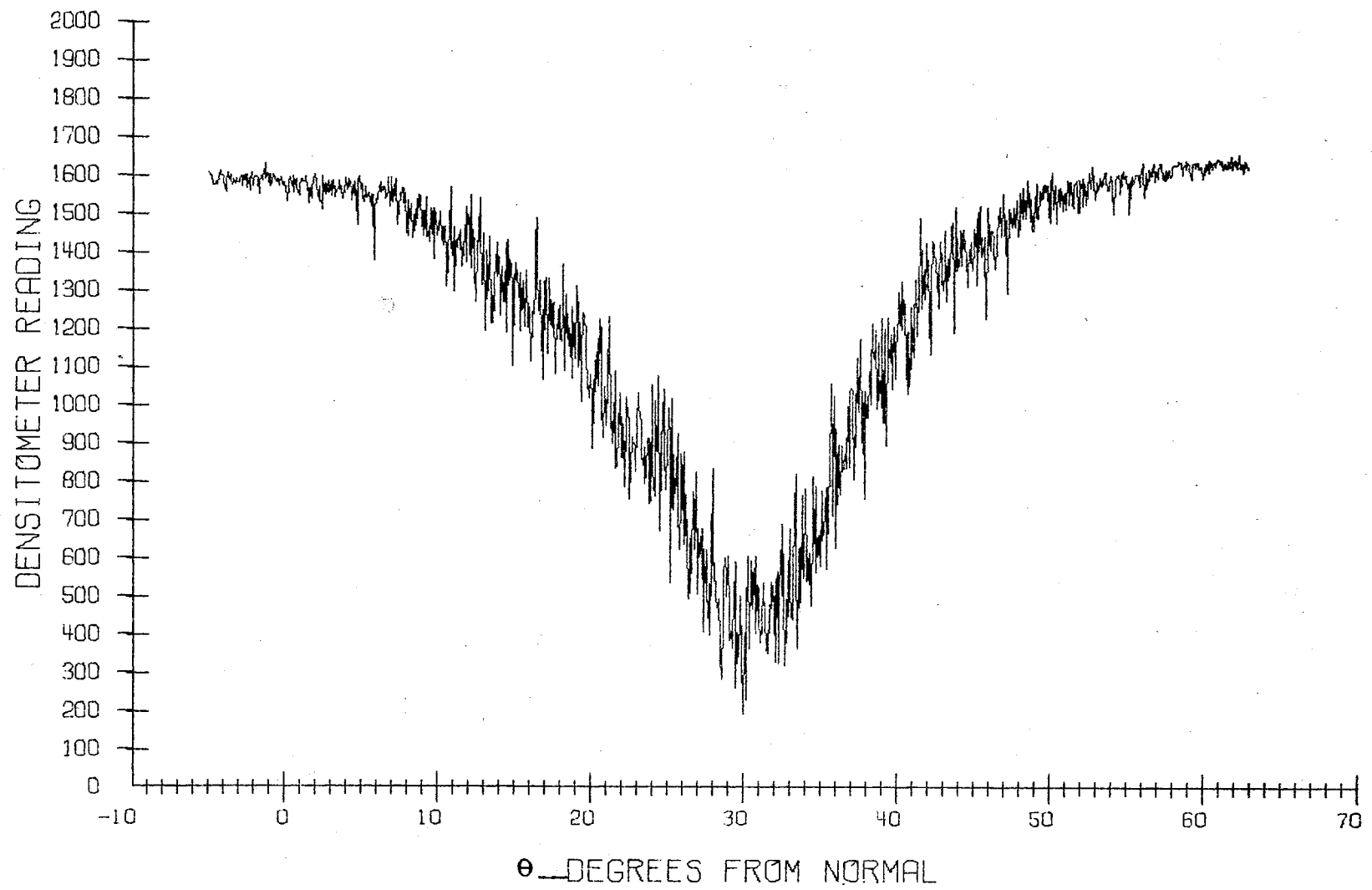


Figure 35. Raw Data—Sample 2— $\psi = 30^\circ$

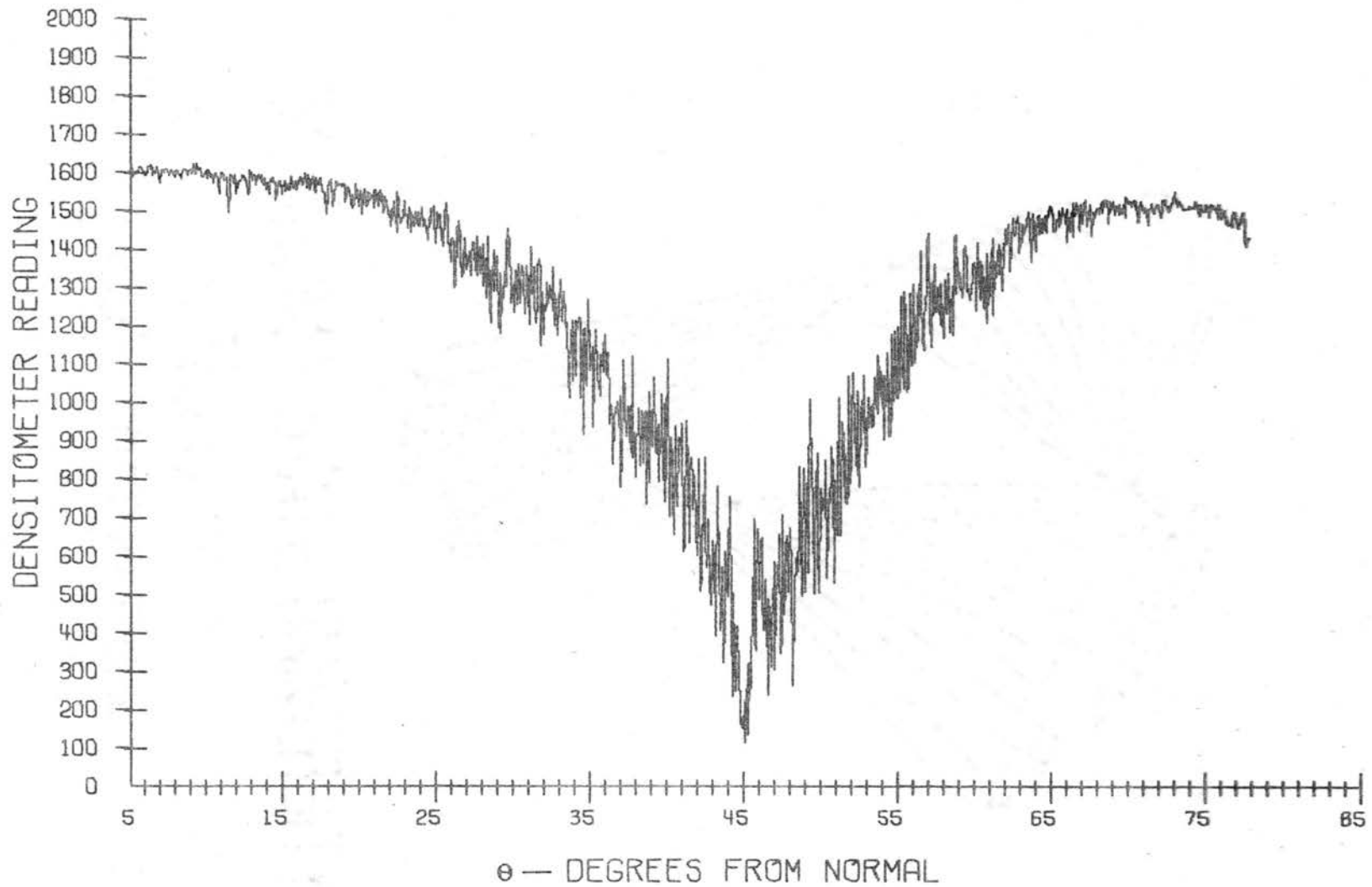


Figure 36. Raw Data - Sample 2 - $\psi = 45^\circ$

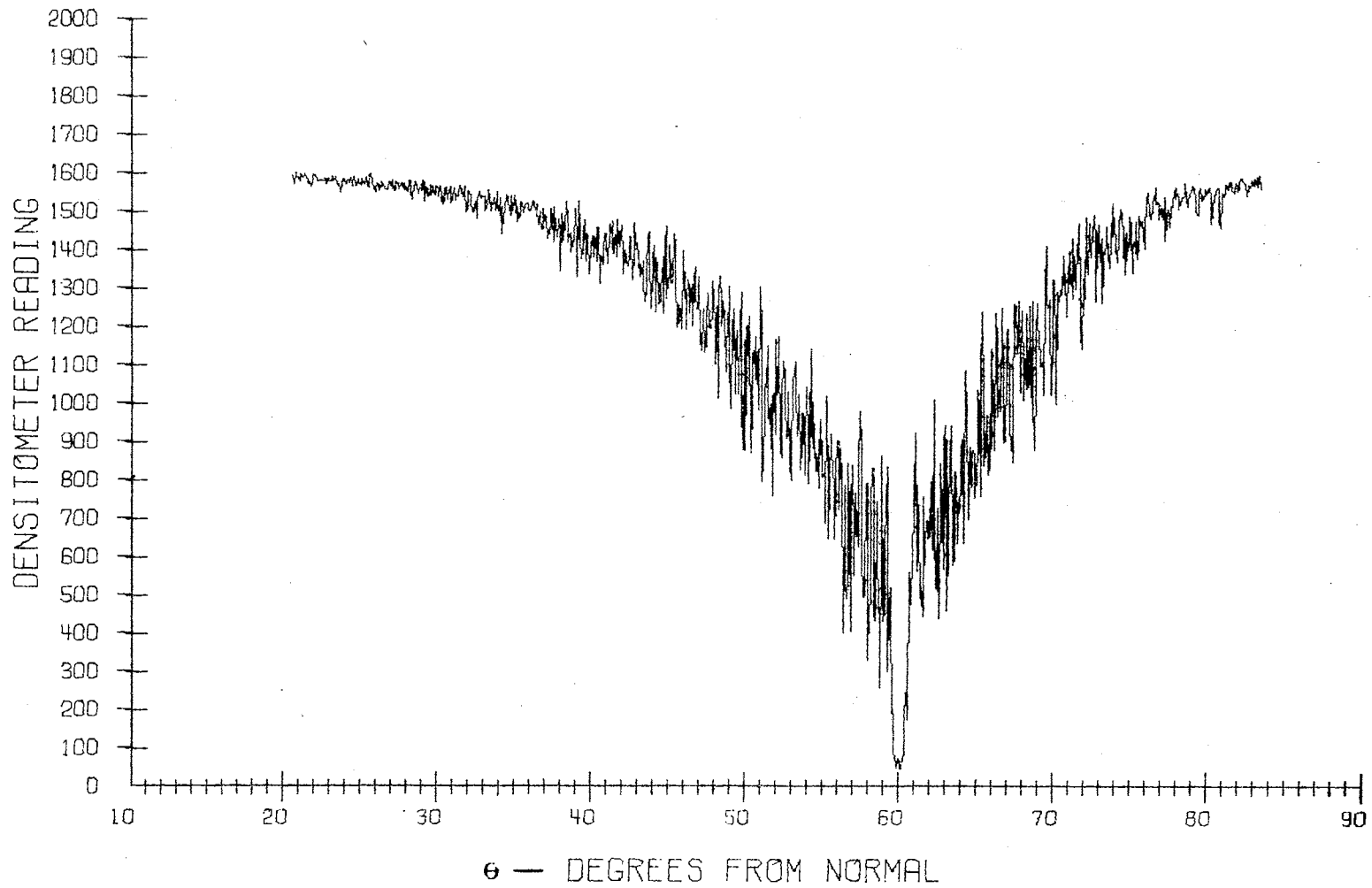


Figure 37. Raw Data - Sample 2 - $\psi = 60^\circ$

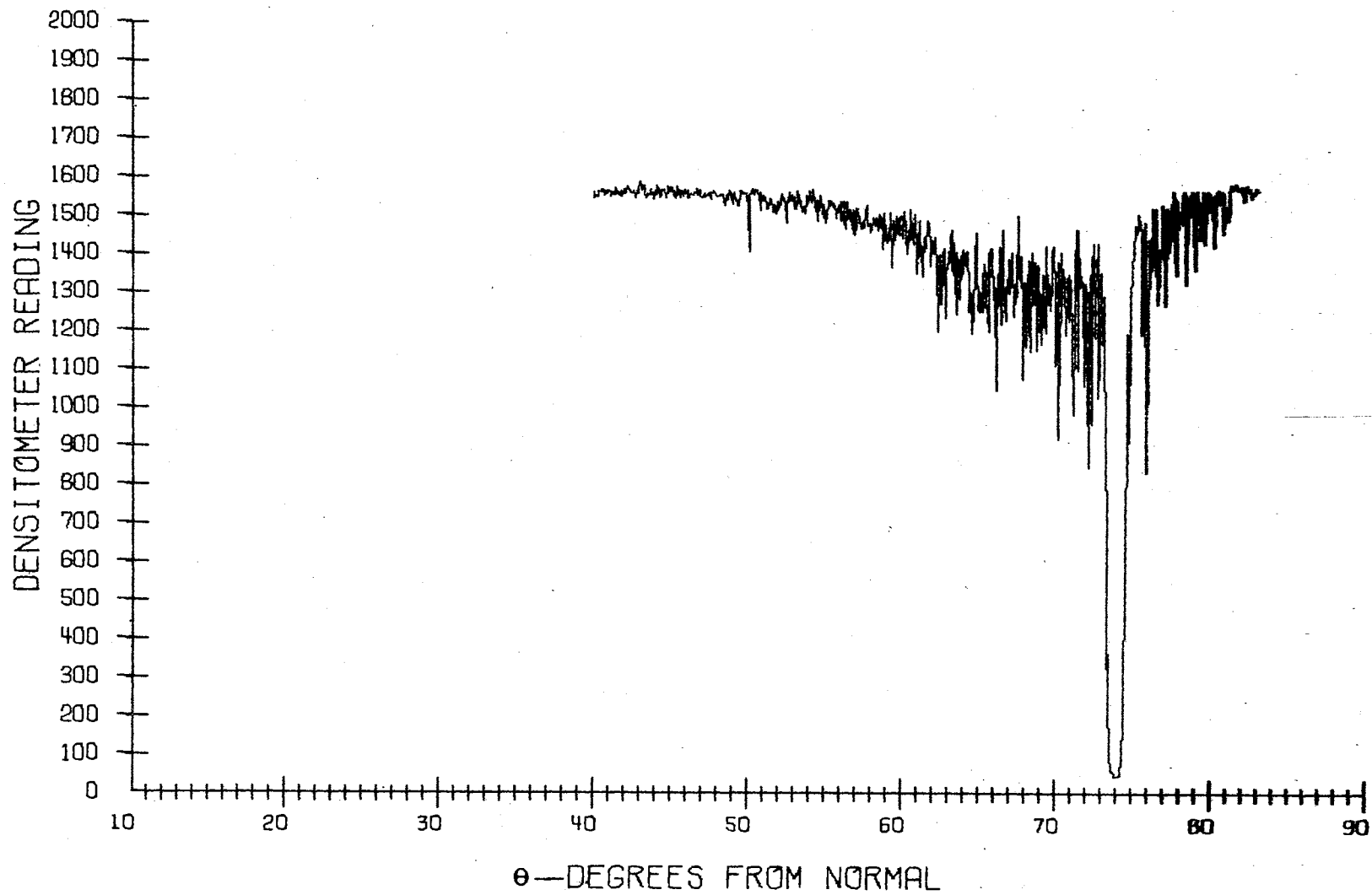


Figure 38. Raw Data - Sample 2 - $\psi = 75^\circ$

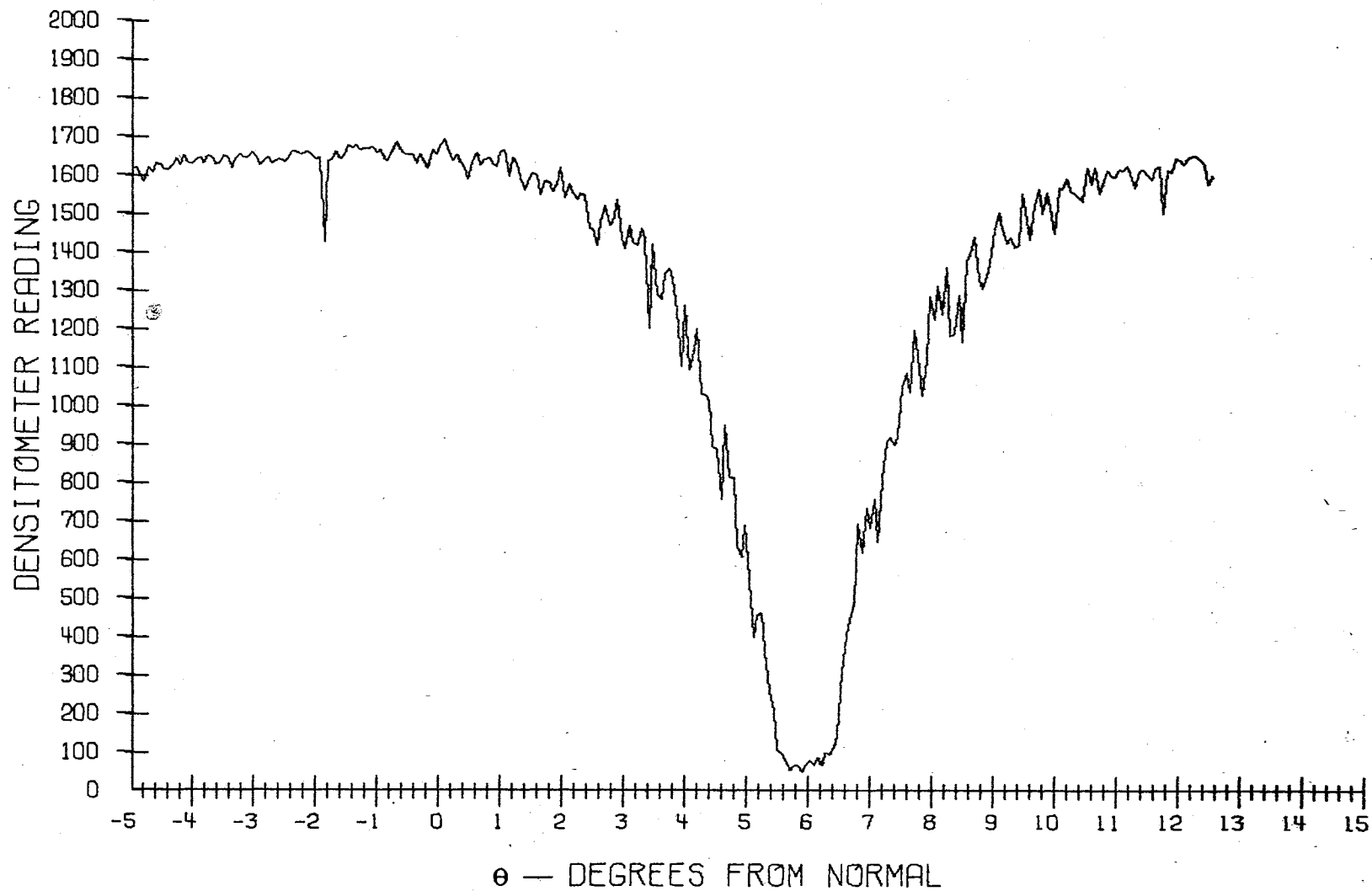


Figure 39. Raw Data - Sample 3 - $\psi = 5^\circ$

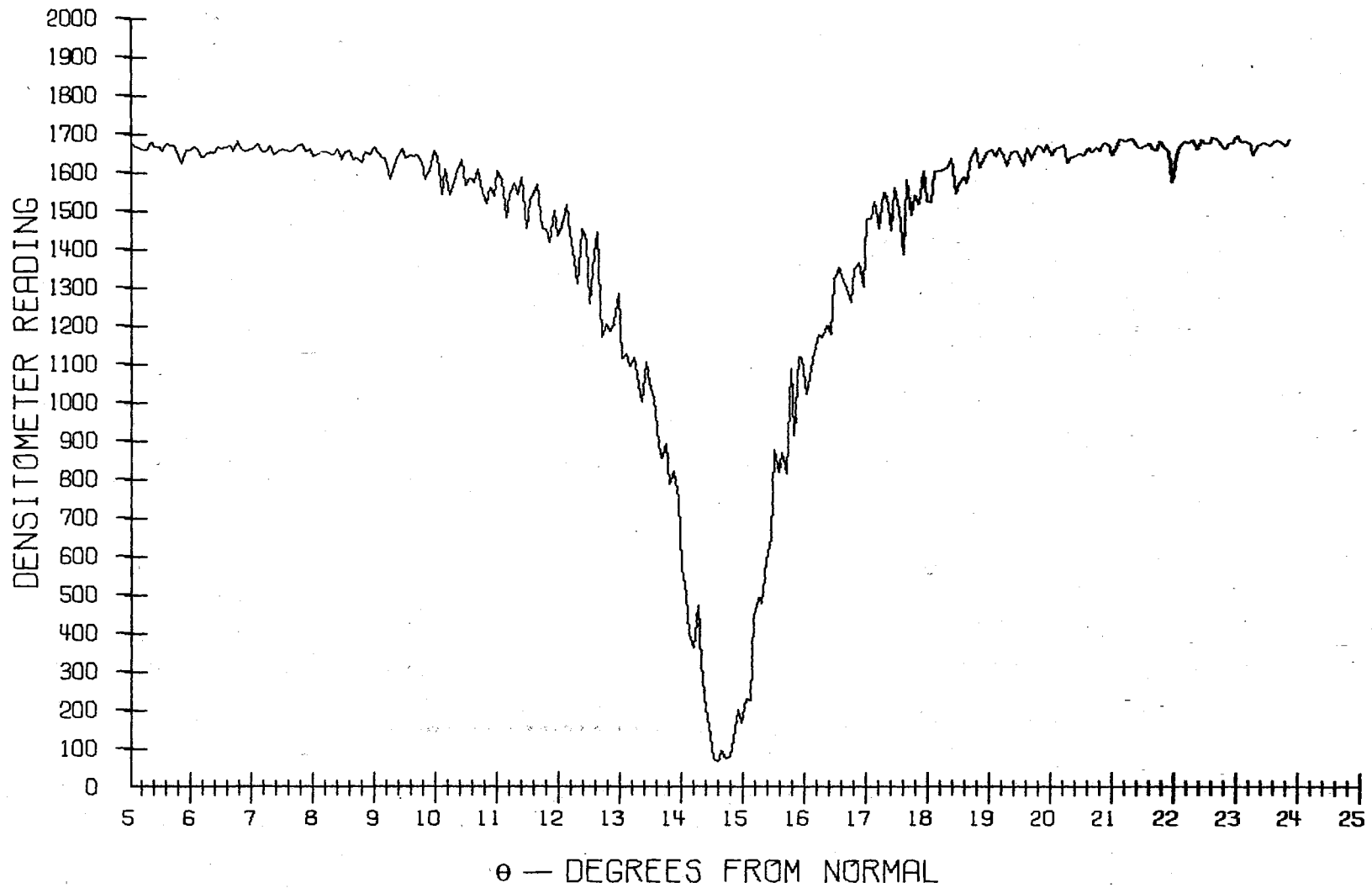


Figure 40. Raw Data - Sample 3 - $\psi = 15^\circ$

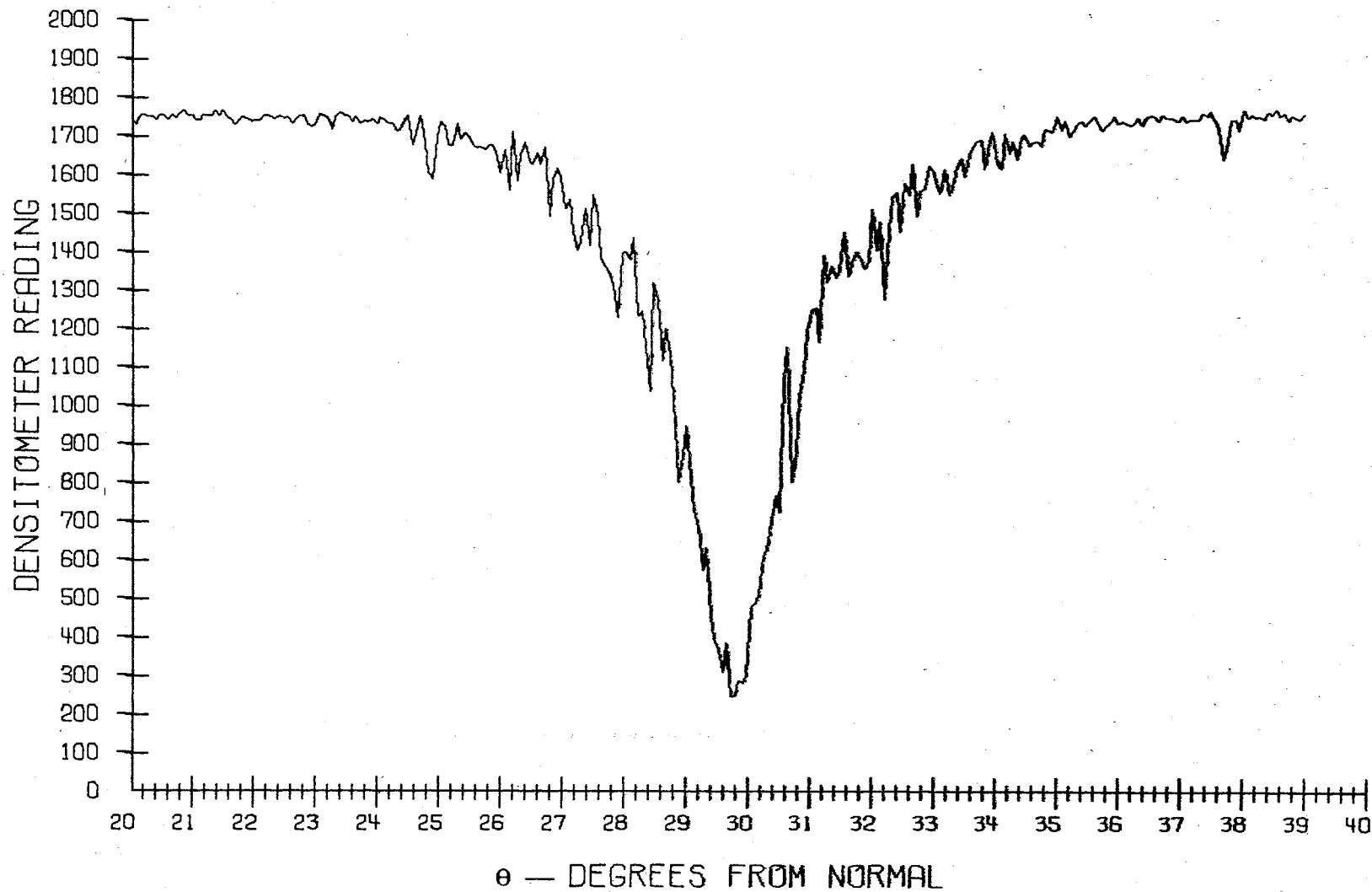


Figure 41. Raw Data - Sample - $\psi = 30^\circ$

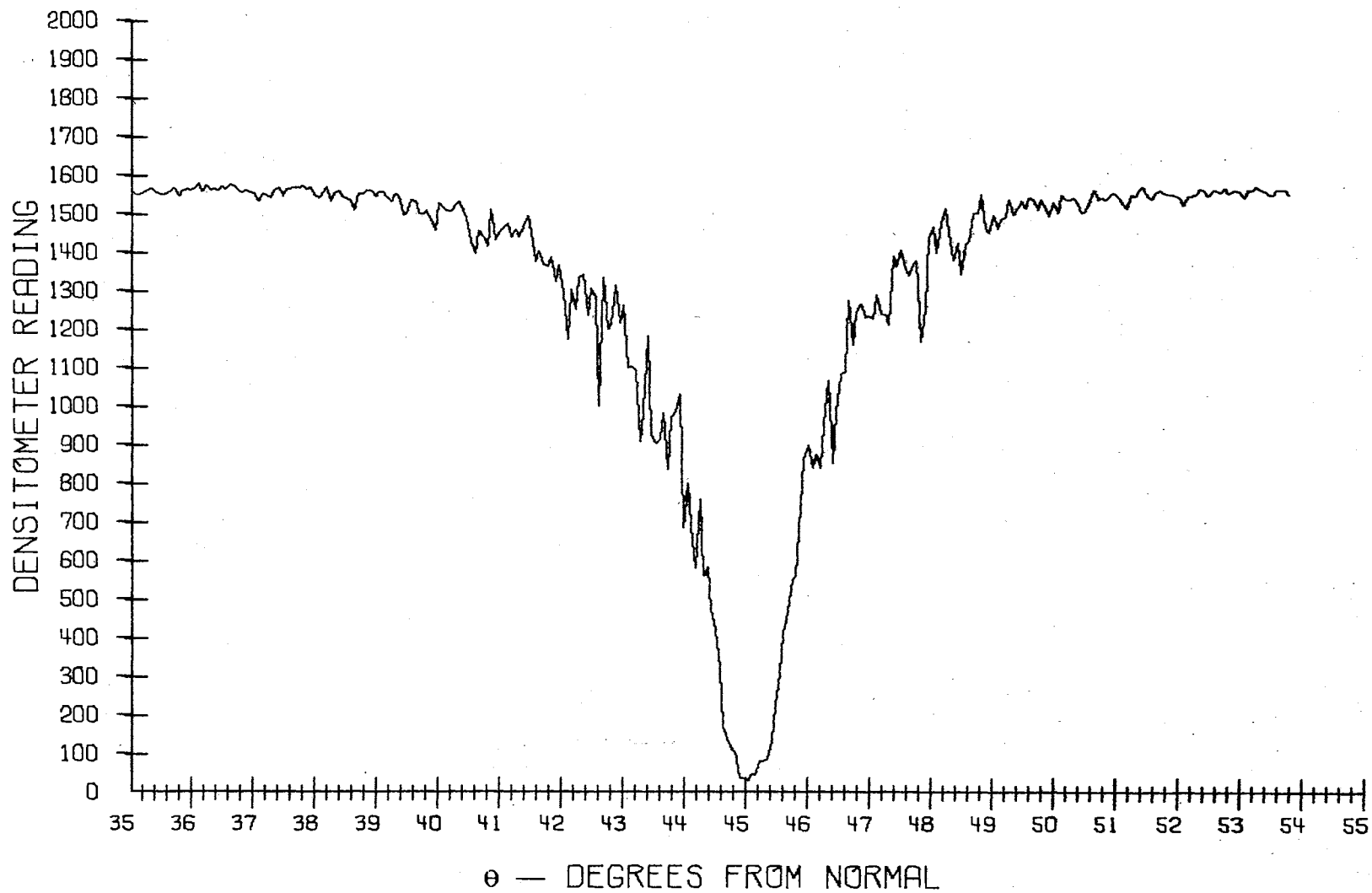


Figure 42. Raw Data - Sample 3 - $\psi = 45^\circ$

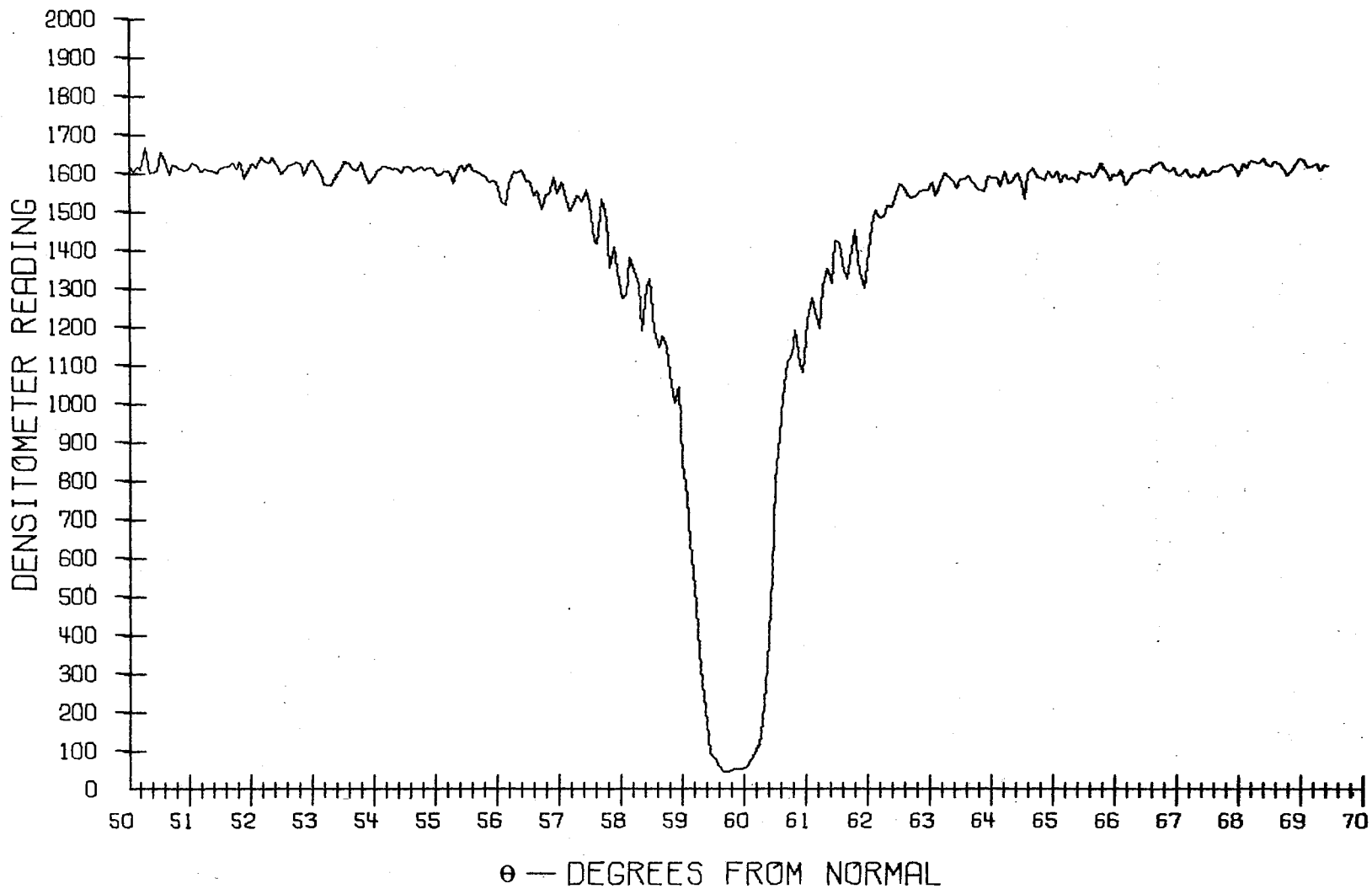


Figure 43. Raw - Sample 3 - $\psi = 60^\circ$

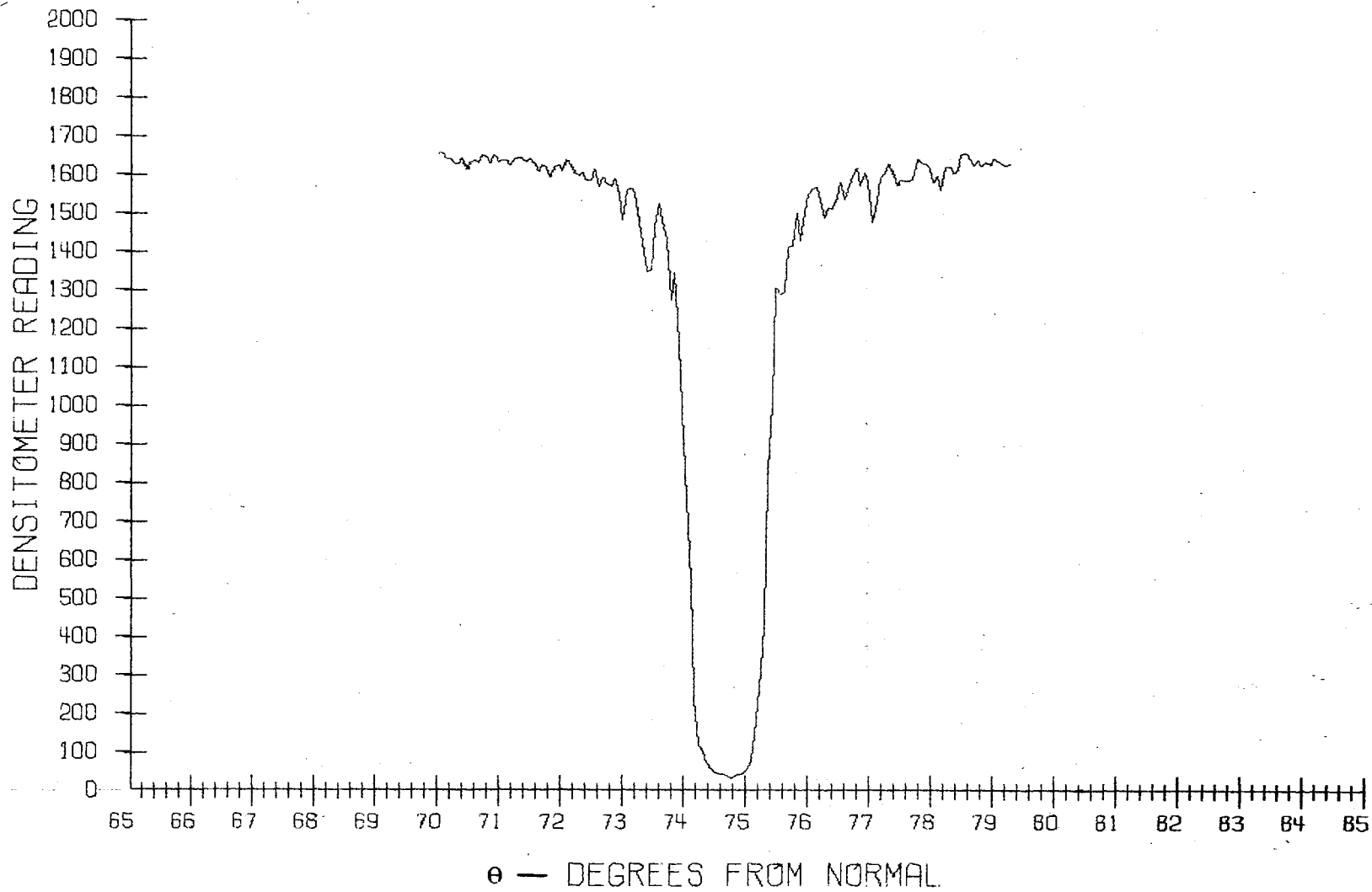


Figure 44. Raw Data - Sample 3 - $\psi = 75^\circ$

APPENDIX B
THEORETICAL PREDICTIONS
VERSUS DATA

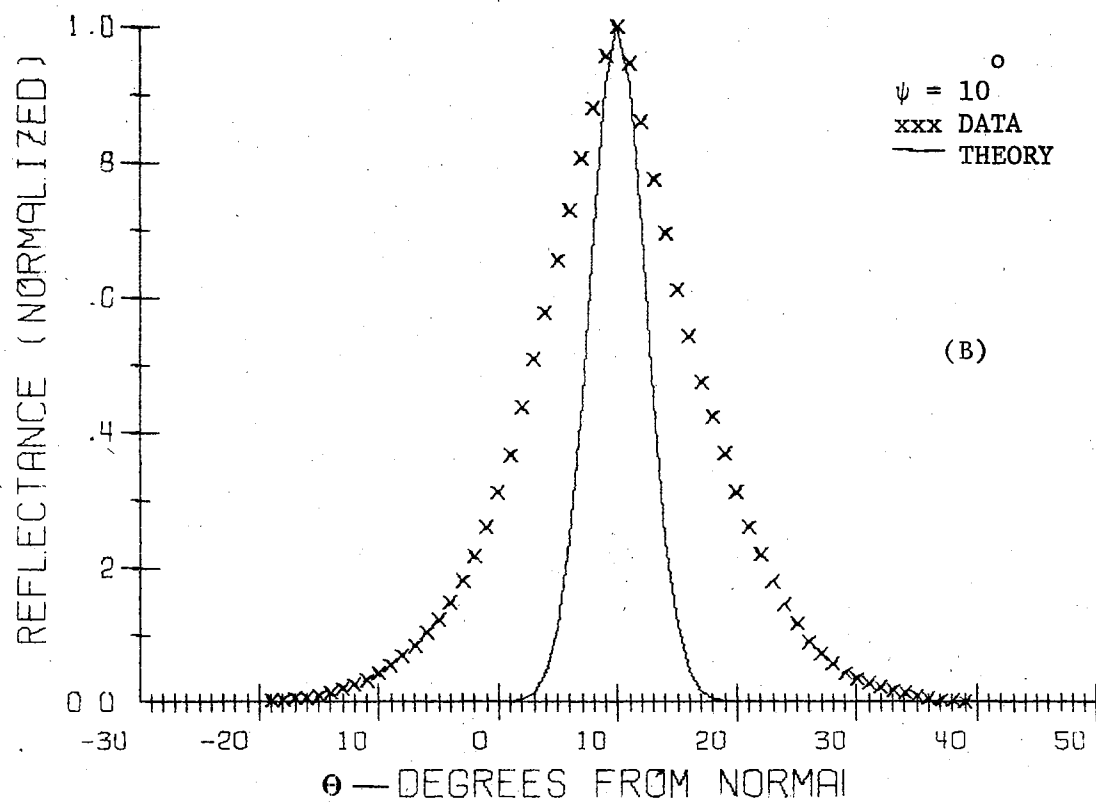
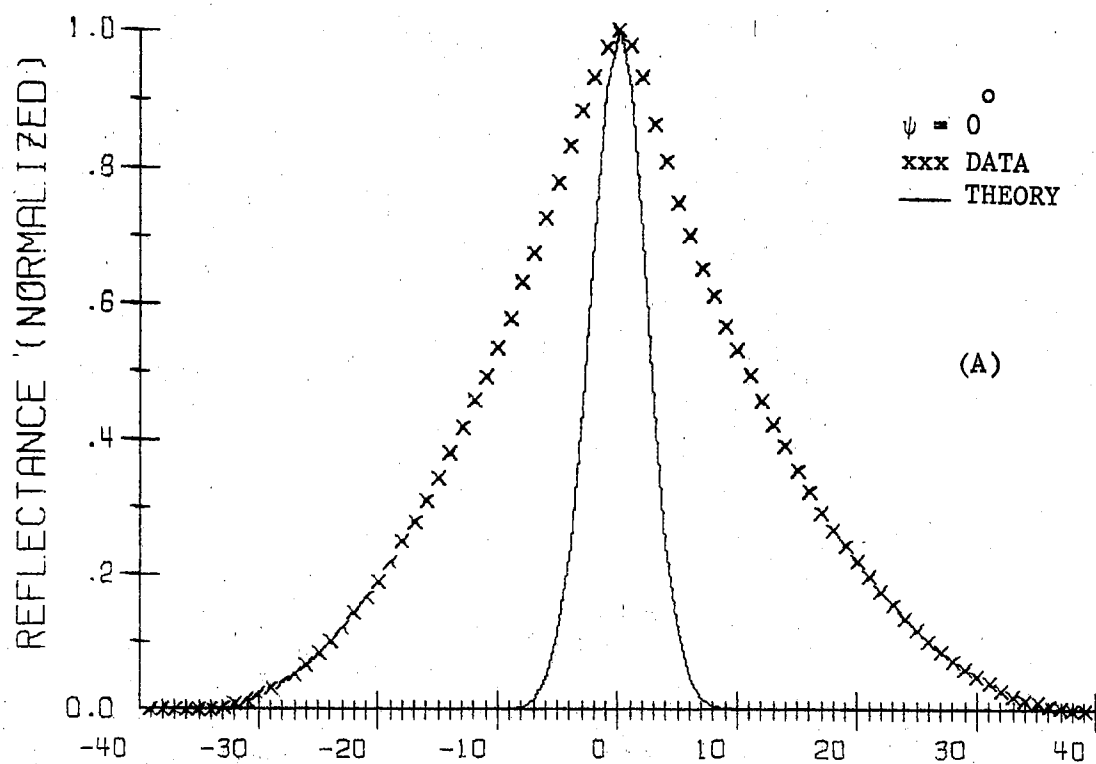


Figure 45. Theory Versus Data - Sample 1 - $\psi = 0^\circ$ and 10°

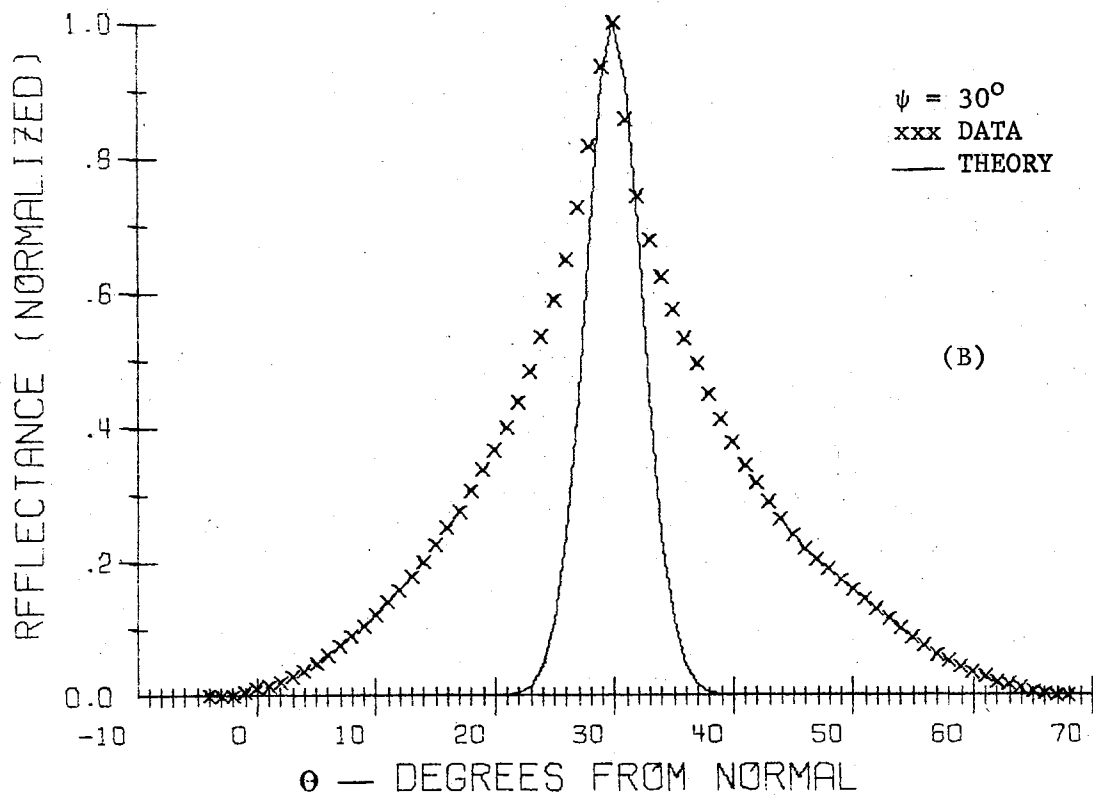
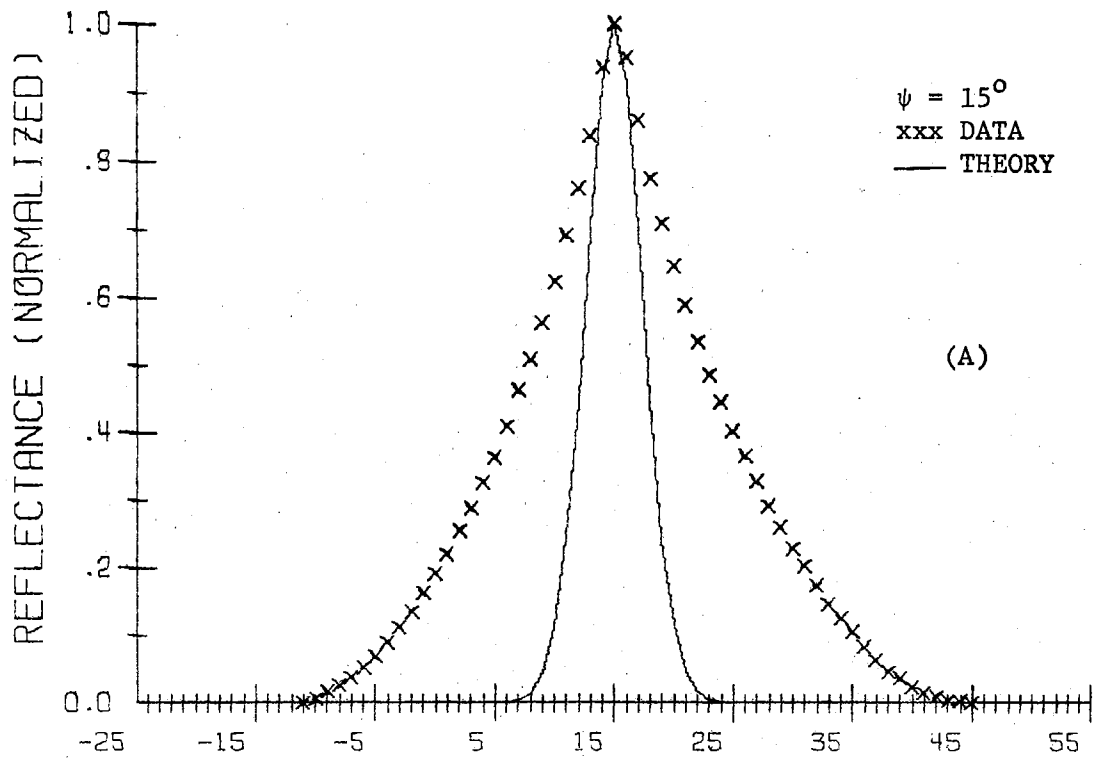


Figure 46. Theory Versus Data - Sample 1 - $\psi = 15^\circ$ and 30°

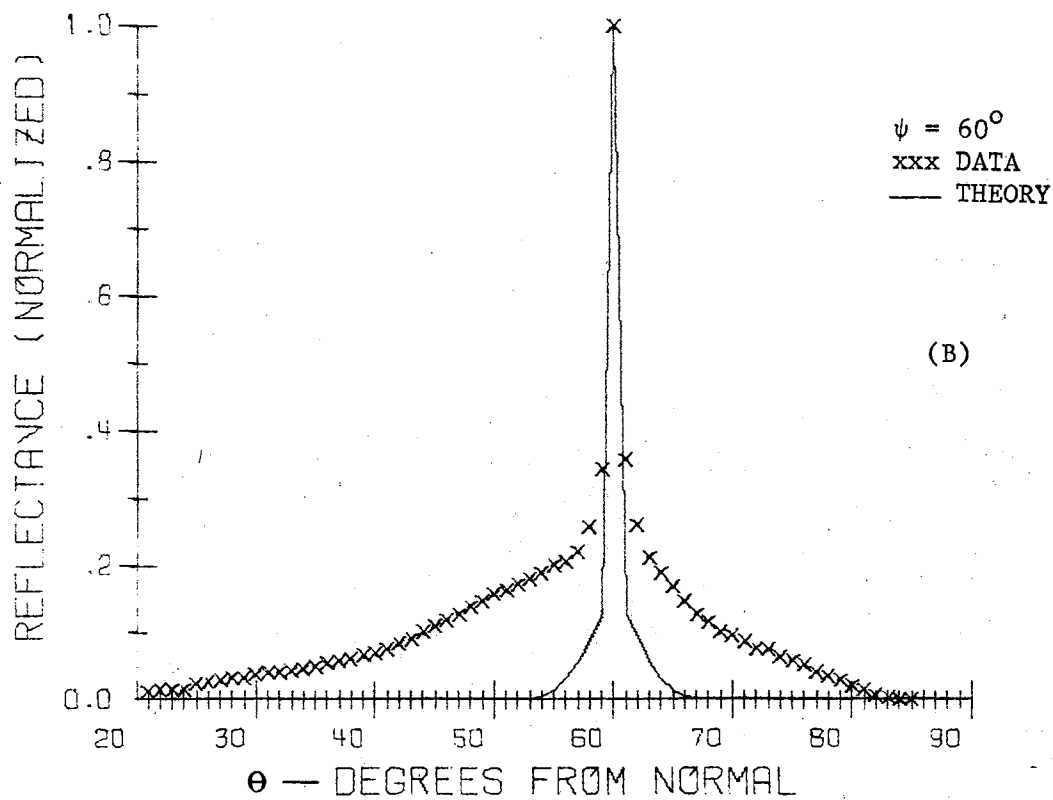
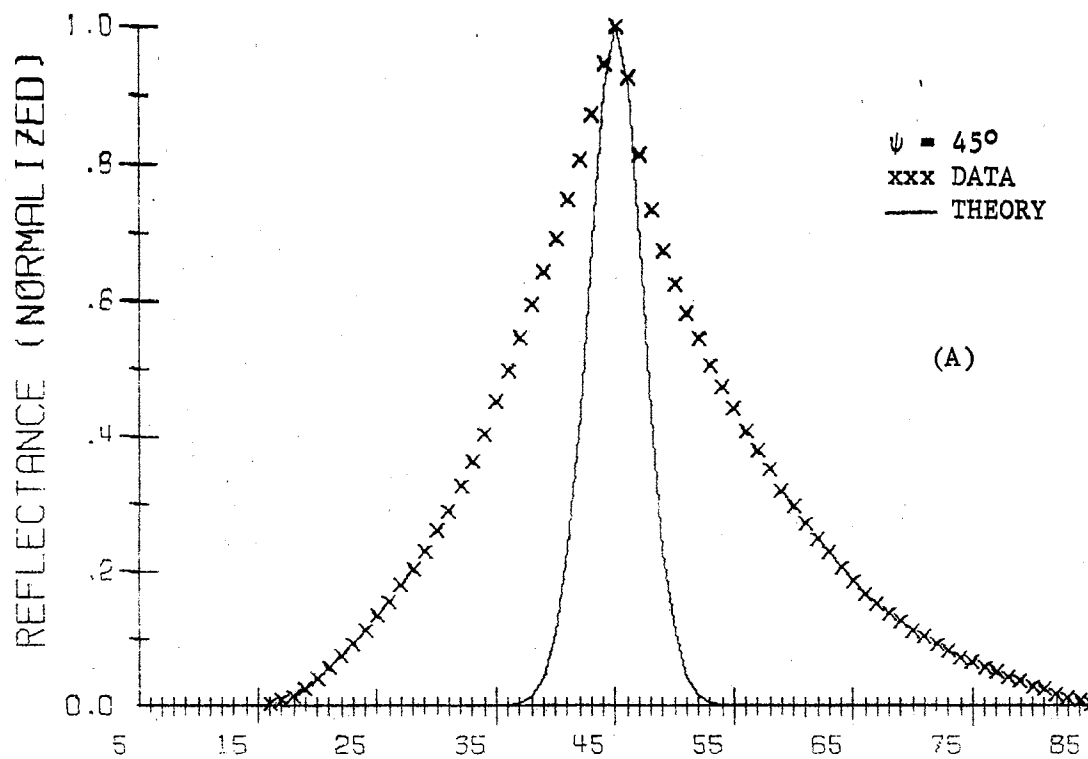


Figure 47. Theory Versus Data - Sample 1 - $\psi = 45^\circ$ and 60°

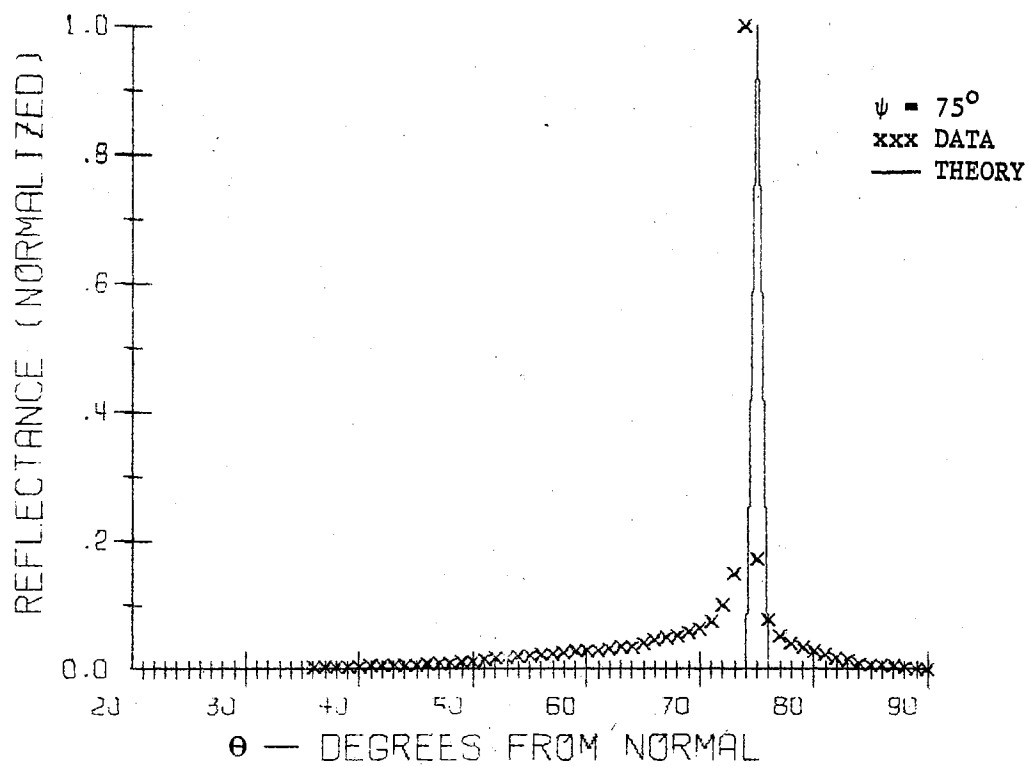


Figure 48. Theory Versus Data - Sample 1 -
 $\psi = 75^\circ$

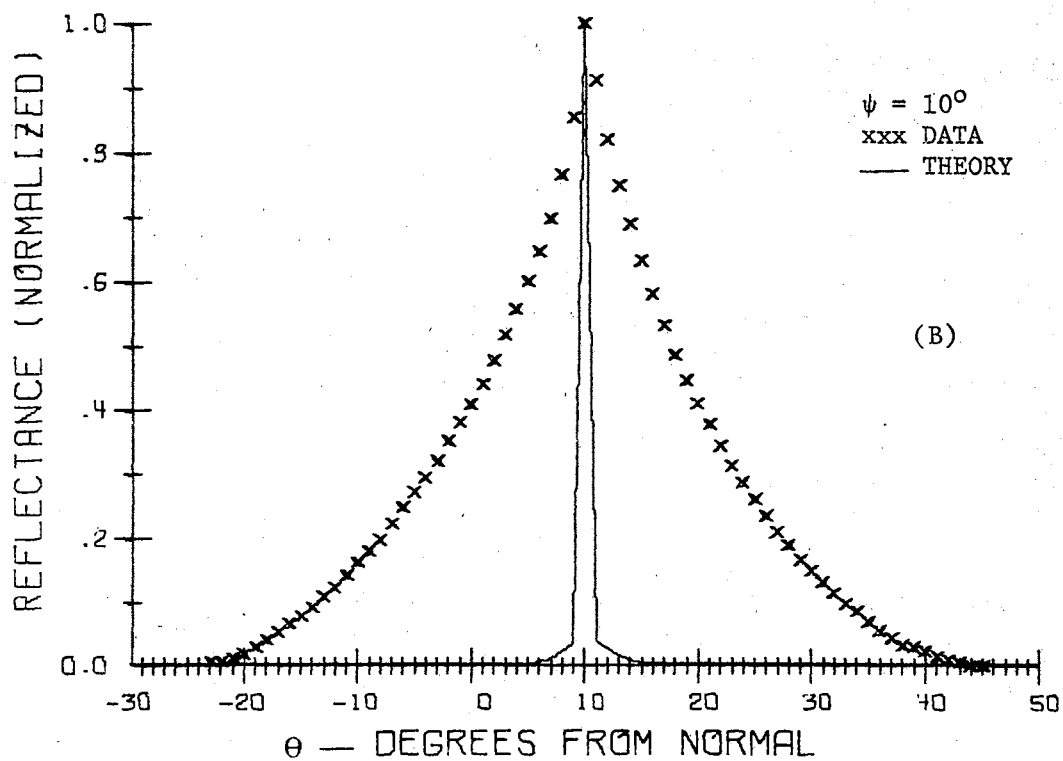
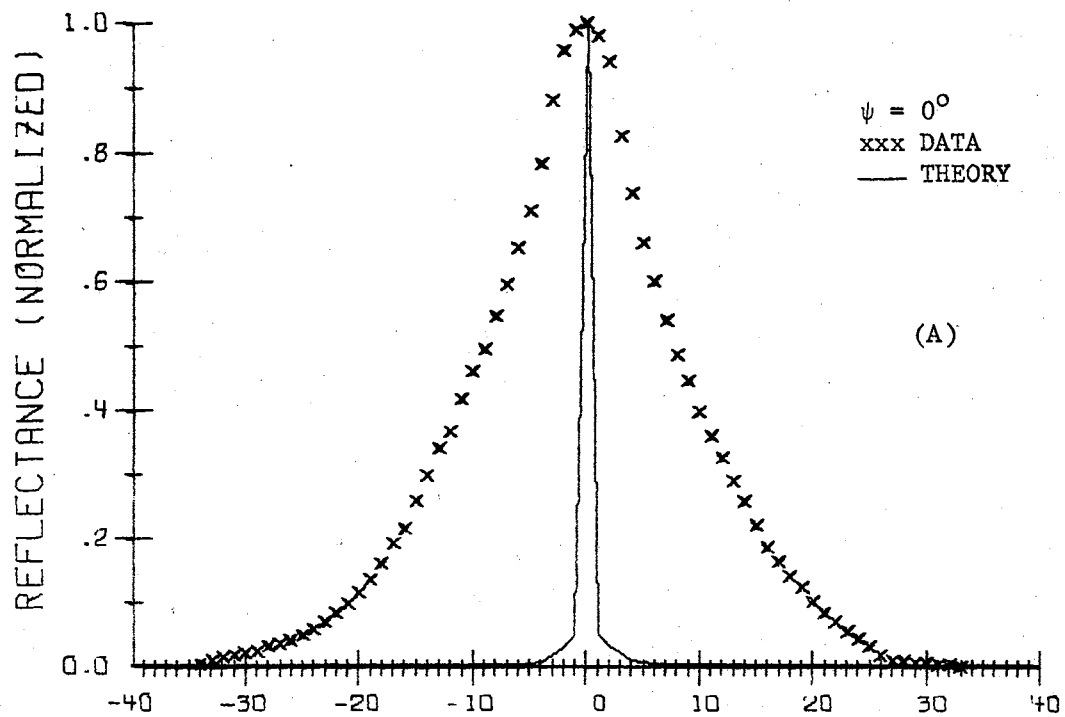


Figure 49. Theory Versus Data - Sample 2 - $\psi = 0^\circ$ and 10°

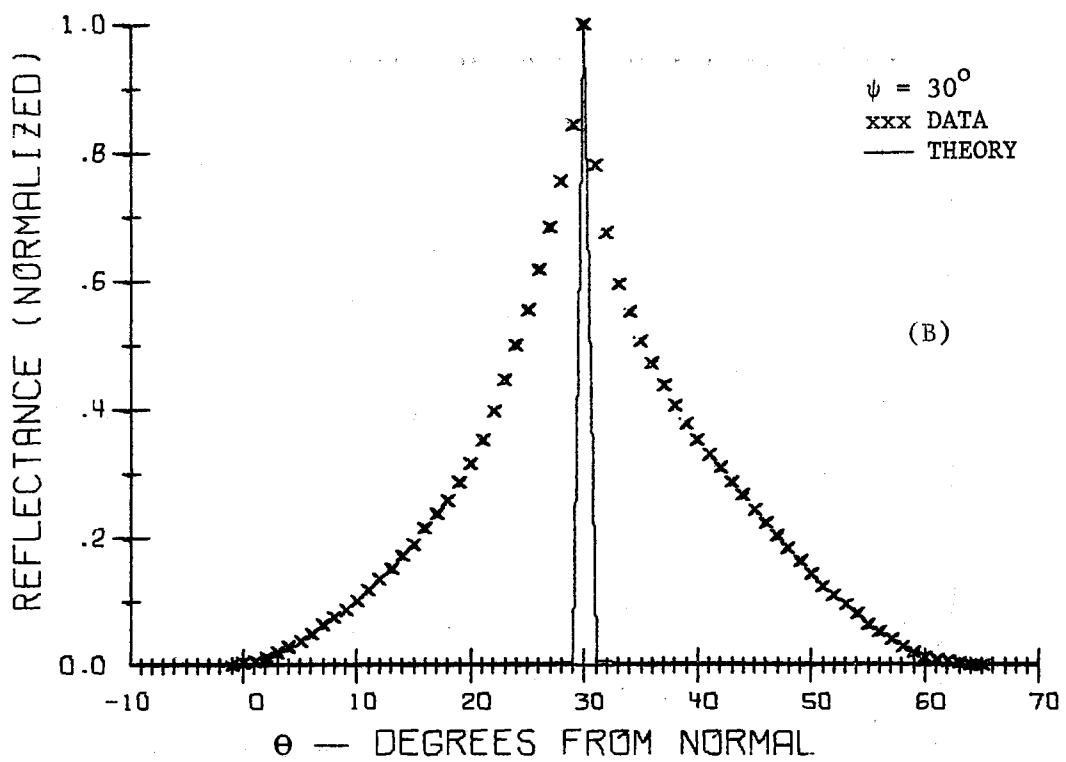
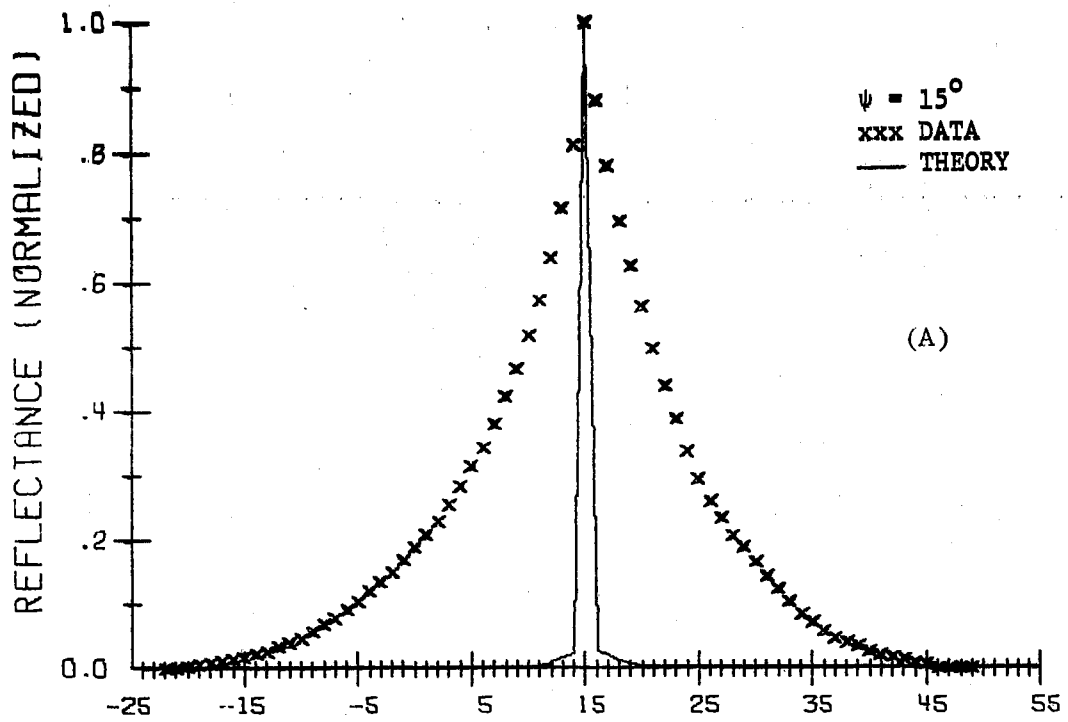


Figure 50. Theory Versus Data - Sample 2 - $\psi = 15^\circ$ and 30°

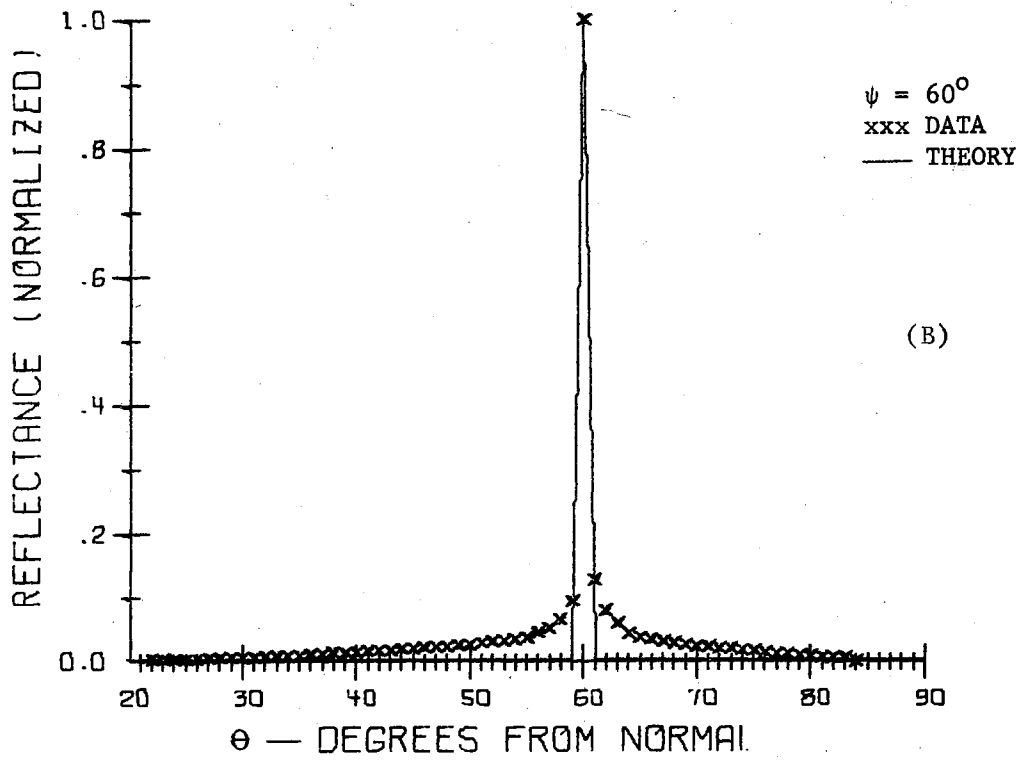
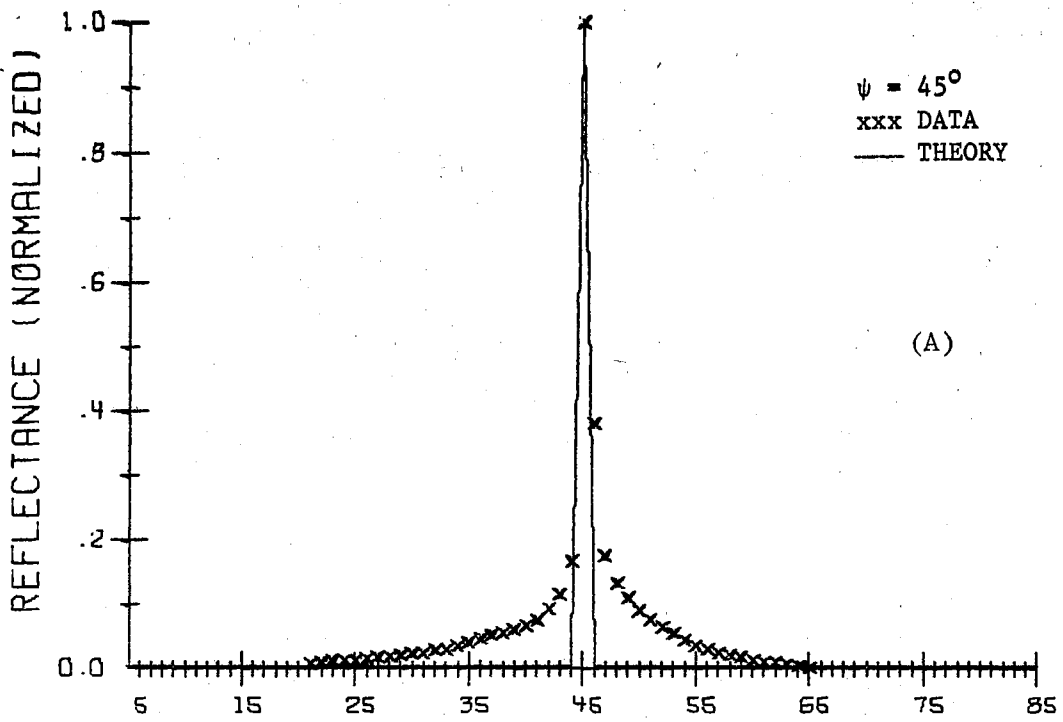


Figure 51. Theory Versus Data - Sample 2 - $\psi = 45^\circ$ and 60°

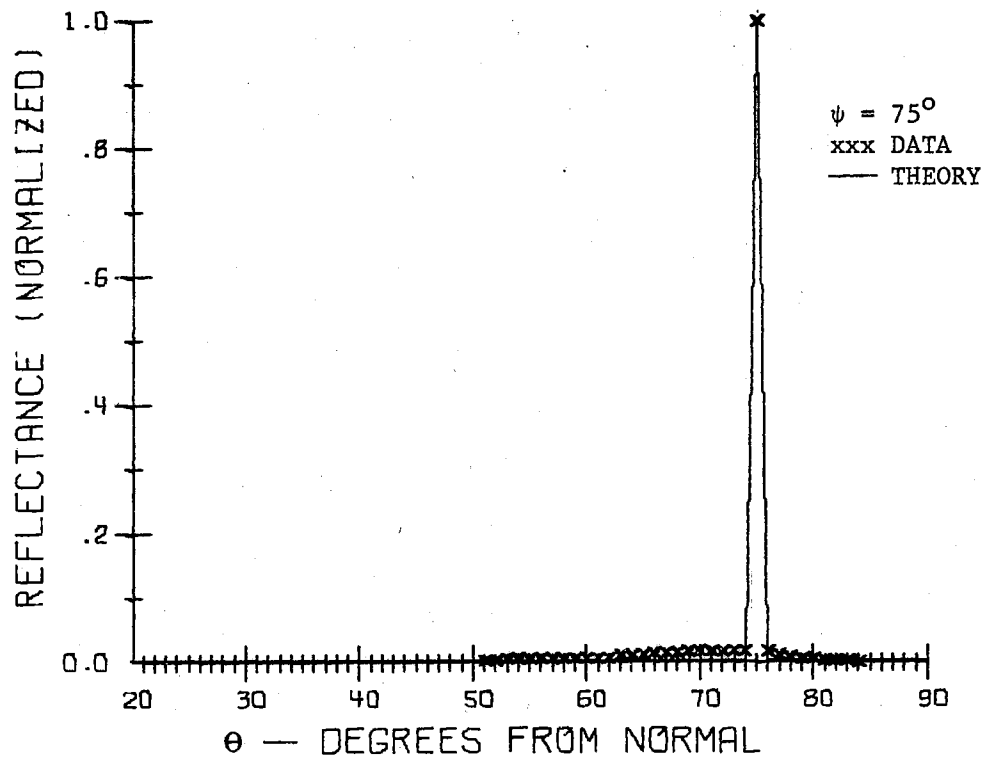


Figure 52. Theory Versus Data - Sample 2 - $\psi = 75^\circ$

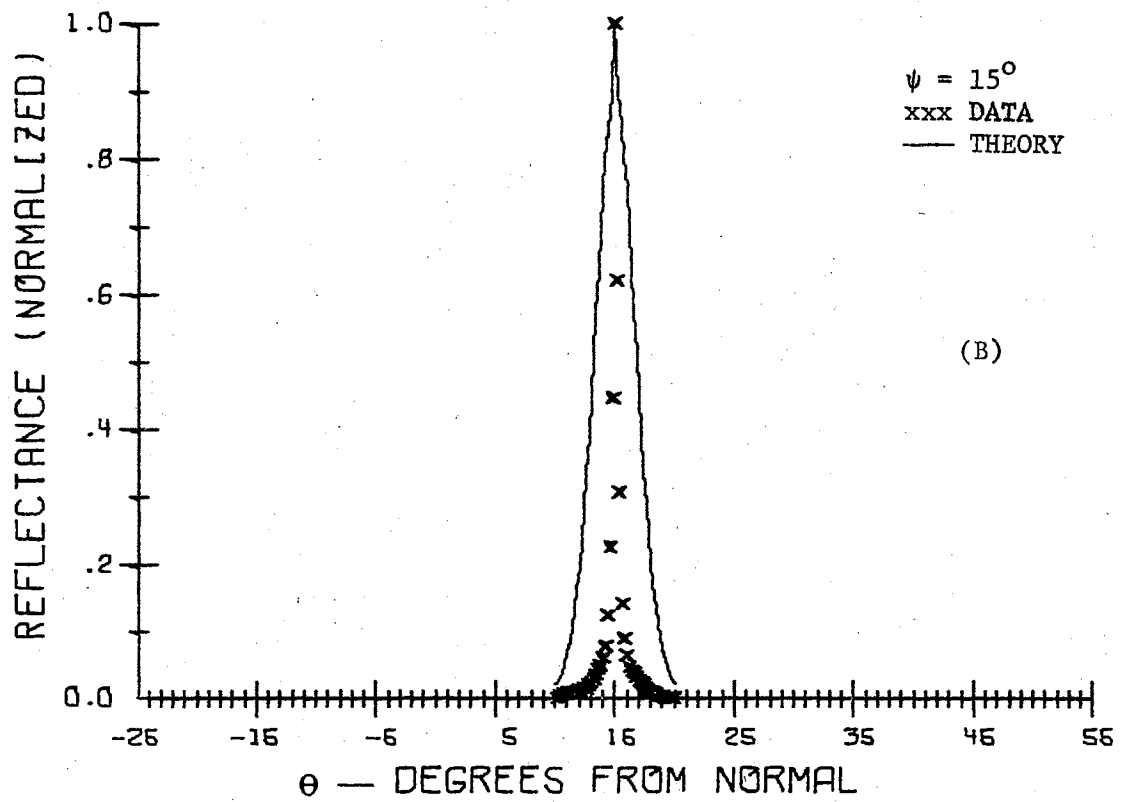
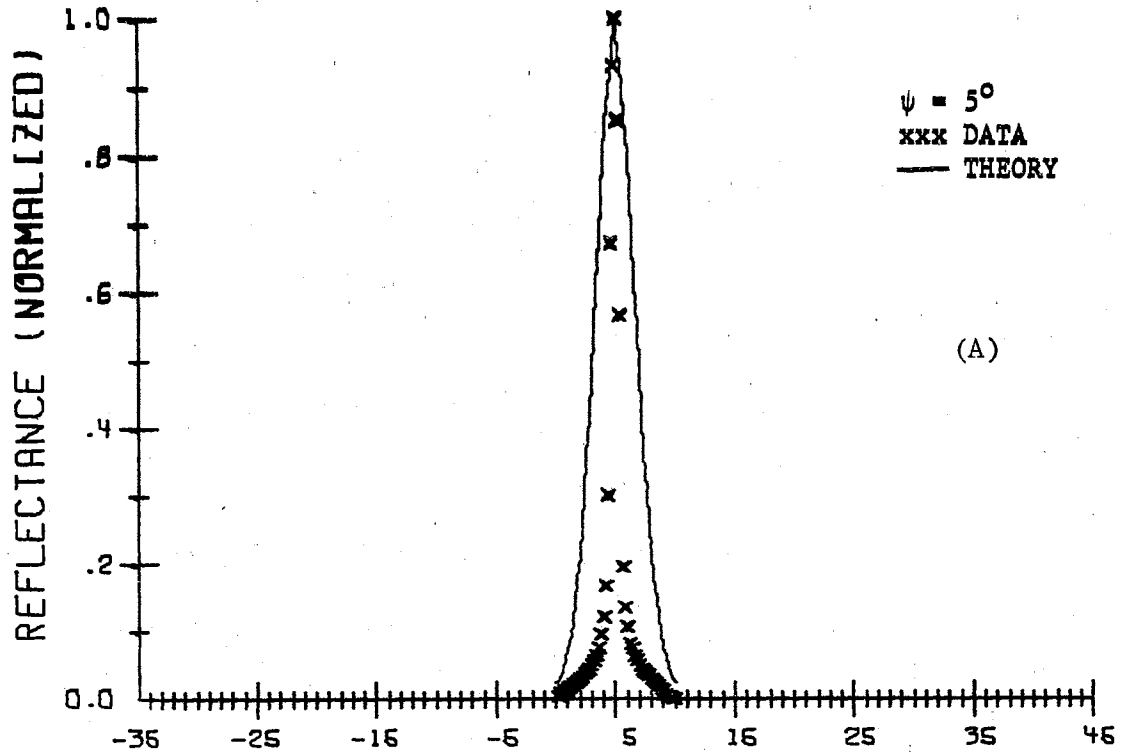


Figure 53. Theory Versus Data - Sample 3 - $\psi = 5^\circ$ and 15°

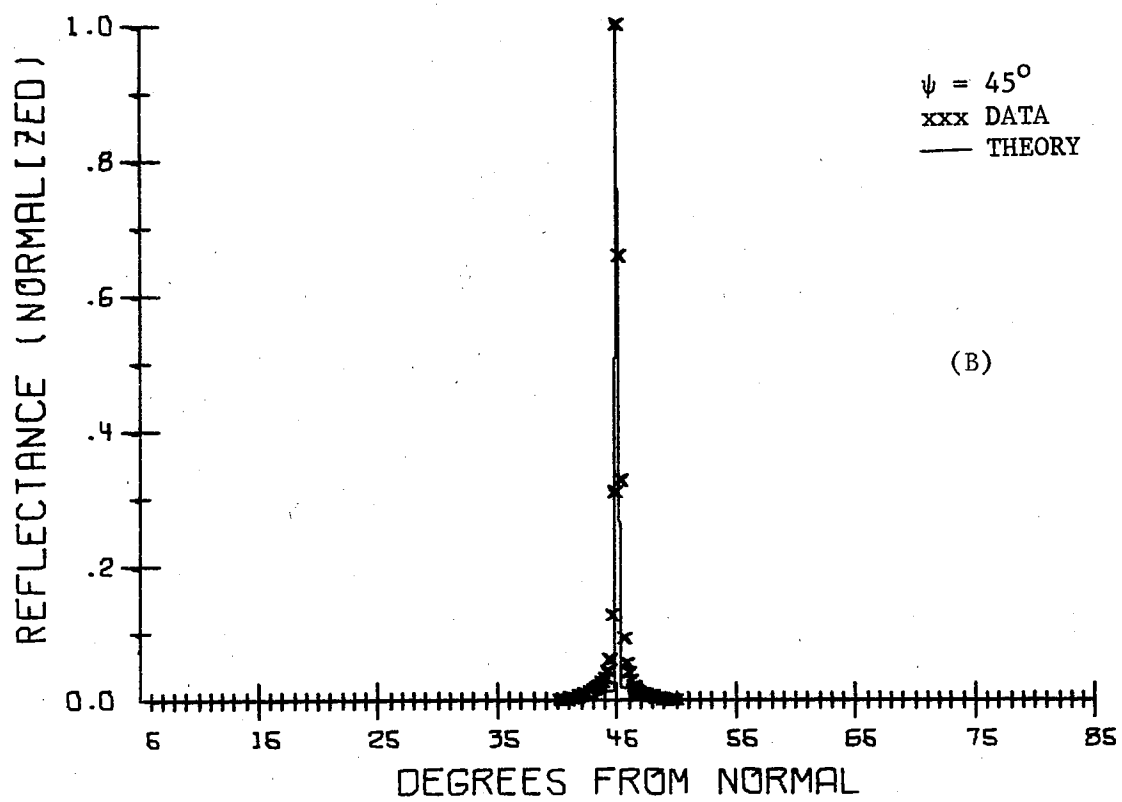
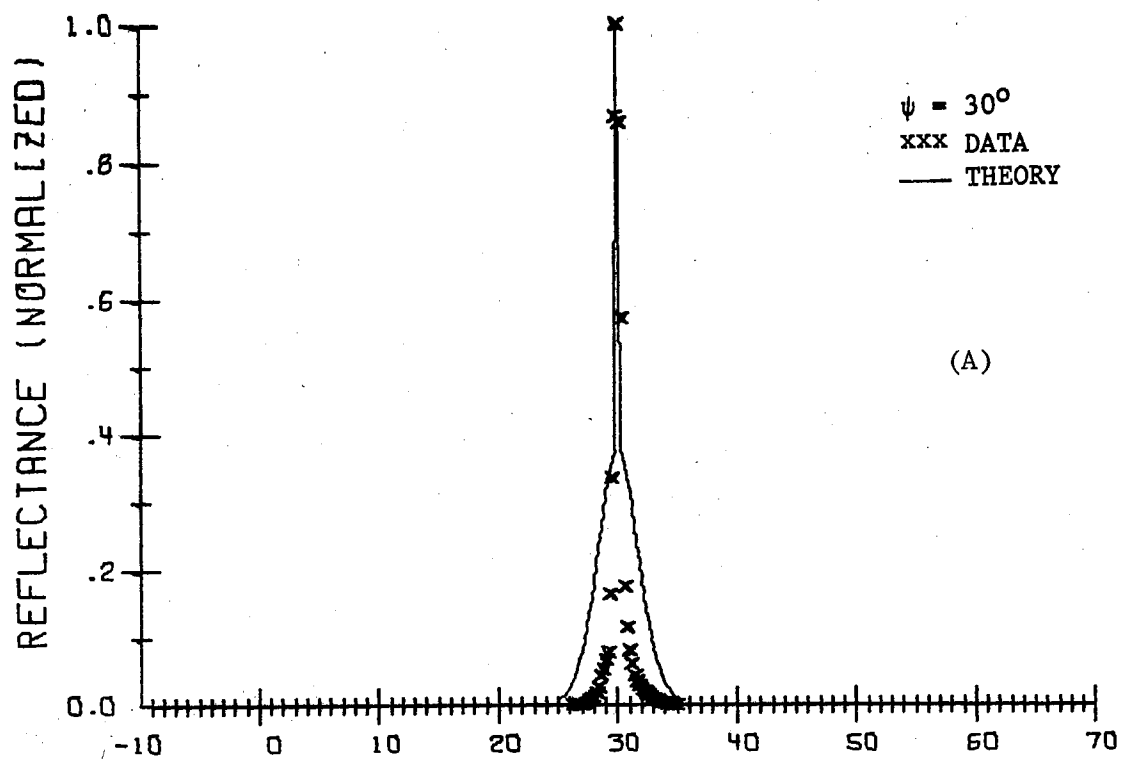


Figure 54. Theory Versus Data - Sample 3 - $\psi = 30^\circ$ and 45°

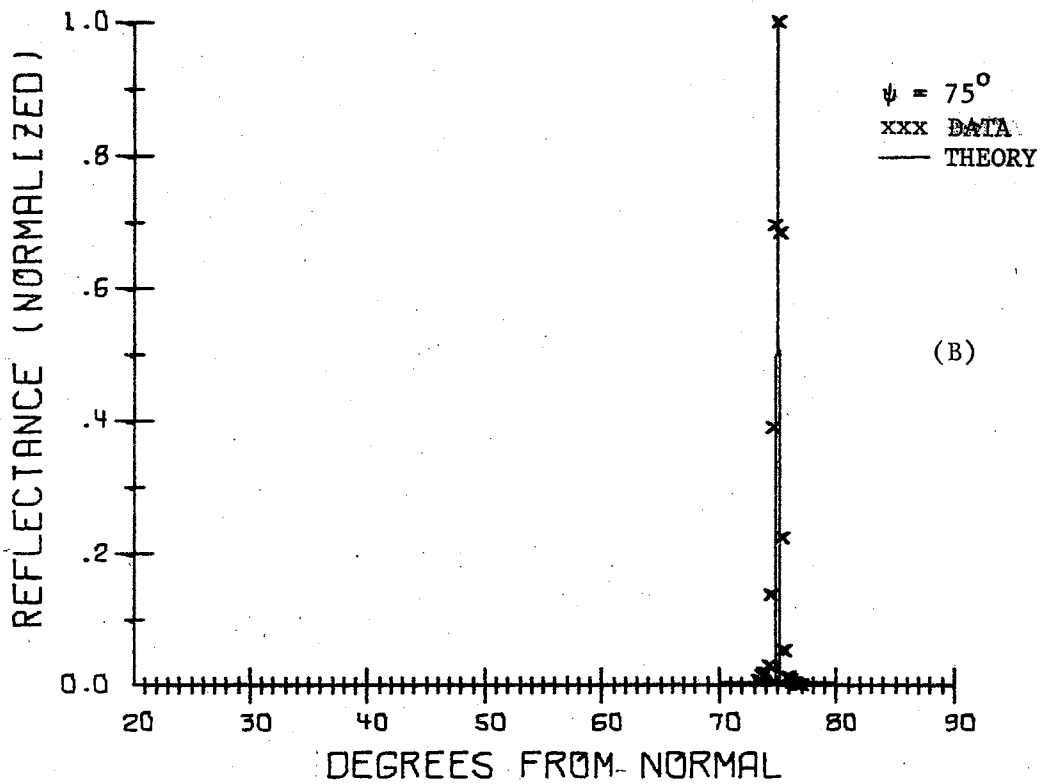
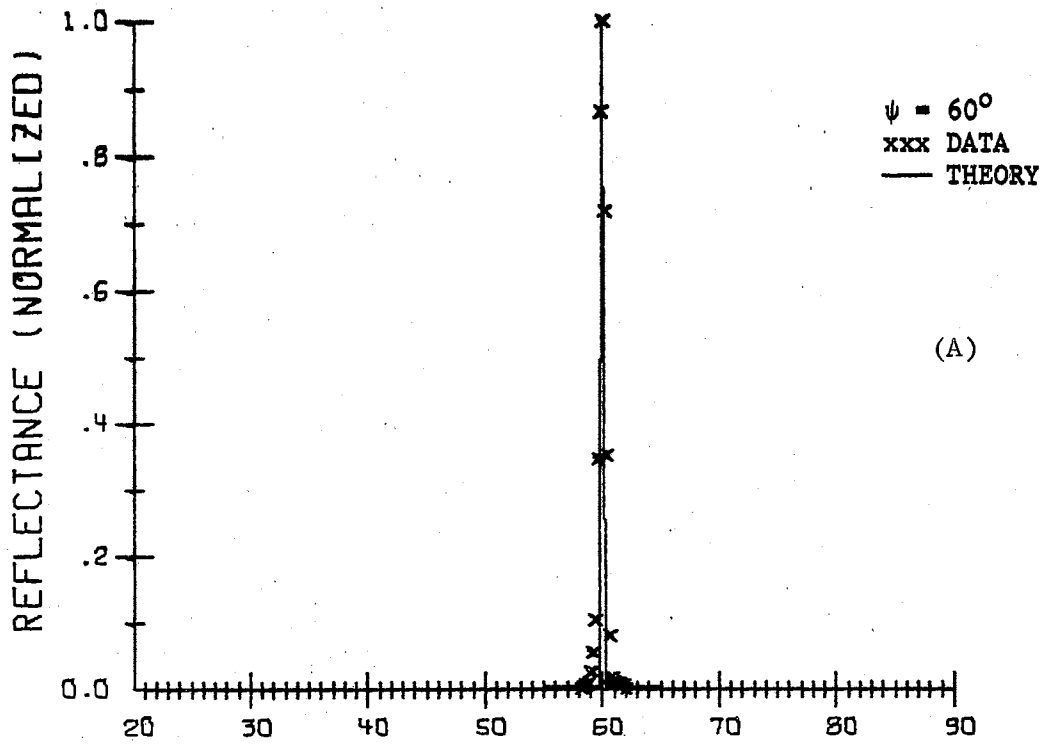


Figure 55. Theory Versus Data - Sample 3 -
 $\psi = 60^\circ$ and 75°

APPENDIX C

THEORY VERSUS DATA COMPUTER PROGRAM

PROGRAM FEWTD3 (INPUT,OUTPUT,TAPES=INPUT,TAPE6=OUTPUT,TAPES)

C
C
C
C
C

CALCULATES THEORETICAL REFLECTANCES AND PLOTS VERSUS DATA

REAL LENGTH,LTH
 DIMENSION PSII(8), CNTHET (2), THET (180), SUM(100), FACT(100), R(10
 10), COEF(20), R1(180), R2(100), AUTOD(2), THETDG(100), RDATPL (100)
 DIMENSION YDATA (180), XDATA(180), XSTART(8), XEND(8)
 CALL PLOTS (100.,1,8)
 READ 39, PSII,XSTART,XEND
 AREA=27331000.
 PI=3.1416
 ALAMBDA=0.6328

C
C
C

CHANGE AUTOC-SIGMA-SPREAD FOR EACH SAMPLE

AUTOC=11.9
 SIGMA=.162
 SPREAD=40.

C
C
C

FACTORIALS TO 100

FACT(1)=1.0
 DO 1 I=2,100
 FI=FLOAT(I)
 FACT(I)=FACT(I-1)*FI

1
C
C

CONTINUE

NORMALIZES DATA

CO 38 I1I=1,7
 RNORM=D.
 IREAJ=XEND(I1I)-XSTART(I1I)+1.
 DO 2 I7I=1,180
 YDATA(I7I)= 0.

2

CONTINUE

PSIDT=PSII(I1I)
 READ 40, (YDATA(I),I=1,IREAD)
 IRE=IREAD-8
 DO 3 I5I=5,IRE
 IF (YDATA(I5I).LT.YDATA(I5I-1)) GO TO 3
 RNORM=DATA(I5I)

3

CONTINUE

PRINT 41, YDATA
 DO 4 I2I=1,IREAD
 YDATA(I2I)=YDATA(I2I)/RNORM

```

4  CONTINUE
   PRINT 42, YDATA

C
C  FILLS INCOMING AND OUTGOING THETAS AT 1 DEGREE INTERVALS
C
   XPTST=PSIDT-SPREAD
   XPTEND=PSIDT+SPREAD
   IF (XPTEND.LT.91.) GO TO 5
   XPTEND=90.
   XPTST=20.

5  CONTINUE
   PSI=PSIDT
   PHIDT=0.
   PHI=PHIDT
   IPLTSP=XPTEND-XPTST+1.
   DO 6 I2I=1,IPLTSP
     THET(I2I)=(XPTST+I2I-1.)*.0174533
6  CONTINUE

C
C  THEORETICAL CALCULATIONS
C
   AR=AREA
   PSI=PSI*.0174533
   DO 27 I3=1,IPLTSP
     DO 26 I62=1,2
       IF (I62.EQ.1) GO TO 7
       THETA=THET(I3)
       GO TO 8
7     THETA=PSI
8     CONTINUE
     XA=4.0*PI*SIGMA/ALAMBDA*COS(PSI)
     XA2=XA*XA
     IF (XA2-88.0) 10,10,9
9     FUNCC=0.0
     GO TO 11

10    EXA=1.0/EXP(XA2)
     FUNCC=EXA
11    CONTINUE
     S=SIGMA
     PAR1=(1.0+COS(THETA)*COS(PSI)-SIN(THETA)*SIN(PSI)*COS(PHI))/(COS(THETA)+COS(PSI))
     PAR1=PAR1/COS(PSI)
     F=PAR1
     F2=F*F
     PAR11=F2
     FAC1=PI*AUTOCL*AUTOCL*F2/AR
     PAR2=2.0*PI*SIGMA/ALAMBDA*(COS(THETA)+COS(PSI))
     PAR22=PAR2**2.0

```



```

G=PAR22
PAR3=6
C
C  CALCULATE THE TERMS FOR SUMM

SUM(1)=0.0
SUMM=0.0
SUMF1=0.
SUMF2=1.
M=100
DO 17 I=1,M
FI=FLOAT(I)
PAR4=-(PI*PI/FI*AUTOC/ALAMBD*AUTOC/ALAMBD*(SIN(PSI)*SIN(PSI)+SIN(T
LHETA)*SIN(THETA)-2.0*SIN(PSI)*SIN(THETA)*COS(PHI)))
IF (PAR4) 12,14,14
12  PAR4NE=-PAR4
    IF (PAR4NE.GT.88.0) GO TO 13
    SUM(I)=PAR3**FI/(FACT (I)*FI)*1.0/EXP(-PAR4)
    GO TO 16

13  SUM(I)=0.0
    GO TO 16

14  CONTINUE
    IF (PAR4.6T.88.0) GO TO 15
    SUM (1)=PAR3**FI/(FACT(I)*FI)*EXP(PAR4)
    GO TO 16

15  SUM(T)=PAR3**FI/(FACT(I)*FI)*EXP(87.0)
16  SUMM=SUMM+SUM(I)
17  CONTINUE
    IF (88.0-PAR22) 18,19,19
18  FUNCIC=0.0
    GO TO 20
19  FUNCIC=FAC1*1.8/EXP(PAR22)*SUMM
20  CONTINUE
    IF (ABS(THETA-PSI).LT.0.00001) GO TO 21
    DD1=0.
    GO TO 22
21  DD1=1.0
22  IF (ABS(PHI).LT.0.00001) GO TO 23
    DD2=0.0
    GO TO 24
23  DD2=1.0
24  FUNC=FUNC*DD1*DD2+FUNCIC
    IF (ABS(THETA-PSI).GT.0.00001) GO TO 25
    FUNCN=FUNC
25  CONTINUE
26  CONTINUE
    R1(I3)=FUNC/FUNCN
27  CONTINUE
    PRINT 43, R1

```

C
C
C
C

PLOTS THEORETICAL REFLECTANCES

```

CAL AXIS (0.5,0.5,XPTST,XPTEND,.06250,1.,10.,4HF5.0,0.0,19HDEGREE
1S FROM NORMAL,19)
CALL AXIS (8.5,0.5,0.0,1.0,3.50,0.1,0.2,4HF8.1,90.,24HREFLECTANCE
1(NORMALIZED),24)
YY=R1(1)*3.50+0.5
IF (XPTST.GT.0.) GO TO 28
XX=THET(1)/.0174533*.8625+0.5+AES(XPTST)*.0625
GO TO 29
28 CONTINUE
XX=THET(1)/.0174533*.0625+0.5-XPTST*.0625
29 CONTINUE
CALL PLOT (XX,YY,3)
CAL PLOT (XX,YY,2)
DO 32 I3I=2,IPLTSP
YY=R1(I3I)*3.50+0.5
IF (XPTST.GT.0.) GO TO 30
XX=THET(I3I)/.0174533*.0625+0.5+ABS(XPTST)*.0625
GO TO 31
30 CONTINUE
XX=THET(I3I)/.0174533*.0625+0.5-XPTST*.0625
31 CONTINUE
CALL PLOT (XX,YY,2)
32 CONTINUE
C
C PLOTS REFLECTANCE DATA
YY=YDATA(1)*3.50+0.5
IF (XSTART (I1I).GT.0.) GO TO 33
XX=(XPTST+(XSTART(I1I)-XPTST))*0.0625+0.5+ABS(XPTST)*.3625
GO TO 34
33 CONTINUE
XX=(XPTST+(XSTART (I1I)-XPTST))*0.0625+0.5-XPTST*.0625
34 CONTINUE
CALL PLOT (XX,YY,3)
CALL PLOT (XX,YY,2)
DO 37 I2I=2,IREAD
YY=YDATA(I2I)*3.50+0.5
IF (XSTART(I1I).GT.0.) GO TO 35
XX=(XPTST+(XSTART(I1I)-XPTST)+(I2I-1.))*0.0625+0.5+ABS(XPTST)*.0625
GO TO 36
35 CONTINUE
XX=(XPTST+(XSTART(I1I)-XPTST)+(I2I-1.))*0.0625+0.5-XPTST*.0625
36 CONTINUE
37 CALL SYMBOL (XX,YY,.87,4,0.,-1)
CALL PLOT (10.,0.,-3)
38 CONTINUE
RETURN
C

```

```

39  FORMAT (*F10.7)
40  FORMAT (5X,F5.8)
41  FORMAT (15(2X,F5.0))
42  FORMAT (15(1X,F6.4))
43  FORMAT(15(1X,F6.4))
    END

```

LENGTH INCLUDING I/O BUFFERS

ASSIGNMENTS

ASSIGNMENTS

880103	5	-	00142	7	-	000174	8	-	000176
000207	10	-	060211	11	-	000216	12	-	000337
000360	14	-	000362	15	-	000400	16	-	000413
000422	19	-	000424	20	-	000432	21	-	00044D
000442	23	-	000447	24	-	000451	25	-	000463
000463	28	-	000541	39	-	000546	36	-	000570
000576	33	-	000620	34	-	000626	35	-	000655
000666	37	-	000666	39	-	001004	40	-	001005
001011	42	-	001014	43	-	001017			001005

ASSIGNMENTS

003620	AR	-	003644	AREA	-	003615	AUTOC	-	003621
002514	CNTHET	-	001076	COEF	-	002040	DDL	-	003675
003676	EXA	-	003653	F	-	003656	FACT	-	001530
003661	FI	-	003625	FUNC	-	003677	FUNCG	-	003652
003674	FUNCN	-	003700	F2	-	003657	G	-	003664
003624	IPLTSP	-	003643	IRE	-	003633	IREAD	-	003630
003626	I2I	-	003635	I3	-	003645	I3I	-	003703

VITA

Fred Edwin Walter

Candidate for the Degree of

Doctor of Philosophy

Thesis: AN INVESTIGATION OF BI-DIRECTIONAL REFLECTANCE FROM RANDOMLY ROUGH ENGINEERING SURFACES

Major Field: Mechanical Engineering

Biography:

Personal Data: Born at Bearcreek, Montana, August 12, 1935, the son of Harry E. and Lillian R. Walter.

Education: Attended grade school in Red Lodge, and Billings, Montana, and graduated from Billings Senior High School in 1953; received the Bachelor of Science degree from Montana State University, with a major in Mechanical Engineering, in May, 1958; received the Master of Science degree from the University of Wyoming, with a major in Mechanical Engineering, in February, 1963; completed requirements for the Doctor of Philosophy degree, Oklahoma State University, in May, 1972.

Professional Experience: Entered the United States Air Force in 1958 and is now a Major; since 1961 has been working as a mechanical engineering officer in the areas of packaging design and evaluation, layout and installation of mechanized materials handling systems, test design and theoretical analysis of the survivability and vulnerability of facilities.